

11. SITE 935¹

Shipboard Scientific Party²

HOLE 935A

Date occupied: 18 April 1994

Date departed: 22 April 1994

Time on hole: 4 days, 05 hr

Position: 5°25.612'N, 47°33.893'W

Bottom felt (drill pipe measurement from rig floor, m): 3496.5

Distance between rig floor and sea level (m): 10.99

Water depth (drill pipe measurement from sea level, m): 3485.5

Penetration (m): 372.60

Number of cores (including cores having no recovery): 40

Total length of cored section (m): 372.00

Total core recovered (m): 268.60

Core recovery (%): 72

Oldest sediment cored:

Depth (mbsf): 372.60

Nature: Silty clay

Earliest age: Pleistocene

Principal results: Site 935 (proposed Site AF-15) is located on the flank of the Aqua Channel, the oldest "Channel 1" conduit (Table 1 in "Introduction" chapter, this volume). This part of the Aqua Channel was abandoned when upchannel avulsion formed the Brown segment of "Channel 1" (Figs. 3B and 9 in "Introduction" chapter, this volume). The site was one of a series designed to characterize the development of the levees of the Amazon Channel, the most recently active course of which lies about 15 km to the west of Site 935, on the Brown and Amazon segment. Site 935 also was intended to sample the underlying, flat-lying, high-amplitude reflection packets (HARPs) and to determine the age of the Unit R Debris Flow and the underlying Green levee crest of the Lower Levee Complex. A limited logging program was undertaken to characterize the HARP units, the debris-flow deposit, and the buried levee crest.

The site was selected from a *Conrad* seismic profile (C2514; 0222UTC on 3 Dec. 1984), which our pre-site survey showed was mis-navigated by about 0.9 nmi to the east. The site was further shifted 0.5 km west of the proposed location, off the crest of the Green levee, to increase the chances of recovering sediment at the top of the Green stratigraphic interval.

Hole 935A was cored by APC to 104.6 mbsf and recovered 111.33 m (106.4%). The hole was then cored by XCB to 372.6 mbsf, with 59.4% recovery in this lower part of the hole. Temperature measurements were made at 51 and 80 mbsf using ADARA and at 132 mbsf using WSTP, showing a geothermal gradient ranging from 35°/km near the surface to 25°/km at depth, with a linear mean of 32°/km. There was gas expansion

in many cores, destroying sedimentary structures in most sand beds. Honeycomb structure, suggestive of gas hydrate, was found at 4.1–5.0 mbsf. Methane was found throughout the hole, but higher hydrocarbons were not detected. Logging was hindered by poor hole conditions near 200 mbsf. The Quad-combo and FMS tools were run from 64 to 180 mbsf and 230 to 290 mbsf.

Six lithologic units are recognized:

Unit I (0–0.65 mbsf) is a Holocene foraminifer-nannofossil clay, bioturbated, with up to 38% carbonate. The unit includes five indurated brown crusts between 0.36 and 0.65 mbsf.

Unit II (0.65–98.50 mbsf) consists of thin bedded mud with beds and laminae of silt and sand. Subunit IIA (to 5.94 mbsf) is a slightly to moderately bioturbated clay. Subunit IIB (to 21.20 mbsf) consists of silty clay with silt laminae. Subunit IIC (to 43.40 mbsf) consists of silty clay with infrequent laminae and thin beds of silt and fine sand. Subunit IID (to 98.50 mbsf) is similar to Subunit IIC, but has more frequent and thicker laminae and beds (<3 cm) of silt and fine sand, with cross lamination in about 5% of the sand beds. Magnetic remanence intensity in this subunit is more than double that in under- and overlying sediment. Subunits IIA and IIB correspond to the Amazon-Brown levee flank 15 km from the channel; Subunits IIC and IID correspond to the Aqua levee flank less than 1 km from the channel.

Unit III (98.50–199.30 mbsf) corresponds to high-amplitude reflection packets (HARPs) in seismic-reflection profiles. The unit consists of fine to coarse sand beds, commonly with mud clasts, alternating with silty clay with laminae and thin beds of silt and fine sand. Recovery was only 52.3% in this unit. Subunit IIIA (to 151.67 mbsf) consists of thick beds of medium sand intercalated with thick silty clay intervals that generally have contorted bedding, suggesting that mass transport has occurred. Subunit IIIB (to 199.30 mbsf) is principally clay with laminae and thin beds of silt and sand, with a thick bed of coarse to medium sand at the base of the subunit. At 173–179 mbsf, the clay is moderately bioturbated and contains a few foraminifers, suggesting relatively slow hemipelagic sedimentation.

Unit IV (199.30–276.30 mbsf) consists of very dark gray silty clay, with <5% contorted beds of silty clay with organic detritus. Clasts of carbonate-rich clay occur at 219–226 mbsf. Pore-water sulfate concentrations of 1.0–3.3 mM are found at 223 and 250 mbsf. The unit is interpreted as a mass-transport deposit (slides and/or debris-flow deposits) and corresponds to a unit of incoherent reflections in seismic-reflection profiles (the "Unit R Debris Flow").

Unit V (276.30–286.04 mbsf) is a foraminifer-nannofossil-rich and -bearing clay, with ephemeral black color mottling and banding. This unit has high total sulfur content (0.9%–1.8%).

Unit VI (286.04–372.06 mbsf) corresponds to the flank of the Green levee. The unit consists of silty clay with laminae and thin beds of silt and fine sand. Subunit VIA (to 310.32 mbsf) is silty clay with rare silt laminae. Subunit VIB (to 363.00 mbsf) is silty clay with silt laminae and thin beds of silt and fine sand, some of which are cross laminated. The frequency of silt and sand beds decreases downhole. Subunit VIC (to 372.06 mbsf) consists of silty clay with discontinuous laminae and thin beds of silt.

Clasts of nannofossil- and foraminifer-bearing clay are found in sand beds in Unit III and as blocks in Unit IV. Most clasts in Unit III are of Zone CN15b. A coarse sand near the base of Unit III contains reworked

¹Flood, R.D., Piper, D.J.W., Klaus, A., et al., 1995. *Proc. ODP, Init. Repts.*, 155: College Station, TX (Ocean Drilling Program).

²Shipboard Scientific Party is as given in the list of participants in the contents.

foraminifers including *G. menardii*. Most blocks in Unit IV have low abundance of nannofossils, but one clast contains a rich nannofossil assemblage similar to that in Unit V, indicating that substantial reworking has occurred.

The bioturbated clay interval at 173–179 mbsf near the base of Unit III contains a few nannofossils. The presence of clasts within the underlying unit containing Zone CN15b nannofossil assemblages (<85 ka) indicates that the base of Unit III must be younger than 85 ka. The sparse foraminifer assemblage includes *P. obliquiloculata*, indicating an age >40 ka. The absence of *G. menardii* and *G. tumida* is consistent with an age of <85 ka.

Unit V contains a nannofossil assemblage lacking both *P. lacunosa* and *E. huxleyi*. The foraminifer assemblage is a warm (interglacial) assemblage including *G. tumida flexuosa* and *G. hexagonus*.

Five oscillations in magnetic declination and inclination from 35 to 42 mbsf are interpreted as secular variation cycles. No geomagnetic excursion was detected at this site.

The clay-sized mineral fraction of mud was systematically examined by XRD at this site. The data show that smectite/kaolinite is highest in the Holocene calcareous clay (Unit I), in the HARP unit (Unit III) and at the top of the Green levee (Units V and VI). Illite/kaolinite tends to be higher in the same intervals. Kaolinite is most abundant in the Amazon-Aqua interval (Unit II) and the mass-transport deposit (Unit IV).

In general, organic-carbon content ranges from 0.8% to 1.0% with atomic carbon:nitrogen ratios ([C/N]_a) of 6 to 10. Two organic-rich sand units have organic-carbon contents of 2.0% and 4.9% and [C/N]_a ratios of 20 and 34, characteristic of vascular plant debris. Four bitumen analyses show predominance of odd-carbon-numbered *n*-alkanes with maximum concentrations of *n*-C₂₉H₆₀ and *n*-C₃₁H₆₄, suggesting derivation from higher terrestrial plants.

Site 935 is an important chronologic reference for the Middle and Lower Levee complexes. Hemipelagic sediment dated between 40 and 85 ka is found 25 m above the "Unit R Debris Flow" (Unit IV). More important, the Green levee is capped by interglacial sediment (Units V and VIA) that shows many characteristics similar to the extreme latest Pleistocene–Holocene section. Our shipboard interpretation is that this interval represents isotopic Stage 9, but this remains to be confirmed by shore-based taxonomic and isotopic studies.

SETTING AND OBJECTIVES

Introduction

Site 935 (proposed Site AF-14) was one of a series of sites designed to characterize the development of the most recently active channel of the Amazon Fan (the Amazon Channel). It is located on

the flank of the Aqua Channel, one of the paleo-channel pathways from which the present channel branched. Environments sampled include overbank deposits and high-amplitude reflection packets (HARPs). The site also had a stratigraphic objective to determine the age of the Unit R Debris Flow and the underlying Green levee of the Lower Levee Complex (Manley and Flood, 1988). A limited logging program was undertaken to characterize the HARP units, the debris-flow deposit, and the buried levee crest.

Setting

Site 935, on the western (left) levee of the Aqua Channel, sampled sediment related to the development and demise of a portion of the Amazon Channel system (Fig. 1). Regional mapping of reflection units suggests that this site is located 33 km down-fan from the site of the bifurcation of the Amazon-Brown Channel from the Aqua Channel near Site 940. The levee is underlain by a generally flat-lying HARP. The surficial levee and HARP lie on top of a transparent unit interpreted to be a debris-flow deposit. This deposit has covered an underlying levee system (the Green system of Manley and Flood, 1988). Sediment with datable microfossils was expected to overlie the Green levee crest.

The site was selected from a *Conrad* seismic profile (C2514; 0222UTC on 3 Dec. 1984; Fig. 2). However, our pre-site survey showed that this line was misnavigated by about 0.9 nmi to the east. We located Site 935 slightly west of the buried Green levee crest on our *JOIDES Resolution* profile (2245UTC on 15 April 1994; Fig. 3).

A 3.5-kHz profile at the site (Fig. 4) shows that the uppermost 33 ms (about 29 m) are overbank deposits from the Amazon Channel, underlain by overbank deposits from the Aqua Channel. The seismic-reflection data show that the levee-crest strata associated with the Aqua system are about 90 ms (80 m) thick (Fig. 2 and 3). This overlies one or more units of high-amplitude subparallel reflections (HARPs), 100 ms (90 m) thick, that may represent sandier deposits formed in the early stages of channel avulsion. The HARP units overlie a 80 ms (76 m) thick acoustically incoherent unit with surface hyperbolic diffractions (interpreted as a debris flow) that covers the levee flank of the Green Channel-levee System, which is the topmost system in the Lower Levee Complex (Manley and Flood, 1988). The *JOIDES Resolution* seismic profile shows onlap of reflections toward the buried levee crest, thus suggesting either partial removal of the levee crest or preferential deposition in the valley between levees. Site 935 was shifted from the proposed location off the crest of the Green levee to a saddle in the levee to increase the chances of recovering the top of the Green stratigraphic interval.

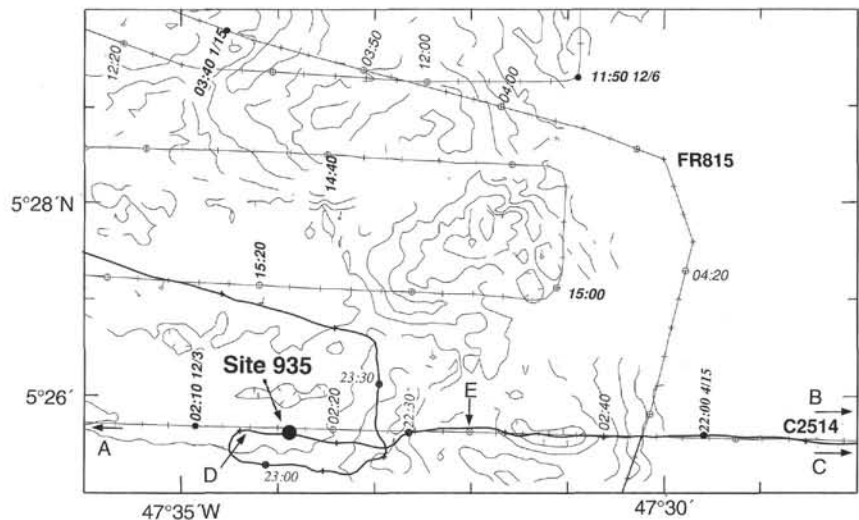


Figure 1. Location of Site 935 showing *Conrad* (C) and *Farnella* (FR) ship tracks with seismic profiles. A–B is seismic profile in Figure 2; C–D is seismic profile in Figure 3; D–E is 3.5-kHz profile in Figure 4.

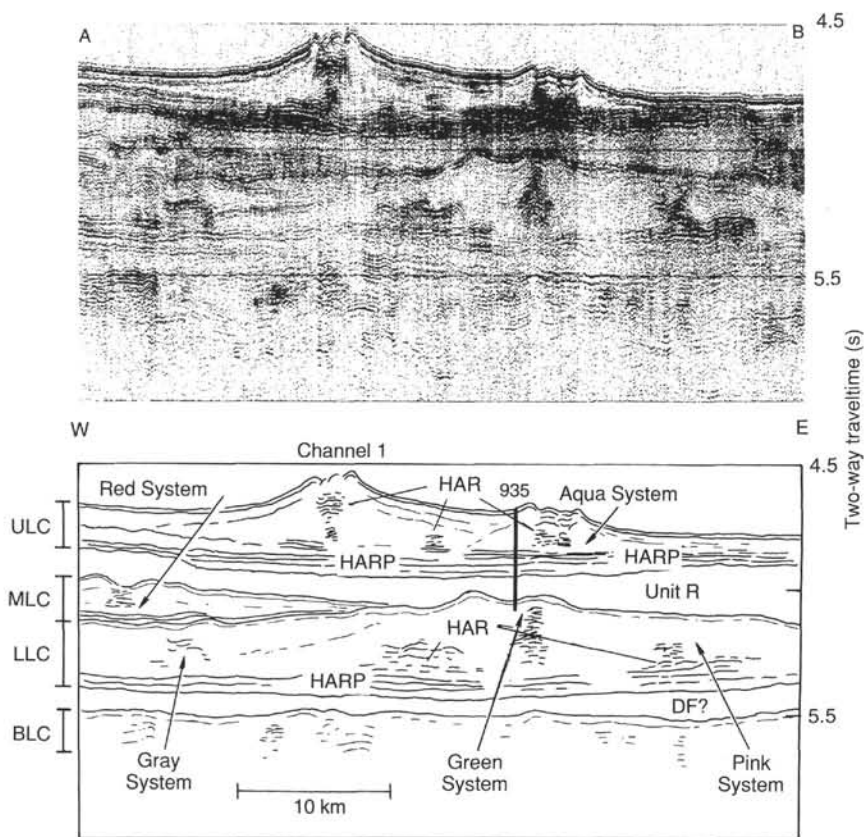


Figure 2. Interpreted seismic reflection profile through Site 935 (from Flood et al., 1991). Line A-B on Figure 1. ULC = Upper Levee Complex, MLC = Middle Levee Complex, LLC = Lower Levee Complex, BLC = Bottom Levee Complex, DF = debris flow.

Objectives

The principal objectives at Site 935 were:

1. To sample the anticipated mud and carbonate clay section above the Green levee to provide a date for the end of activity on this levee.
2. To sample the expanded section in the Aqua levee to provide one element of a transect along the Amazon/Brown/Aqua levee systems.
3. To sample the HARP unit as part of an along-channel study of HARP facies and evolution.
4. To characterize the Unit R Debris Flow deposit to learn the nature of the sediment from which it is made and the properties of sediment at its boundaries.

The logging objectives were to characterize the HARP, levee, and debris-flow acoustic facies by their log response, particularly to establish thickness and patterns of sand beds that are poorly recovered by coring.

OPERATIONS

Transit: Site 934 to Site 935 (AF-14)

The 9-nmi transit in dynamic positioning mode from Site 934 to Site 935 took 8.1 hr at 1.1 kt. When the ship arrived at 05°25.612'N, 47°33.893'W, we deployed a beacon at 0345 hr 18 April.

Hole 935A

We positioned the bit at 3490.5 mbrf and spudded Hole 935A at 0630 hr 18 April. The distance from sea level to rig floor, which depends on the ship's draft, was approximately 10.99 m for Hole 935A. Core 1H recovered 3.52 m of sediment, and the mud line was defined

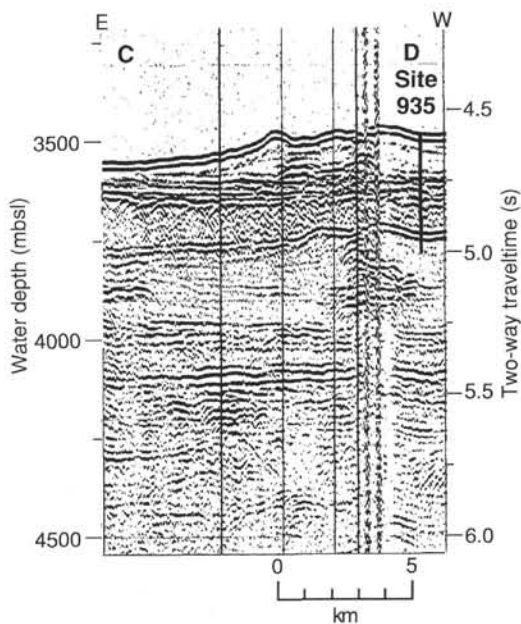


Figure 3. JOIDES Resolution seismic reflection profile of Site 935. Line C-D on Figure 1.

to be at 3496.5 mbrf (Table 1). Cores 1H through 12H were taken from 0 to 104.6 mbsf (3496.5–3601.1 m), recovering 111.33 m (106.4%). Many of the cores recovered at Site 935 began to extrude sediment from the core liner due to gas expansion once the liner was taken out of the core barrel. Core disturbance was minimized by drilling small holes in nearly all of the core liners to allow gas to escape.

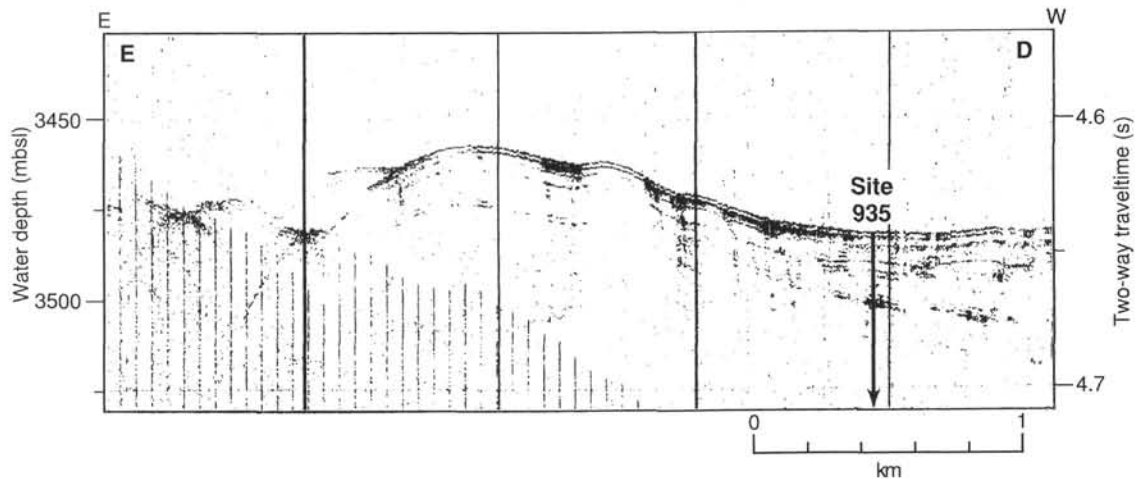


Figure 4. JOIDES Resolution 3.5-kHz profile through Site 935. Line D-E on Figure 1.

Table 1. Site 935 coring summary.

Core	Date (1994)	Time (UTC)	Depth (mbsf)	Length cored (m)	Length recovered (m)	Recovery (%)
155-935A-						
1H	April 18	1050	0.0-3.5	3.5	3.52	100.0
2H	April 18	1140	3.5-13.0	9.5	9.64	101.0
3H	April 18	1240	13.0-22.5	9.5	10.13	106.6
4H	April 18	1400	22.5-32.0	9.5	10.42	109.7
5H	April 18	1450	32.0-41.5	9.5	10.29	108.3
6H	April 18	1610	41.5-51.0	9.5	10.46	110.1
7H	April 18	1655	51.0-60.5	9.5	10.00	105.2
8H	April 18	1745	60.5-70.0	9.5	9.33	98.2
9H	April 18	1855	70.0-79.5	9.5	10.34	108.8
10H	April 18	1940	79.5-89.0	9.5	10.80	113.7
11H	April 18	2030	89.0-98.5	9.5	10.28	108.2
12H	April 18	2120	98.5-104.6	6.1	6.12	100.0
13X	April 18	2255	104.6-112.7	8.1	0.00	0.0
14X	April 19	0005	112.7-122.3	9.6	4.68	48.7
15X	April 19	0110	122.3-132.0	9.7	9.15	94.3
16X	April 19	0355	132.0-141.1	9.1	2.66	29.2
17X	April 19	0525	141.7-151.4	9.7	9.05	93.3
18X	April 19	0625	151.4-160.9	9.5	5.73	60.3
19X	April 19	0725	160.9-170.4	9.5	0.00	0.0
20X	April 19	0840	170.4-180.0	9.6	8.47	88.2
21X	April 19	1100	180.0-189.6	9.6	5.68	59.1
22X	April 19	1220	189.6-199.3	9.7	1.14	11.7
23X	April 19	1400	199.3-209.0	9.7	1.11	11.4
24X	April 19	1610	209.0-218.6	9.6	0.70	7.3
25X	April 19	1815	218.6-228.2	9.6	7.15	74.5
26X	April 19	2030	228.2-237.8	9.6	7.60	79.1
27X	April 19	2230	237.8-247.4	9.6	6.60	68.7
28X	April 20	0050	247.4-257.1	9.7	6.35	65.4
29X	April 20	0250	257.1-266.7	9.6	8.85	92.2
30X	April 20	0440	266.7-276.3	9.6	6.92	72.1
31X	April 20	0610	276.3-286.0	9.7	8.03	82.8
32X	April 20	0750	286.0-295.7	9.7	6.68	68.8
33X	April 20	0925	295.7-305.3	9.6	8.90	92.7
34X	April 20	1100	305.3-315.0	9.7	6.13	63.2
35X	April 20	1225	315.0-324.7	9.7	7.99	82.4
36X	April 20	1345	324.7-334.3	9.6	9.44	98.3
37X	April 20	1530	334.3-343.9	9.6	6.61	68.8
38X	April 20	1700	343.9-353.5	9.6	5.59	58.2
39X	April 20	1830	353.5-363.0	9.5	0.00	0.0
40X	April 20	2000	363.0-372.6	9.6	6.03	62.8
Coring totals				372.0	268.6	72.20

Note: An expanded version of this coring summary table that includes lengths and depths of sections, location of whole-round samples, and comments on sampling disturbance is included on the CD-ROM in the back pocket of this volume.

Parts of Cores 10H, 31X, 33X, and 36X extruded from the liner onto the rig floor. Core 1H was difficult to remove from the barrel and may have been slightly disturbed. The core barrel only partially stroked while taking Core 12H. Cores 3H through 12H were oriented using the Tensor tool. ADARA heat-flow measurements were attempted during Cores 4H, 6H, and 9H.

XCB Cores 13X through 40X were taken from 104.6 to 372.6 mbsf (3601.1-3869.1 mbrf), coring 268.0 m and recovering 157.24 m (58.7%). The combined APC/XCB recovery was 72.1%. A WSTP temperature measurement was taken prior to Core 16X.

The hole was circulated clean with a sepiolite/seawater mixture. We pulled the pipe up to 61.5 mbsf (3558.0 mbrf) and, while lowering it back down, the hole was blocked at 188.5 mbsf (3683.0 m). We reamed out the bridge (about 2 m thick), but the bit encountered fill at 3841.0 mbrf. The 28 m of soft fill was reamed out, and the go-devil was pumped to open the LFV. We then pulled the pipe up to 80.2 mbsf (3576.7 mbrf) and set up to pick up 20 m to log the upper hole. The hole was logged in two sections. During the first Quad-combo run, the tool tagged a bridge at 184.5 mbsf (3681.0 mbrf), and we decided to log the hole above and below the bridge. The Quad-combo run above the bridge required 4.3 hr. The FMS tool tagged the bridge at 171.5 mbsf (3668.0 mbrf) and required 3.6 hr to log.

We washed and reamed with the bit down to 3690.0 mbrf and then lowered the bit to 212.0 mbsf (3708.5 mbrf). The second run of the Quad combo tagged bottom at 298.5 mbsf (3795.0 mbrf; 74.1 m above the total depth [TD] of the hole) and required 5.75 hr. The second FMS tagged bottom at 270.5 mbsf (3767 mbrf; 102.1 m above TD) and required 3.8 hr.

The bit cleared the seafloor at 0245 hr and cleared the rig floor at 0845 hr 22 April.

LITHOSTRATIGRAPHY

Introduction

Hole 935A was drilled to a depth of 372.6 mbsf through the western levee of the Aqua Channel-levee System, acoustic Unit R, and the uppermost part of the Green Channel-levee System of the Lower Levee Complex. Incomplete recovery, especially within the interval 185 through 220 mbsf (Cores 935A-21X through - 24X; Fig. 5), and drilling disturbance (both sand liquefaction and biscuit formation), limited our ability to determine lithology, primary structure, and precise unit boundaries for some intervals. Expansion of methane gas

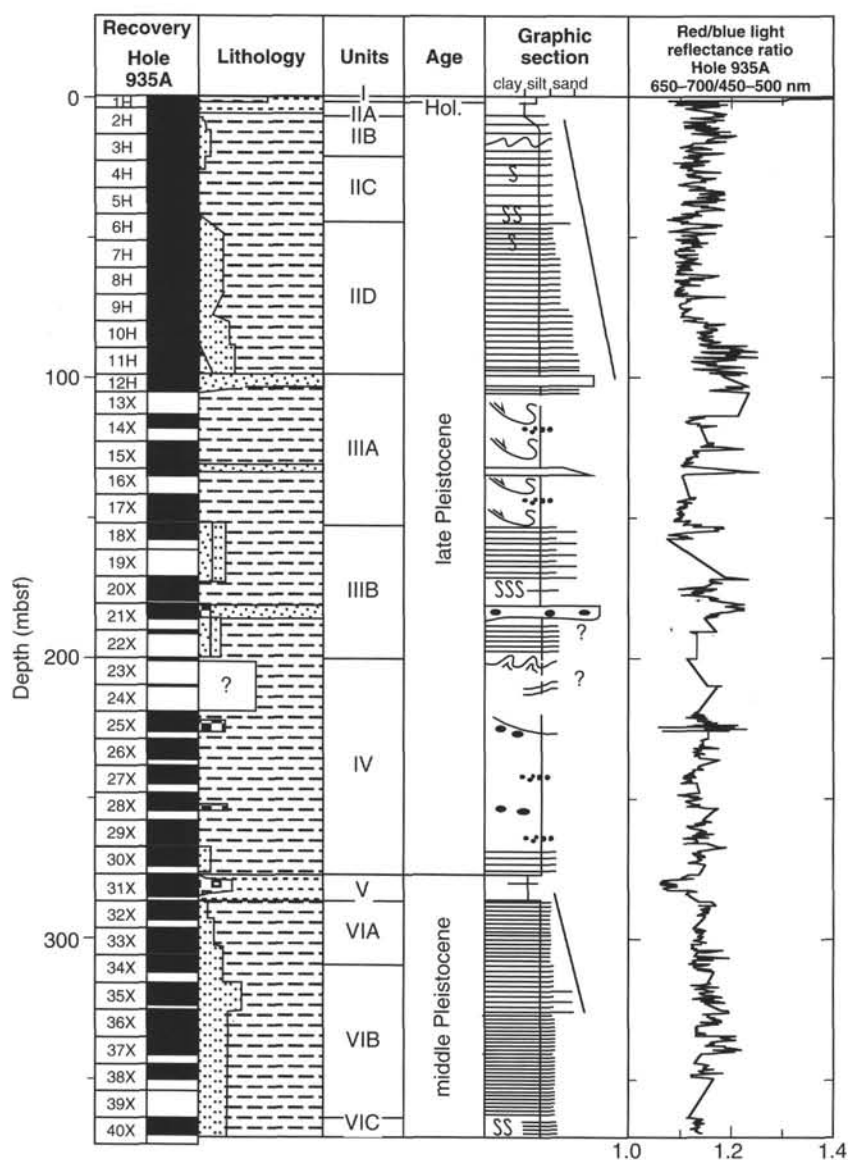


Figure 5. Composite stratigraphic section for Site 935 showing core recovery, simplified summary of lithology, depths of unit boundaries, age, a graphic section with generalized grain-size and bedding characteristics, and downhole variations in light-reflectance values. The lithologic symbols are explained in Figure 1 of the "Explanatory Notes" chapter, this volume.

during core recovery commonly affected the sediment by disrupting the primary sedimentary structures in many silt and sand beds, and by producing void spaces within many of the core sections (see "Lithostratigraphy" section, "Explanatory Notes" chapter, this volume).

Description of Lithostratigraphic Units

Unit I

Intervals: 155-935A-1H-1, 0-65 cm
Age: Holocene
Depth: 0-0.65 mbsf

Unit I consists of 0.65 m of foraminifer-nannofossil-rich clay, which shows a gradational color change from yellowish brown (10YR 5/4; 0-0.36 mbsf) through light brownish gray (2.5Y 6/2; 0.36-0.50 mbsf), to gray (5Y 5/1; 0.50-0.65 mbsf). The sediment is moderately bioturbated and shows slight, ephemeral, black (N2) color mottling throughout. The unit contains five distinct, indurated, diagenetic, dark grayish brown (2.5YR 4/2) clay crusts (at intervals 935A-1H-1, 36, 39, 46, 50, and 65 cm). Similar iron-rich crusts were analyzed previously and correlated throughout the Amazon Fan and adjacent Guiana Basin (Damuth, 1977; see "Introduction" chapter,

this volume). The carbonate content of the unit is approximately 38% (see "Organic Geochemistry" section, this chapter).

Unit II

Interval: 155-935A-1H-1, 65 cm, through -11H-CC
Age: late Pleistocene to Holocene
Depth: 0.65-98.50 mbsf

Unit II consists of 97.85 m of terrigenous clay, silty clay, silt, and very fine sand. The sediment ranges in color from olive gray (5Y 4/2) to very dark gray (5Y 3/1) and is stained to varying degrees by diagenetic hydrotroilite, which imparts a black color (N2) as irregular patches and/or color bands and laminae (see "Introduction" chapter, this volume). The carbonate content of Unit II is low, with an average value of less than 2%. Unit II has been subdivided into four subunits based on the frequency of silt laminae and thin beds of silt and very fine sand.

Subunit IIA

Subunit IIA extends from 0.65 to 5.94 mbsf (interval 935A-1H-1, 65 cm, through -2H-2, 94 cm) and consists of dark olive gray (5Y 3/

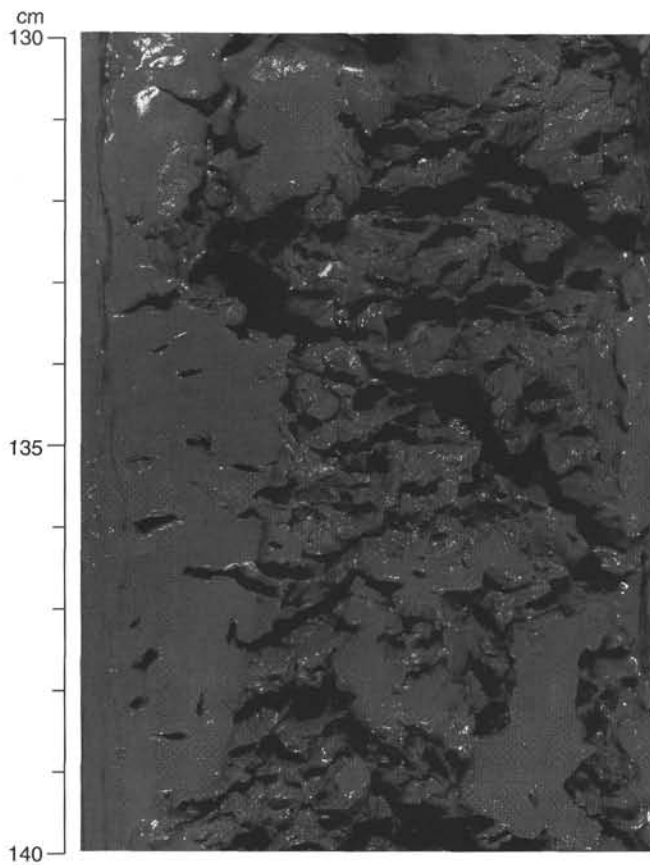


Figure 6. Honeycomb-like core expansion and fracture fabric between 4.15 and 5.03 mbsf within Subunit IIA. The fabric may represent a gas hydrate melt (interval 155-935A-2H-1, 130–140 cm).

2), slightly to moderately bioturbated, mottled clay. Black (N2) mottles are concentrated between 1.75 and 3.52 mbsf (interval 935A-1H-1, 35 cm, through -1H-CC, 25 cm). Honeycomb-like core expansion and fracture (Fig. 6) was observed between 4.15 and 5.03 mbsf (interval 935A-2H-1, 65 cm, through -2H-2, 3 cm). This structure is similar to the “mousse” structure described from Leg 146 (Westbrook, Carson, Musgrave, et al., 1994) and has been interpreted as related to the melting of gas hydrates.

Subunit IIB

Subunit IIB extends from 5.94 to 21.20 mbsf (interval 935A-2H-2, 94 cm, through -3H-6, 70 cm) and is characterized by dark gray (5Y 4/1), olive gray (5Y 4/1), and dark olive gray (5Y 3/2) silty clay that contains silt laminae. The boundary between Subunits IIA and IIB was placed at the uppermost occurrence of silt laminae. On average, five silt laminae occur per meter of core. Faint color banding, in part highlighted by the presence of hydrotroilite, occurs from the top of the subunit to 13.14 mbsf (interval 935A-2H-2, 94 cm, through -2H-CC, 33 cm); below this interval, to the bottom of the subunit at 21.20 mbsf, there is no color banding. An interval of sediment deformation, highlighted by contorted silt laminae, occurs between 14.50 and 17.95 mbsf (Sections 935A-3H-2 through -3H-4, 45 cm).

Subunit IIC

Subunit IIC extends from 21.20 to 43.40 mbsf (interval 935A-3H-6, 70 cm, through -6H-2, 40 cm) and consists of very dark gray (5Y 3/1) and dark olive gray (5Y 3/2) silty clay containing silt laminae and thin beds of silt and fine sand. The boundary between Subunits

IIB and IIC is placed at the first thin bed that consists of silt and very fine sand. This subunit contains, on average, less than five silt laminae and/or beds per meter. Black (N2) color banding and mottling, and moderate levels of bioturbation are common throughout.

Subunit IID

This subunit extends from 43.40 to 98.50 mbsf (interval 935A-6H-2, 40 through -11H-CC), and consists of very dark gray (5Y 3/1) and dark olive gray (5Y 3/2) silty clay with laminae and 1- to 15-cm-thick beds of silt and fine sand. The sequence between the top of the subunit and 80.21 mbsf (935-10H-1) contains between five and 20 silt laminae and/or thin beds per meter (Fig. 7), exhibits black (N2) color banding and mottles, and is moderately bioturbated. Cross-lamination is evident in approximately 5% of the beds. Based on the sequences of primary sedimentary structures in all of the beds, these are either T_{bde} or T_{cdc} turbidites. A thin section from an interval of color-banded silty clay contains a few sharp-based laminae less than 1.5 mm thick. One of these is compositionally graded, with silt grains more abundant at the base (Fig. 8A). Another lamina from the same interval consists of asymmetric ripple forms with amplitude and wavelength values of about 0.7 mm and 15 mm, respectively (Fig. 8B). These features have sharp bases and tops, and no internal lamination. The sequence between 80.21 and 98.50 mbsf (Cores 935A-10H-2 through -11H-CC) contains more than 20 silt laminae and/or thin to medium (2–15 cm thick) beds of silt and fine sand per meter. This 18.29-m-thick interval is faintly color banded; mottling is absent. Some of the medium beds are well graded (for example, beds in Section 935A-11H-5).

Unit III

Interval: 155-935A-12H-1 through -23X-1, 0 cm
Age: late Pleistocene
Depth: 98.50–199.30 mbsf

Unit III consists of 100.80 m of fine to coarse sand interbedded with silty clay (Fig. 9). Some of the sand intervals contain mud clasts. The upper boundary of this unit is at the first occurrence of medium-grained sand at 98.50 mbsf. This unit has been divided into two subunits on the basis of the structure of the silty clay and the texture of sand intervals.

Subunit IIIA

Subunit IIIA is 53.17 m thick (interval 935A-12H-1 through -18X-1, 27 cm). The recovered sediment consists of thick beds of olive gray (5Y 5/2), well-sorted medium sand, intercalated with dark gray (5Y 4/1) silty clay (Fig. 9). The sequence between 102.73 and 113.08 mbsf (interval 935A-12H through -14X-2, 38 cm) consists of dark gray silty clay, which contains laminae of silt and very fine sand. The sequence from 113.08 to 131.45 mbsf (interval 935-14X-1, 38 cm, through -15X-CC) consists of very dark gray silty clay, some of which is highly contorted, with local distorted sand blebs and patches. The interval 935A-16X-1 through -16X-2, 27 cm, contains a thick, normally graded bed of dark grayish brown coarse to fine sand. The primary fabric of this sand was destroyed by the combined effects of drilling and core handling. The interval below the sand to the base of the subunit at 151.67 mbsf (interval 935A-16X-2, 27 cm, through -18X-1, 27 cm) consists of very dark gray (5Y 3/1) silty clay with moderately contorted folds that have a “wood-grain” appearance. This pattern has been reported at other sites and occurs where contorted beds are segmented into drilling biscuits (see “Lithostratigraphy” section, “Explanatory Notes” chapter, this volume).

Subunit IIIB

Subunit IIIB is 47.63 m thick (interval 935A-18X-1, 27 cm, through -23X-1, 0 cm). The sediment consists of very dark gray (5Y 3/1) clay with laminations and thin beds of silt and fine sand with a

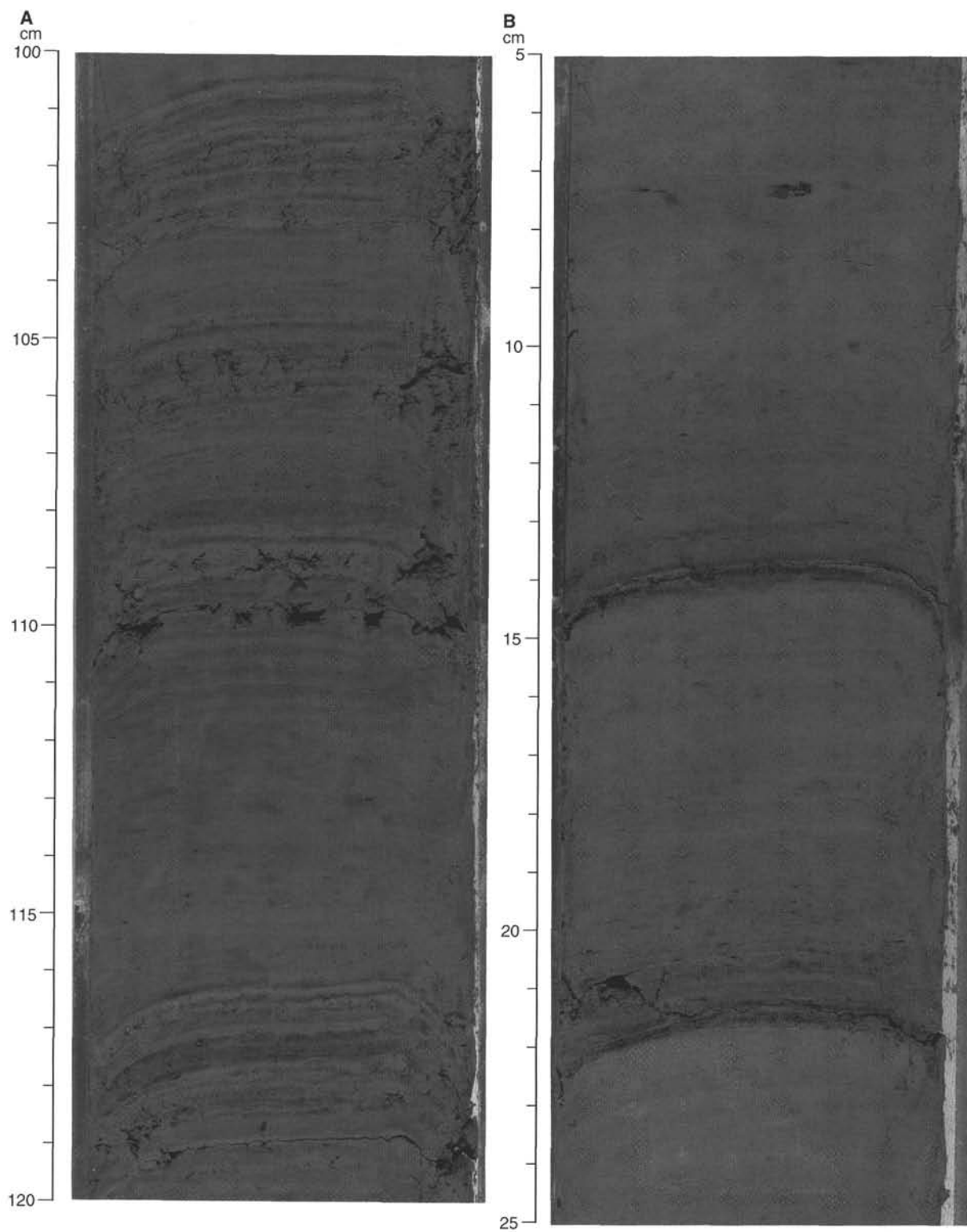


Figure 7. **A.** Thin silt and fine sand laminae couplets, which alternate with color-banded, mottled, and moderately bioturbated silty clay (interval 155-935A-7H-1, 100–120 cm). **B.** Silt and fine sand laminae with sharp basal contacts highlighted by hydrotroilite (interval 155-935A-8H-2, 5–25 cm).

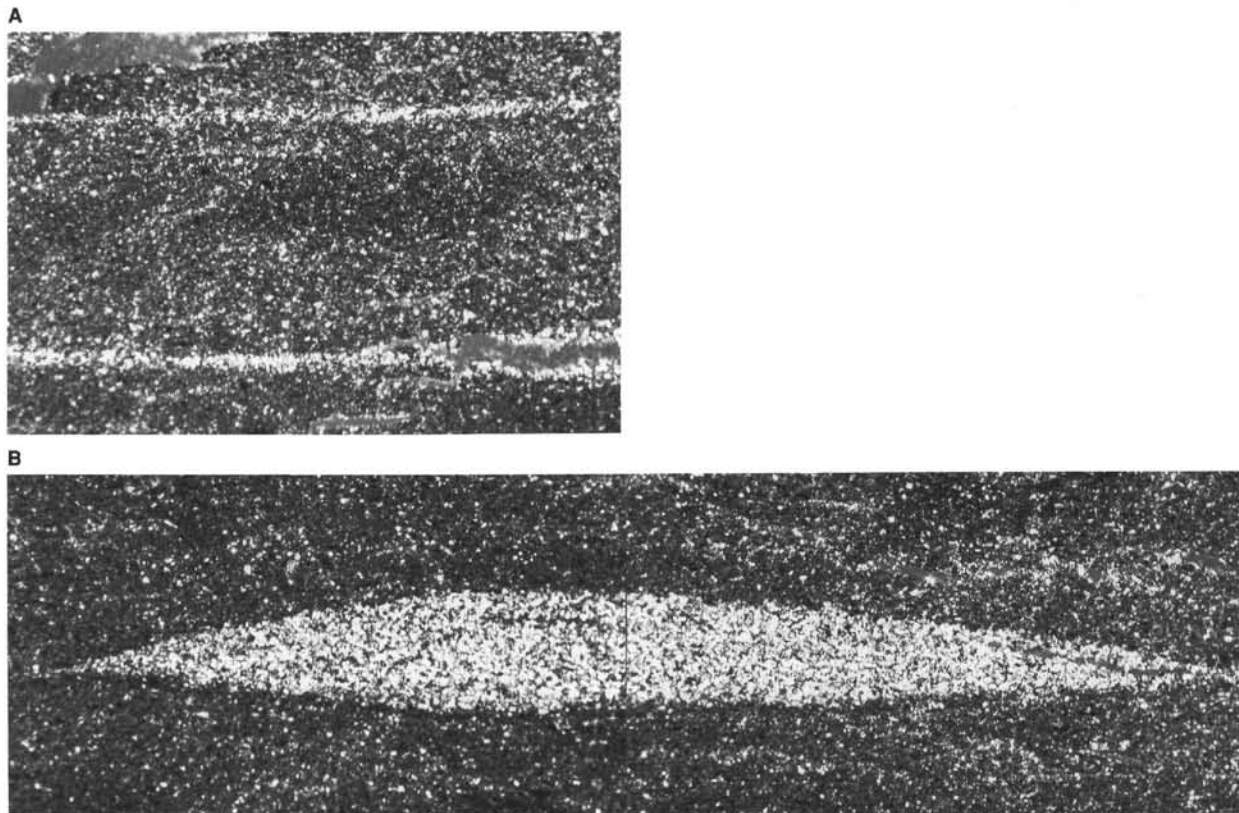


Figure 8. Photomicrograph of color-banded silty clay from Subunit IID (interval 155-935A-8H-3, 134–140 cm) illustrating (A) a content-graded silt-mud couplet about 1.25 mm thick, and (B) an asymmetric silt microripple from a starved-ripple train. Wavelength is approximately 15 mm.

massive medium to coarse sand in Core 21X (Fig. 9). A mixed lithology of very dark gray (5Y 3/1) and black (N2) intercalated clay, silty clay, and fine sand containing organic detritus occurs from 170.40 to 171.15 mbsf (interval 935A-20X-1, 0–75 cm). A moderately bioturbated and mottled dark olive gray (5Y 3/1) silty clay is present from 173.40 to 178.87 mbsf (Sections 935A-20X-3, 0 cm, through -20X-CC). From 180.00 to 199.30 (Cores 935A-21X through -23X-1, 0 cm), the subunit consists of olive gray (5Y 3/2), massive, medium to coarse sand, which contains very dark gray (5Y 3/1) and grayish brown (10YR 4/2), 1- to 3-cm-diameter clasts of foraminifer-nannofossil-rich and -bearing mud (Fig. 10), and a 3-cm-diameter, well-rounded clast of fine sandstone (Fig. 11).

Unit IV

Interval: 155-935A-23X through -31X
Age: late Pleistocene
Depth: 199.30–276.30 mbsf

This unit consists of thin intervals of contorted beds together with a sequence of structureless, very dark gray (5Y 3/1) silty clay. The structureless silty clay extends from Cores 935A-25X through -29X. The contorted interval at the top of this unit (Fig. 12) consists of silty clay with silt laminae, both containing organic detritus, but such intervals compose less than 5% of the unit. The interval 218.60 through 225.75 mbsf (Core 935A-25X) contains 10- to 15-cm-thick greenish gray (5GY 5/1), carbonate-rich clasts (Fig. 13), one of which contains 32.7% carbonate.

Unit V

Interval: 155-935A-31X-1, 0 cm, through -CC, 51 cm
Age: middle Pleistocene
Depth: 276.30–286.00 mbsf

Unit V consists of 9.70 m of dark greenish gray (5GY 3/1) to very dark gray (5Y 3/1) foraminifer-nannofossil-rich and -bearing clay (maximum 26.8% carbonate). Ephemeral black (N2) color mottling occurs to varying degrees throughout (Fig. 14). Faint color banding is present in the uppermost 3 m of the unit.

Unit VI

Interval: 155-935A-32X-1 through -40X-CC
Age: middle Pleistocene
Depth: 286.00–369.03 mbsf

Unit VI is an 83.03-m-thick sequence of very dark gray (5Y 3/1) silty clay containing silt laminae and thin beds of silt and fine sand. The upper boundary of the unit is identified by the highest occurrence of a silt lamina below Unit V. Some of the beds within the unit appear graded, and less than 5% display cross-lamination. The unit has been subdivided into three subunits on the basis of the frequency and nature of the laminae and thin beds.

Subunit VIA

Subunit VIA consists of 24.32 m of very dark gray (5Y 3/1) silty clay with silt laminae (interval 935A-32X-1, 0 cm, through -34X-4, 52 cm). The silt laminae occur with a frequency of approximately three per meter. Mottling, bioturbation, and color banding are present throughout the unit.

Subunit VIB

Subunit VIB comprises 52.68 m of very dark gray (5Y 3/1) silty clay with laminae and 1- to 3-cm-thick beds of silt and fine sand (interval 935A-34X-4, 52 cm, through -39X). The top of this subunit is placed at the upper contact of the first silt bed in Unit VI. Some of the beds are T_{de} turbidites. The average frequency of beds and laminae in the sequence 315.40 to 334.30 mbsf (interval 935A-35X-1, 40 cm,

through -36X) is approximately 40 per meter. This number decreases to between 10 and 15 per meter from 334.30 to the base of the subunit at 363.00 mbsf (Cores 935A-37X through -39X).

Subunit VIC

Subunit VIC (Core 935A-40X) consists of 6.03 m of dark olive gray (5Y 3/2) silty clay with “wispy” discontinuous laminae and distorted and discontinuous thin beds of silt (Fig. 15). This subunit is moderately bioturbated, and it appears that bioturbation has in part destroyed the silt laminae.

Mineralogy

Mineralogy was determined by estimation of mineral volume percentages in smear slides and X-ray diffraction (XRD) analysis of <2 μ m separates.

Smear-slide Synthesis

The silt fraction of the silty clay, the dominant lithology at this site, is composed of 40%–50% quartz, 12%–20% feldspar, 2%–7% mica, and 7%–25% accessory minerals. The accessories include common hornblende, augite and opaques, and rare zircon, spinel, and monazite. Organic detritus forms approximately 5% within some samples. Unit IV lithologies include sand-bearing clayey silt beds (20% sand, 45% silt, and 35% clay; e.g., Sample 935A-25X-3, 102–103 cm) and sandy mud beds (e.g., Sample 935A-30X-1, 98–99 cm).

X-ray Diffraction

X-ray diffraction analysis was performed on the <2- μ m fraction of the dominant silty clay lithologies in most cores recovered at Site 935. The results are summarized in Table 2 and Figure 16. Kaolinite shows a relative decrease from 95 to 200 mbsf and from 250 to 300 mbsf. The depth intervals where kaolinite is relatively low in abundance include the finest-grained intervals of the succession, suggesting a grain-size control on clay-mineral composition.

Spectrophotometry

Light reflectance was low throughout the sediment column recovered at Site 935. For all wavelength bands from 400 to 700 nm, reflectance values range between 10% and 25%. Changes in reflectance are dominated by high-frequency variability resulting from black color banding or mottling, gas partings, and silt/sand laminations. Significant correlations between light reflectance and lithologies can be made using the ratio of the red (650–700 nm) and blue (450–500 nm) spectrum reflectance (Fig. 5), which varies around a mean value of 1.15, determined by the dominant lithology of very dark gray silty clays. The occurrence of silt and sand laminations interbedded in the clay causes high-frequency variability (noise), which is most obvious in Unit II. Black mottling or color bands, for example in Subunits IIA, IID, and VIA, correspond to intervals displaying red/blue values slightly below 1.15. Positive deviations from the mean, indicating the occurrence of iron oxyhydroxides (increased red reflectance), correspond to the brownish calcareous clay in Unit I and to thicker (>10 cm) sand layers, which contain red-stained quartz grains. Also, the downcore increase in the numbers and thickness of silt and sand beds in Subunits IID and VIB is marked by an increase of the red spectrum reflectance relative to that of the blue spectrum.

Although carbonate contents are similar within the calcareous clays of Units I and V, their red/blue reflectance is distinctly different. Whereas red/blue ratios in Unit I are characterized by enhanced red reflectance due to high iron oxyhydroxide content, the occurrence of reduced iron phases causes enhancement of the blue spectrum in

Unit V, leading to the largest negative red/blue deviation from the mean. Similar low red/blue reflectance ratios correspond to the calcareous clay clasts found in Unit IV (Core 935A-25X).

Discussion

Units II and VI have similar lithologies in that their upper subunits lack coarse-grained beds, but their lower subunits are characterized by common silt laminae, silt beds, and laminae and beds of very fine to fine sand. These fining-upward turbidite sequences have been observed most at other sites during Leg 155. Both Unit II (Subunit IIC) and Unit VI (Subunit VIB) show a higher frequency of silt and sand beds toward their bases. The frequency of these turbidites probably indicates periods of enhanced sediment supply to this area of the fan and/or a stage in the evolution of each channel-levee complex. A summary of turbidite sequences recovered within levee sequences during this leg is presented in a foldout in the back pocket of this volume.

Units III and IV contain lithologies indicative of mass-transport deposits. Unit III consists of massive fine- through coarse-grained sand beds, some of which contain mud clasts and organic detritus. Beds with abundant mud clasts are interpreted as debris-flow deposits, whereas the massive sand beds are thought to represent channel and/or sheet-flow deposits. Blocks of silty clay up to 20 m thick, some of which contain contorted fabric, are intercalated within the debris-flow and channel/sheet-flow deposits. The nature and scale of the contorted sediment within some of the blocks, together with a microfossil assemblage indicative of a slope environment, indicate that some of these blocks may have been subjected to soft-sediment deformation as a result of slump or slide processes on the continental slope. These blocks are now components of one or more debris-flow deposits situated more than 250 km from the present-day slope. Unit IV also contains an assemblage of contorted sediment, isolated clasts, and organic detritus that is interpreted as a mass-transport deposit. The massive structureless silty clay in Unit IV has been tentatively interpreted as a block lying within a debris-flow deposit. This block also contains a reworked microfossil assemblage indicative of a slope environment.

Because there is no evidence of shear along block contacts in either unit, and because Site 935 is approximately 250 km from the continental slope, it seems probable that these blocks were transported to this site as components of debris flows. Internal contortion within these blocks could be the result of transport within the debris flow. Blocks of this size (and much larger) are found within debris-flow deposits at abyssal depths. For example, Masson et al. (1993) reported large (>100 m) rafted blocks originating from the African continental rise, lying on top of, and within, the Saharan Debris Flow Deposit, more than 1,000 km from the source.

BIOSTRATIGRAPHY

Calcareous Nannofossils

Calcareous nannofossils recovered are from the Holocene nannofossil Zone CN15b through the Pleistocene nannofossil Zone CN14b (Table 3). Nannofossils are abundant and well preserved in the hemipelagic mud of Holocene age. Diverse and well-preserved *Emiliania huxleyi* acme assemblages (Zone CN15b) occur in the mud-line sample. At a depth of 0.5 mbsf (Sample 935A-1H-1, 50–52 cm), only traces of poorly preserved nannofossils are found. The abundance and preservation increases from 0.5 mbsf to a depth of 1 mbsf (Sample 935A-1H-1, 101–103 cm), similar to the abundance pattern observed around the “iron-rich crust” in previous sites. Below 3.5 mbsf (Sample 935A-1H-CC, 24–25 cm) nannofossils become rare and poorly preserved, which is characteristic of the glacial-age sediment recovered during Leg 155. Calcareous nannofossils are absent from

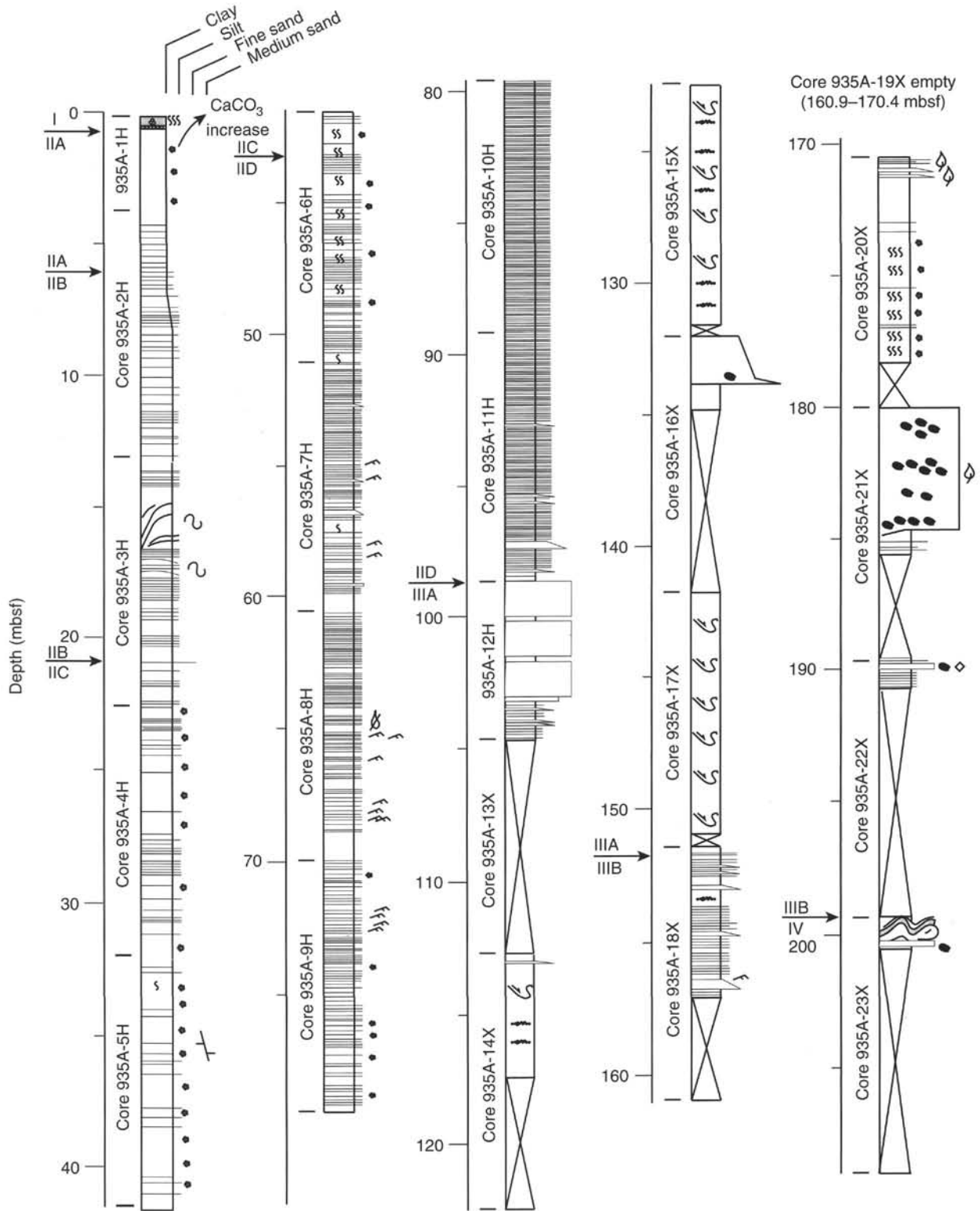


Figure 9. Graphic sedimentological columns for Site 935 showing grain-size variation (width of columns), bed thickness, and sedimentary structures; symbols and preparation of these columns are explained in the "Lithostratigraphy" section of the "Explanatory Notes" chapter, this volume. Arrows indicate the positions of unit and subunit boundaries. The upper part of the column is shown in the strike section of the foldout (back pocket, this volume) for comparison of levee sequences on the middle and upper fan.

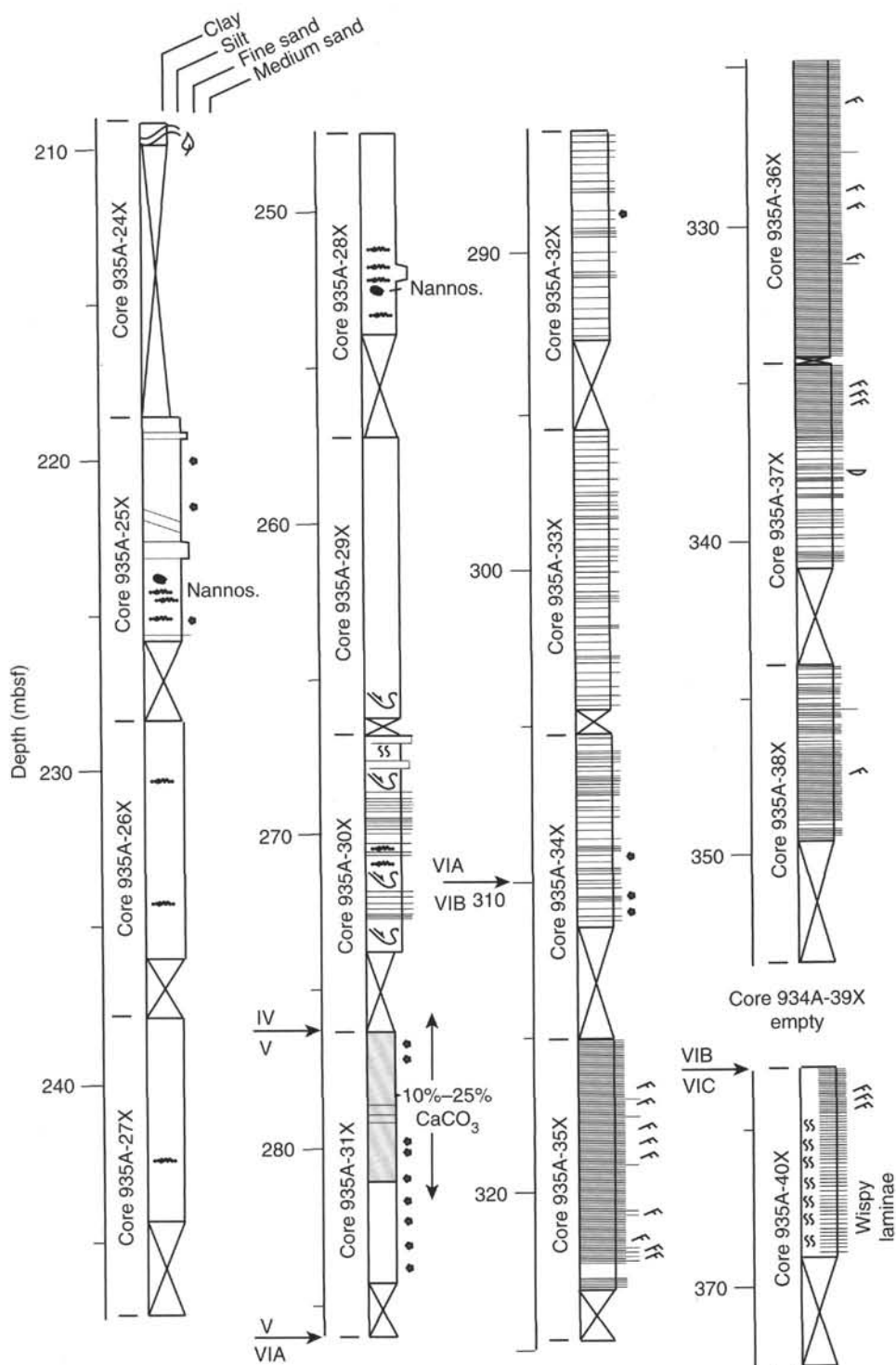


Figure 9 (continued).

the pre-Holocene levee sequence of clay with beds of silt and silty sand from 3.51 mbsf to 99.2 mbsf in Unit II (Samples 935A-1H-CC, 24–25 cm, through -11H-CC, 38–39 cm) and occur sporadically in the upper part of the underlying Unit III from 104.6 to 131.4 mbsf (Samples 935A-12H-CC, 11–12 cm, through -15X-CC, 38–39 cm). Well-preserved nannofossils reappear in high abundance in a calcareous clast within the brown silty clay of Subunit IIIA at 133.7 mbsf

(Sample 935A-16X-2, 23 cm). In the underlying Subunit IIIB, at 172 mbsf, composed of clays, light-colored carbonate bands contain rare and poorly preserved nannofossils from Zone CN15 along with the cold-water species *Coccolithus pelagicus* (Samples 935A-20X-2, 24–26 cm; -2, 35–37 cm; -2, 60–62 cm; -2, 65–69 cm). The coarse sand units at 182 mbsf in Subunit IIIB contain clasts of pelagic clay that have rich assemblages representing Zone CN15b (Samples

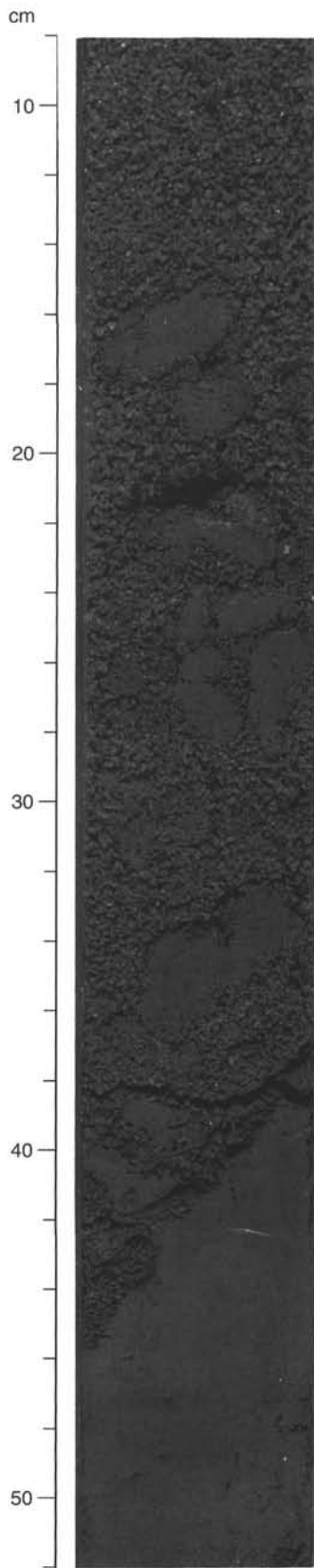


Figure 10. Mud clasts within a coarse- to medium-sand matrix at the base of Subunit IIIB (interval 155-935A-21X-4, 8–52 cm).

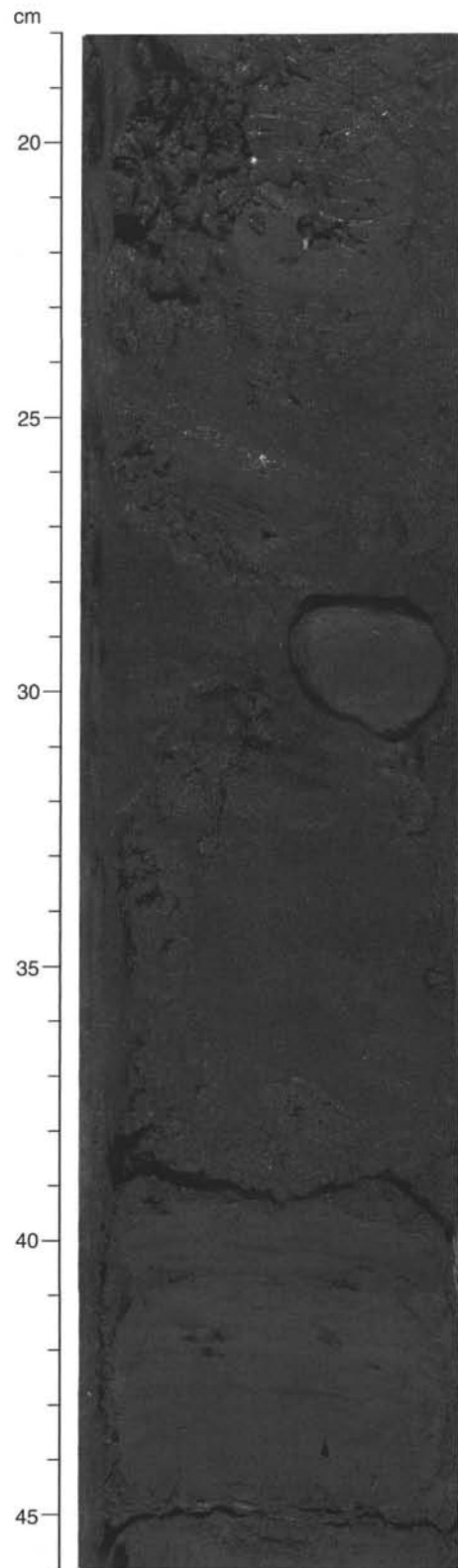


Figure 11. Well-rounded, 3-cm-diameter, fine sandstone clast within silty clay matrix (28.5–31 cm). Angular mud clasts occur within a medium-sand matrix (18–27.5 cm). At 39 cm is the sharp basal contact of the sand with silty clay containing silt laminae at 39 cm (interval 155-935A-22X-1, 18–46 cm).

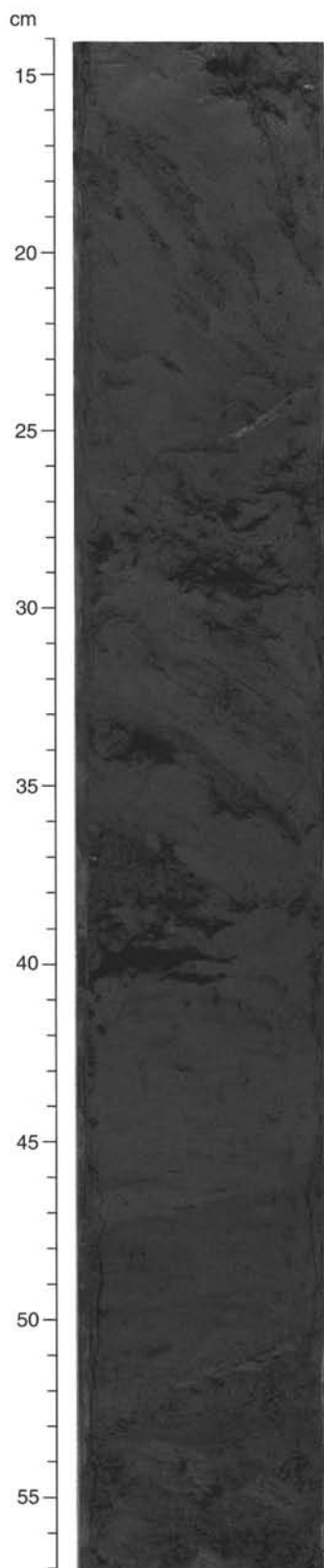


Figure 12. Dipping, deformed beds and laminae at the top of Unit IV (interval 155-935A-23X-1, 14–57 cm).

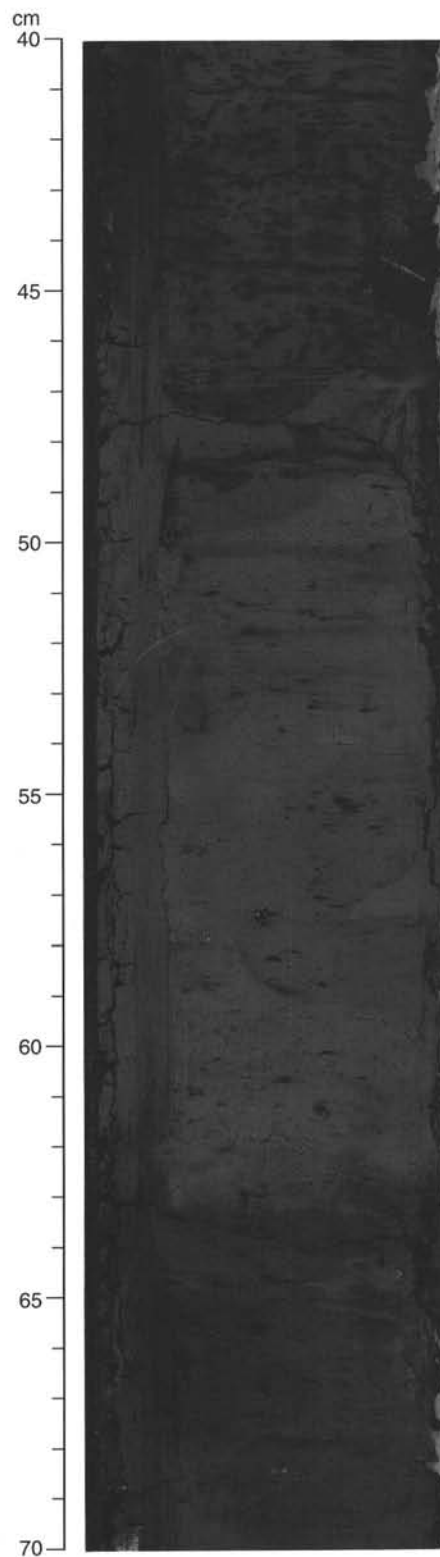


Figure 13. Carbonate-rich mud clast (47–63 cm) within mottled and moderately bioturbated silty clay (interval 155-935A-25X-4, 40–70 cm).

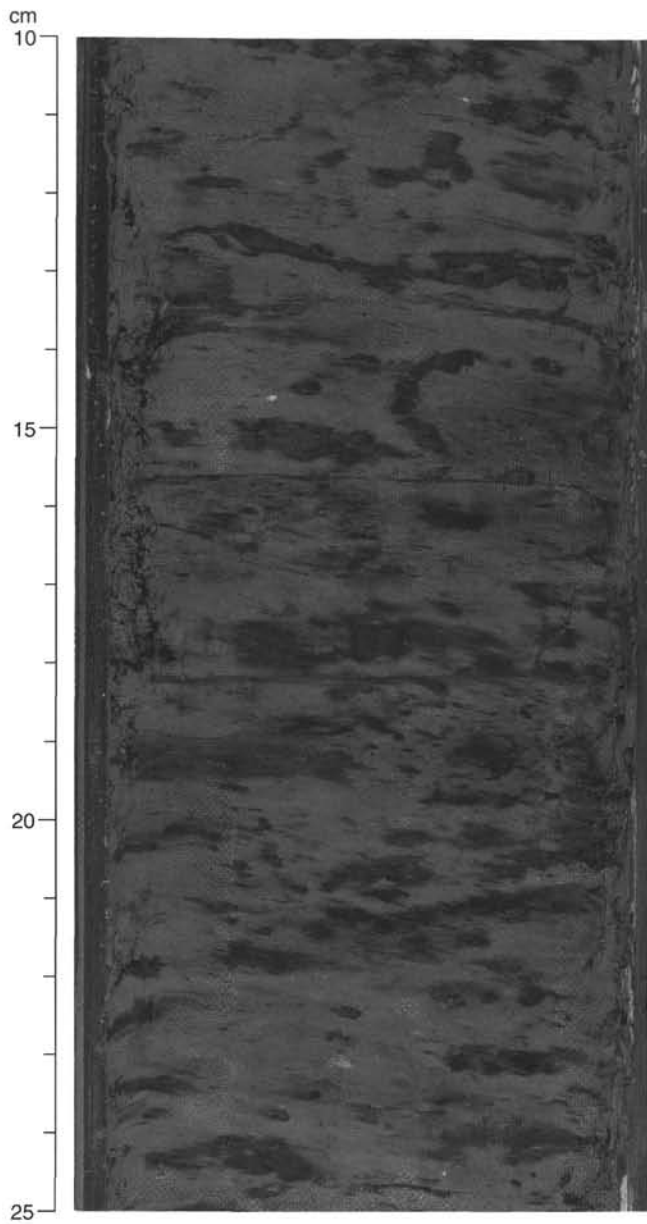


Figure 14. Ephemeral black (N₂) color mottling in Unit V (interval 155-935A-31X-4, 10–25 cm).

935A-21X-1, 79 cm, and -1, 61 cm). One clast within the same coarse sand unit contains rare nanofossils (Sample 935A-21X-2, 91 cm).

A major change in assemblage composition takes place within the rare nanofossil-bearing intervals of the Unit IV mass-transport deposit from 200 mbsf to 273 mbsf (Samples 935A-23X-CC, 13–14 cm, through 935A-30X-CC, 37–38 cm). In a light-colored band of hemipelagic mud at 225.14 mbsf (Sample 935A-25X-5, 54–59 cm), interpreted as a clast, a well-preserved assemblage dominated by species of *Gephyrocapsa* appears. This assemblage includes common *Helicosphaera inversa*. As *P. lacunosa* and *E. huxleyi* are absent, an age of 0.26–0.46 Ma is assigned to this assemblage (Zone CN14b). The lower part of Unit IV is barren of calcareous nanofossils from 225.7 to 273.6 mbsf (Samples 935A-26X-CC, 53–54 cm, through -30X-CC, 37–38 cm).

Well-preserved nanofossils, dominated by species of the genus *Gephyrocapsa* (average size of 4 to 5.5 μm), reappear in the foramin-

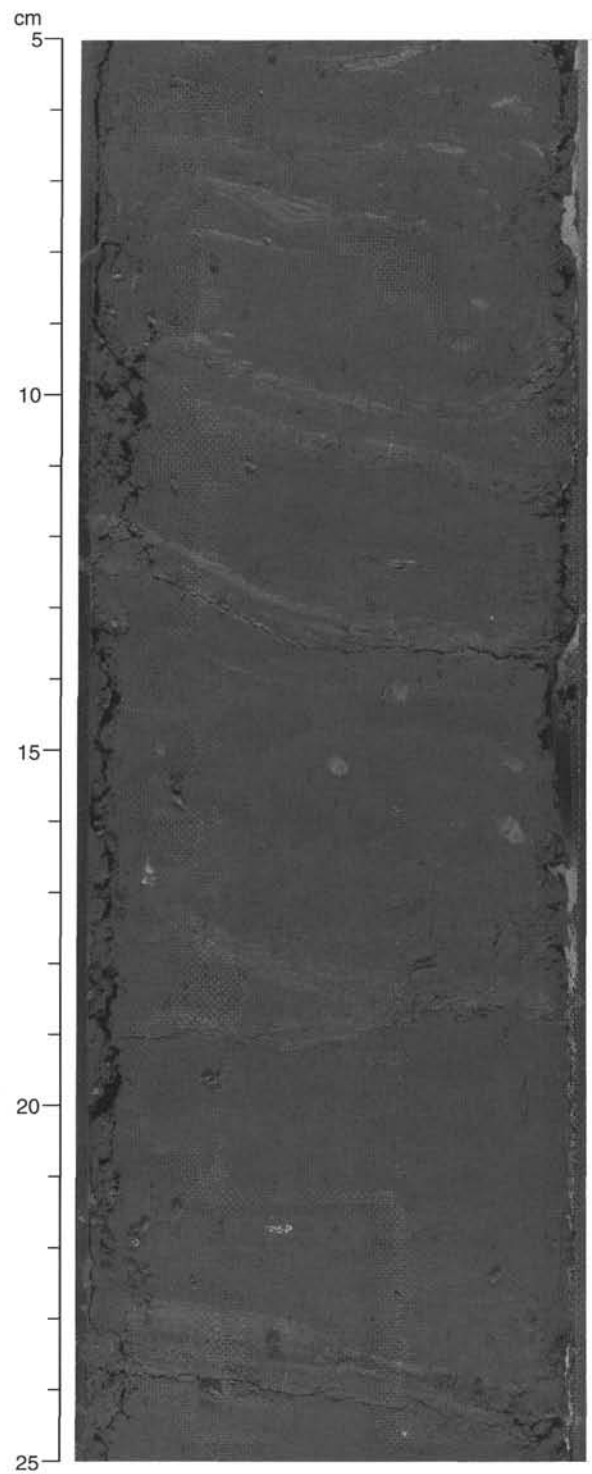


Figure 15. “Wispy” and discontinuous silt and fine sand laminae, thin beds and blebs in Subunit VI (interval 155-935A-40X-2, 5–25 cm).

ifer-nanofossil-bearing clay of Unit V at 276.6 mbsf (Sample 935A-31X-1, 30–32 cm). The entire Core 935A-31X, 276 to 284 mbsf, is characterized by this assemblage. The absence of *P. lacunosa* and *E. huxleyi*, and the presence of *Helicosphaera inversa*, place Core 935A-31X in Zone CN14b. A substantial reworking into the mass-transported deposit of Unit IV is indicated, because the assemblages

Table 2. Relative peak intensities of the main minerals (<2 μm fraction) within representative lithologies at Site 935.

Core, section, interval (cm)	Depth (mbsf)	Relative intensities of primary peaks (<2 μm fraction)					
		Smectite	Mica + Illite	Kaolinite	Quartz	Feldspars	Total clay minerals
155-935A-							
1H-1, 14–16	0.14	165	130	150	100	43	445
2H-2, 40–41	5.40	187	187	214	100	63	588
3H-7, 110–111	15.60	172	153	212	100	69	537
3H-7, 8–9	22.08	223	171	228	100	64	623
5H-4, 80–81	37.30	255	216	270	100	*	741
7H-5, 130–131	57.88	226	207	233	100	*	667
9H-2, 53–55	72.03	170	161	191	100	*	522
11H-5, 75–76	95.75	225	164	169	100	70	558
14X-3, 42–43	116.12	220	187	184	100	59	592
15X-3, 50–51	125.80	352	227	188	100	66	767
19X-1, 50–51	157.63	250	212	214	100	71	676
23X-1, 39–40	199.69	270	160	215	100	60	645
25X-3, 63–64	222.23	214	175	208	100	65	598
27X-3, 25–26	241.05	146	125	217	100	*	488
28X-2, 100–101	249.90	180	161	230	100	*	571
29X-4, 130–131	262.90	403	244	264	100	*	911
33X-4, 58–59	300.78	412	244	253	100	*	908
35H-3, 95–06	318.95	196	172	243	100	*	611
37X-2, 104–105	336.84	477	268	265	100	*	1010
40X-2, 32–33	364.82	138	213	261	100	*	612

Notes: See "Lithostratigraphy" section in the "Explanatory Notes" chapter, this volume, for XRD methods. * denotes non-detection.

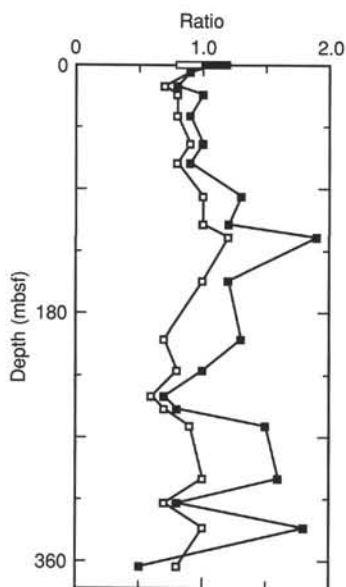


Figure 16. Peak intensities in XRD analyses of clay minerals from Hole 935A relative to kaolinite, from Table 2. Solid squares = smectite/kaolinite; open squares = illite (+ mica)/kaolinite.

in the lower 50 m of the mass-transported Unit IV are identical to the hemipelagic section of the underlying Unit V at 223.3 and 276.6 mbsf (Samples 935A-25X-4, 21 cm, and -31X-1, 11–13 cm, respectively).

During Leg 154, a continuous Pliocene–Pleistocene stratigraphic section was recovered at Site 925 where numerous large specimens (>5 μm) of *Gephyrocapsa* occurred just above the extinction of *P. lacunosa* (at 0.46 Ma) (Curry, Shackleton, Richter, et al., in press). It is thus possible that the *Gephyrocapsa* event observed in the sites of Leg 155 is only slightly younger than 0.46 Ma. A few atypical specimens of *P. lacunosa* were observed at 276.6 and 284.3 mbsf in Samples 935A-31X-1, 30–31 cm, and -31X-CC, 50–51 cm, but were regarded as reworked. No nannofossils are present in the lowermost part of Hole 935A, 292.6 to 369 mbsf (Samples 935A-32X-CC, 44–45 cm, through -40X-CC, 76–77 cm).

Planktonic Foraminifers

The boundary between Ericson Zones Z and Y (downhole disappearance of *G. menardii* and *G. tumida*) is between 0.81 and 3.51 mbsf (Samples 935A-1H-1, 80–82 cm, and -1H-CC, 14–24 cm; Fig. 17; Table 4), taking into account possible downhole contamination of core-catcher samples.

Foraminifers are found in low abundances from 13 to 178 mbsf (Samples 935A-2H-CC, 22 cm, through -20X-CC, 29–38 cm). This interval has been defined as the Y Zone on the basis of the absence of *G. menardii* and *G. tumida*. Within this zone, samples in sand layers contain only *G. menardii* and *G. tumida* in the size range of 350 and 500 μm from 133 to 134 mbsf (Samples 935A-16X-1, 110–112 cm, and -16X-CC, 19–28 cm). No other sizes or species were found in this interval. This suggests the assemblage is reworked. *P. obliquiloculata* is found at 178 mbsf, near the base of lithologic Subunit IIIB (Sample 935A-20X-CC, 29–38 cm). The lack of reworking suggests that the *Yp. obliq.* datum near the base of Subunit IIIB is in place. Clasts found within Subunit IIIB at 182.3 mbsf contain *G. tumida flexuosa* (Sample 935A-21X-2, 77–80 cm), suggesting that interglacial, possibly X Zone, material was reworked into this unit.

Overall abundances of planktonic foraminifers in Unit IV from 200 to 284 mbsf vary from abundant to barren. Unit IV has abundant *G. tumida* and *P. obliquiloculata*, and sporadic occurrences and low abundances of *G. menardii* and *G. tumida flexuosa*. The sediment is preliminarily assigned to the X Zone (older than 85 ka), but is considered reworked because of the following:

1. The discontinuous occurrence of "full interglacial" material, as indicated by the presence of *G. menardii* and *G. tumida flexuosa*,
2. The occurrence of high abundances of shell- and wood fragments,
3. The occurrence of heavily calcified and iron-stained planktonic and benthic foraminifers,
4. The rare occurrence of bathyal benthic foraminifers found usually above a water depth of 2000 m.

Unit V from 276 to 286 mbsf contains a well-preserved foraminifer assemblage. The presence of *G. tumida flexuosa* and *G. calida calida* indicates that this section is of middle to late Pleistocene age. The occurrences of *G. tumida*, *P. obliquiloculata*, *G. hexagonus*, *G.*

Table 3. Calcareous nannofossil and siliceous microfossil abundance data for Hole 935A.

Core, section, interval (cm)	Top interval (mbsf)	Bottom interval (mbsf)	Abundance	Preservation	Zone	Marine	Fresh water	Sponge spicules	Radiolarians	Ericson Zone (inferred from foraminifers)	Age (inferred from foraminifers)
155-935A-											
1H-1, M1	0.00		a	g	CN15b	f	r	f	r	Z	Holocene
1H-1, 35-37	0.35	0.37	a	g		b	b	r	b	Z	Holocene
1H-1, 50-52	0.50	0.52	vr	p		b	b	r	b	Z	Holocene
1H-1, 101-103	1.01	1.03	f	m		b	b	b	b	Z	Holocene
1H-CC, 24-25	3.51	3.52	r	p		b	b	f	b	Z	Holocene?
2H-6, 10.2	11.10		vr	p		b	vr	r	b		
2H-6, 10.7	11.11		vr	p		b	b	b	b		
2H-6, 14	11.14		tr	—		b	b	b	b		
2H-6, 17.4	11.17		tr	—		b	b	b	b		
2H-6, 18.2	11.18		b	—		b	b	b	b		
2H-6, 19.7	11.20		b	—		b	b	b	b		
2H-CC, 32-33	13.16	13.17	b	—		b	b	b	b	Y	late Pleist.
3H-CC, 36-37	23.12	23.13	b	—		b	b	b	b	Y	late Pleist.
4H-4, 72	27.72		tr	—		b	b	b	b		
4H-4, 73	27.73		tr	—		b	b	b	b		
4H-4, 74	27.74		vr	—		b	b	b	b		
4H-4, 77.6	27.78		b	—		b	b	b	b		
4H-4, 79	27.79		tr	—		b	b	b	b		
4H-4, 80	27.80		b	—		b	b	b	b		
4H-4, 83	27.83		b	—		b	b	b	b		
4H-4, 88	27.88		r	p		b	b	b	b		
4H-4, 90.5	27.91		b	—		b	b	b	b		
4H-4, 91.5	27.92		tr	—		b	b	b	b		
4H-CC, 60-61	32.91	32.92	b	—		b	b	b	b	Y	late Pleist.
5H-CC, 40-41	42.28	42.29	b	—		b	b	r	b	Y	late Pleist.
6H-CC, 57-58	51.95	51.96	b	—		b	b	b	b	Y	late Pleist.
7H-CC, 79-80	60.99	61.00	b	—		b	b	f	b	?	?
8H-CC, 52-53	69.82	69.83	b	—		b	b	r	b	Y	late Pleist.
9H-CC, 47-48	80.33	80.34	b	—		b	b	r	b	Y	late Pleist.
10H-CC, 43-44	90.29	90.30	b	—		b	b	b	b	Y	late Pleist.
11H-CC, 38-39	99.27	99.28	b	—		b	b	b	b	Y	late Pleist.
12H-CC, 11-12	104.61	104.62	b	—		b	b	b	b	Y	late Pleist.
14X-CC, 23-24	117.37	117.38	tr	—		b	b	b	b	Y	late Pleist.
15X-CC, 38-39	131.44	131.45	b	—		b	b	b	b	Y	late Pleist.
16X-2, 23	133.73		a	g		b	b	b	b	Y	late Pleist.
16X-CC, 28-29	134.65	134.66	vr	—		b	b	f	b	?	Pleist.
17X-CC, 30-31	150.74	150.75	b	—		b	b	b	b	?	late Pleist.
18X-CC, 23-24	157.12	157.13	b	—		b	b	b	b	?	late Pleist.
20X-2, 24-26	172.14	172.16	b	—		b	b	b	b	?	late Pleist.
20X-2, 35-37	172.25	172.27	r	m		b	b	b	b	—	late Pleist.
20X-2, 60-62	172.50	172.52	f	p		b	b	b	b	—	late Pleist.
20X-2, 65-69	172.55	172.59	vr	p		b	b	b	b	—	late Pleist.
20X-CC, 38-39	178.86	178.87	vr	—		b	b	r	b	Y	late Pleist.
21X-1, 61	182.11		c	g		b	b	b	b	—	late Pleist.
21X-1, 79	182.29		a	g	CN15b?	b	b	b	b	—	late Pleist.
21X-1, 91	182.41		vr	—		b	b	b	b	—	late Pleist.
21X-CC, 57-58	185.67	185.68	vr	—		b	b	f	b	—	Pleist.
22X-CC, 38-39	190.73	190.74	vr	—	CN15a/b	b	b	b	b	X	late Pleist.
23X-CC, 13-14	200.40	200.41	vr	p	CN15a	b	b	vr	b	—	Pleist.
24X-CC, 24-25	209.69	209.70	a	g		b	b	b	b	—	Pleist.
25X-4, 21	223.31		a	g		b	b	b	b	—	late Pleist.
25X-4, 60	223.70		a	g		b	b	b	b	—	late Pleist.
25X-5, 27	224.87		r	g		b	b	b	b	—	late Pleist.
25X-5, 54	225.14		r	p	CN14b	b	b	b	b	—	late Pleist.
25X-5, 54-59	225.14	225.19	a	g		b	b	b	b	—	late Pleist.
25X-CC, 25	225.71		vr	—		b	b	b	b	X	late Pleist.
26X-CC, 53-54	235.79	235.80	b	—		b	b	b	b	—	Pleist.
27X-CC, 32-33	244.39	244.40	b	—		b	b	b	b	—	Pleist.
28X-CC, 34-35	253.74	253.75	b	—		b	b	b	b	—	Pleist.
29X-CC, 22-23	265.94	265.95	b	—		b	b	b	b	—	Pleist.
30X-CC, 37-38	273.61	273.62	b	—		b	b	b	b	—	Pleist.
31X-1, 11-13	276.41	276.43	r	p		b	b	b	b	—	Pleist.
31X-1, 30-32	276.60	276.62	a	g	CN14b	b	b	b	b	?	m.-l. Pleist.
31X-2, 40-42	278.20	278.22	c	g		b	b	b	b	—	m.-l. Pleist.
31X-3, 110-112	280.40	280.42	a	g		b	b	b	b	—	m.-l. Pleist.
31X-5, 10-12	281.77	281.79	a	g		b	b	b	b	—	m.-l. Pleist.
31X-6, 50-52	284.32	284.34	r	p		b	b	b	b	—	m.-l. Pleist.
31X-CC, 50-51	284.32	284.33	f	g		b	b	b	b	?	m.-l. Pleist.
32X-CC, 44-45	292.67	292.68	b	—		b	b	b	b	—	m.-l. Pleist.
33X-CC, 20-21	304.59	304.60	b	—		b	b	b	b	—	m.-l. Pleist.
34X-CC, 22-23	311.42	311.43	b	—		b	b	b	b	?	m.-l. Pleist.
35X-CC, 80-81	322.98	322.99	b	—		b	b	b	b	—	m.-l. Pleist.
36X-CC, 34-35	334.13	334.14	b	—		b	b	b	b	?	m.-l. Pleist.
37X-CC, 20-21	340.90	340.91	b	—		b	b	b	b	—	m.-l. Pleist.
38X-CC, 26-27	349.48	349.49	b	—		b	b	b	b	?	m.-l. Pleist.
39X-CC, 1	362.99		b	—		b	b	b	b	—	m.-l. Pleist.
40X-CC, 76-77	369.02	369.03	b	—		b	b	b	b	—	m.-l. Pleist.

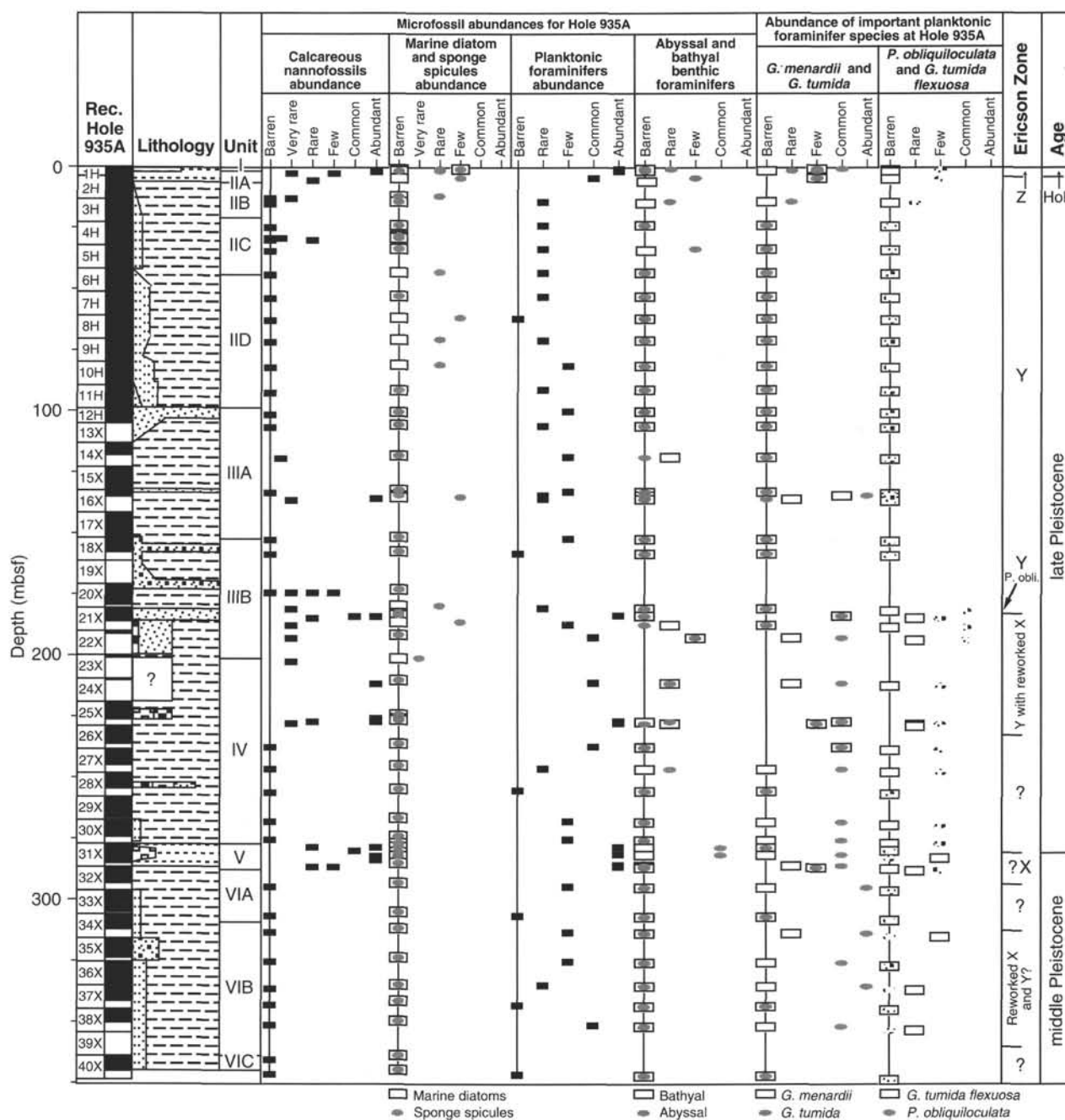


Figure 17. Biostratigraphic summary for Site 935.

menardii, and *G. tumida flexuosa* from 276.6 to 284.3 mbsf indicate that the sediment is from an interglacial, possibly the X Zone (Samples 935A-31X-3, 30–32 cm, and -31X-CC, 41–50 cm). The relatively high abundances of *G. tumida flexuosa* and *G. hexagonus* suggest the age of Unit V might be 120–130 ka (isotopic Stage 5e) by comparison with the work of Pflaumann (1986), who showed that *G. tumida flexuosa* occurs in high abundances in isotopic Stage 5e sediment in the eastern Atlantic, but is rare in earlier interglacials. It is not documented if this is true in the western Atlantic over the Amazon Fan.

Unit VI from 286 to 372 mbsf has low overall foraminifer abundances, with high abundance of *G. tumida* and sporadic occurrence of *G. tumida flexuosa*. The high abundance of iron-stained foraminifer

tests, especially those of *G. tumida flexuosa*, suggests that this sediment may also have been reworked.

Benthic Foraminifers

Two types of benthic foraminifer assemblages are found at Site 935 (Table 4). The upper- to mid-bathyal group is composed of *Bulimina marginata*, *Bolivina striatula*, and *Quinqueloculina* sp. The second group is a deep-water, low-oxygen abyssal group comprising *Uvigerina* spp. and *Pyrgo* spp. In the Holocene sediment, down to 3.51 mbsf (Sample 935A-1H-CC, 24 cm), abyssal species are found. Benthic foraminifers are absent below the Holocene/late Pleistocene boundary to 185.67 mbsf (Sample 935A-21X-CC, 57 cm). Both

Table 4. Foraminifer abundance data for Hole 935A.

Core, section, interval (cm)	Top interval (mbsf)	Bottom interval (mbsf)	<i>Globorotalia menardii</i>	<i>Globorotalia tumida</i>	<i>Globorotalia tumida flexuosa</i>	<i>Pulleniatina obliquiloculata</i>	<i>Globigerinoides ruber</i> (white)	<i>Globigerinoides ruber</i> (pink)	<i>Globorotalia hexagonus</i>	<i>Neogloboquadrina duertrei</i>	<i>Globorotalia trilobus trilobus</i>	<i>Globorotalia inflata</i>	<i>Globorotalia truncatulinoides</i>	<i>Globigerina bulboides</i>	<i>Globigerinoides trilobus sacculifer</i>	<i>Globorotalia fimbriata</i>	<i>Orbulina universa</i>	<i>Globigerinita glutinata</i>	<i>Globigerinoides conglobatus</i>	<i>Globoquadrina conglomerata</i>	<i>Globorotalia crassaformis</i>	<i>Neogloboquadrina pachyderma</i> (right)	<i>Globigerina rubescens</i>	<i>Globorotalia scitula</i>	<i>Globigerina calida calida</i>	<i>Globorotalia tosaensis</i>	Other planktonic foraminifers	Vivianite nodules	Overall foraminifer abundance	Preservation	Abundance of bathyal benthic foraminifers	Abundance of abyssal benthic foraminifers	Ericson Zone	Age			
155-935A-																																					
1H-MI, 0-0	0.00	0.01	F	C	B	F	C	F	B	F	F	B	R	B	F	B	R	B	B	B	B	B	B	B	B	B	B	B	A	G	B	B	B	Z	Holocene		
1H-1, 37-39	0.37	0.39	F	F	B	F	C	F	F	F	F	B	F	B	F	F	R	B	B	B	B	B	B	B	B	B	B	B	A	G	B	B	R	Z	Holocene		
1H-1, 60-61	0.60	0.61	B	F	B	F	C	F	F	F	C	B	F	B	F	R	B	B	B	B	B	B	B	B	B	B	B	B	A	G	B	B	B	Z	Holocene		
1H-1, 80-82	0.80	0.82	B	R	B	F	C	F	F	F	C	B	F	B	F	B	R	B	B	B	B	B	B	B	B	B	B	B	A	G	B	B	B	Z	Holocene		
1H-CC, 14-24	3.42	3.51	F	F	B	F	C	F	R	B	F	F	F	B	F	F	B	B	B	B	B	B	B	B	B	B	B	B	C	G	B	F	Z	Holocene?			
2H-CC, 22-32	13.07	13.16	B	R	B	R	F	R	B	F	F	B	F	B	R	B	B	B	B	B	B	B	B	B	B	B	B	B	R	G	B	R	Y	late Pleist.?			
3H-CC, 27-36	23.03	23.12	B	B	B	B	C	B	C	A	R	B	B	C	B	B	B	B	B	B	B	B	B	B	B	B	B	B	R	M	B	B	Y	late Pleist.			
4H-CC, 51-60	32.82	32.91	B	B	B	B	B	B	B	C	A	B	B	F	C	B	B	B	B	B	B	B	B	B	B	B	B	B	R	M	B	F	Y	late Pleist.			
5H-CC, 31-40	42.19	42.28	B	B	B	B	F	B	B	C	A	B	B	B	F	B	B	B	B	B	B	B	B	B	B	B	B	A	R	G	B	B	Y	late Pleist.			
6H-CC, 48-57	51.86	51.95	B	B	B	B	F	R	B	A	C	B	R	B	F	B	B	B	R	B	B	B	B	B	B	B	B	A	R	G	B	B	Y	late Pleist.			
7H-CC, 70-79	60.90	60.99	B	B	B	B	B	B	B	B	B	B	B	B	B	B	B	B	B	B	B	B	B	B	B	B	B	A	B	G	B	B	?	?			
8H-CC, 43-52	69.73	69.82	B	B	B	B	R	B	B	F	C	B	R	B	A	B	B	B	B	B	B	B	B	B	B	B	B	C	R	G	B	B	Y	late Pleist.			
9H-CC, 38-47	80.24	80.33	B	B	B	B	F	R	B	C	C	B	F	B	A	B	R	B	B	B	B	B	B	B	B	B	B	C	F	M	B	B	Y	late Pleist.			
10H-CC, 34-43	90.20	90.29	B	B	B	B	F	R	B	F	F	B	R	B	F	B	B	B	B	B	B	B	B	B	B	B	B	R	R	G	B	B	Y	late Pleist.			
11X-CC, 29-38	99.18	99.27	B	B	B	B	F	B	B	R	F	B	F	B	F	B	B	B	B	B	B	B	B	B	B	B	B	B	F	M	B	B	Y	late Pleist.			
12X-CC, 2-11	104.52	104.51	B	B	B	B	B	B	B	R	R	B	B	B	R	B	B	B	B	B	B	B	B	B	B	B	B	B	R	G	B	B	Y	late Pleist.			
14X-CC, 14-23	117.28	117.37	B	B	B	B	R	B	B	F	F	B	F	B	F	B	B	B	B	B	B	B	B	B	B	B	B	B	F	F	G	R	B	Y	late Pleist.		
15X-CC, 29-38	131.35	131.44	B	B	B	B	F	B	B	F	C	B	F	B	F	B	B	B	B	B	B	B	B	B	B	B	B	F	F	M	B	B	Y	late Pleist.			
16X-1, 110-112	133.10	133.12	C	A	B	B	B	B	B	B	B	B	B	B	B	B	B	B	B	B	B	B	B	B	B	B	B	B	R	G	B	B	RW	?			
16X-CC, 19-28	134.56	134.65	R	B	B	B	F	R	B	B	B	B	R	B	B	B	B	B	B	B	B	B	B	B	B	B	B	B	?	G	B	B	RW	Pleist.			
17X-CC, 21-30	150.65	150.74	B	B	B	B	F	B	B	C	B	B	C	B	A	B	R	B	B	B	R	B	B	B	B	B	B	A	F	G	B	B	?	Pleist.			
18X-CC, 14-23	157.03	157.12	B	B	B	B	B	B	B	B	B	B	B	B	B	B	B	B	B	B	B	B	B	B	B	B	B	B	B	—	B	B	?	?			
20X-3, 60-62	174.00	174.02	B	B	B	B	C	R	B	C	C	B	C	B	C	B	B	B	B	B	B	B	B	B	B	B	B	C	C	G	B	F	Y	late Pleist.			
20X-5, 24-26	176.64	176.66	B	B	B	B	C	F	B	B	C	C	B	C	B	C	B	B	B	B	B	B	B	B	B	B	B	B	C	M	B	B	Y	late Pleist.			
20X-CC, 29-38	178.77	178.86	B	B	B	C	F	B	B	C	C	B	F	B	C	B	B	B	B	B	B	B	B	B	B	B	B	R	R	G	B	B	Y	late Pleist.			
21X-2, 77-80	182.27	182.30	C	C	R	F	F	F	R	C	C	B	R	B	R	B	B	B	B	B	B	B	B	B	B	B	B	B	A	G	B	B	X	late Pleist.			
21X-CC, 48-57	185.58	185.67	B	B	B	C	B	B	B	A	B	B	C	B	R	B	B	B	B	B	B	B	B	B	B	B	B	B	F	M	R	B	RW	late Pleist.			
22X-CC, 29-38	190.64	190.73	R	C	R	C	C	B	B	C	B	B	F	B	F	B	B	B	B	B	B	B	B	B	B	B	B	B	C	G	F	F	X	late Pleist.			
23X-CC, 4-13	200.31	200.40	R	F	R	C	F	B	B	C	F	B	F	B	F	B	B	B	B	B	B	B	B	B	B	B	B	F	C	G	R	R	X	late Pleist.			
24X-CC, 15-24	209.60	209.69	R	C	B	F	C	R	B	F	C	B	F	B	F	B	F	B	B	B	B	B	B	B	B	B	B	B	C	M	R	R	RW	late Pleist.			
25X-5, 59-64	225.19	225.24	C	C	R	F	F	F	B	F	B	B	F	B	F	B	B	B	B	B	B	B	B	B	B	B	B	B	A	G	B	R	X	late Pleist.			
25X-CC, 19-28	225.65	225.74	F	F	R	F	C	F	B	C	B	B	F	B	F	B	B	B	B	B	B	B	B	B	B	B	B	B	A	M	R	B	X	late Pleist.			
26X-CC, 44-53	235.70	235.79	C	C	B	F	C	R	B	B	F	B	B	B	R	B	B	B	B	B	B	B	B	B	B	B	B	C	C	G	B	B	?	Pleist.			
27X-CC, 23-32	244.30	244.39	B	C	B	F	C	B	R	B	B	C	B	R	R	F	B	B	B	B	B	B	B	B	B	B	B	B	A	R	G	B	R	?	Pleist.		
28X-CC, 25-34	253.65	253.74	B	B	B	B	B	B	B	B	B	B	B	B	B	B	B	B	B	B	B	B	B	B	B	B	B	C	B	—	B	B	?	?			
29X-CC, 13-22	265.85	265.94	B	C	B	F	C	B	B	C	B	B	B	B	C	B	B	B	B	B	B	B	B	B	B	B	B	F	F	G	B	B	?	Pleist.			
30X-CC, 28-37	273.52	273.61	B	C	B	F	C	B	B	C	F	B	F	B	F	B	B	B	B	B	B	B	B	B	B	B	B	C	F	G	B	B	?	Pleist.			
31X-1, 11-13	276.41	276.43	B	B	B	B	C	B	B	C	C	R	C	R	B	B	B	B	B	B	B	B	B	B	B	B	B	B	A	G	B	C	?	late Pleist.			
31X-3, 30-32	279.60	279.62	B	C	F	B	C	B	B	R	C	F	B	R	F	B	B	B	R	B	B	B	B	B	B	B	B	B	A	G	B	C	?	m.-1. Pleist.			
31X-6, 50-52	283.67	283.69	R	C	B	F	C	B	B	R	C	C	B	B	R	F	B	B	B	B	B	B	B	B	B	B	B	B	A	G	B	B	?	m.-1. Pleist.			
31X-CC, 41-50	284.23	284.32	F	F	R	F	C	B	R	F	F	B	R	B	F	B	B	B	B	B	B	B	B	B	B	B	B	B	A	G	B	B	?	(RW) m.-1. Pleist.			
32X-CC, 35-44	292.58	292.67	B	A	B	B	C	B	R	C	B	B	B	R	B	B	B	B	B	B	B	B	B	B	B	B	B	A	F	G	B	B	?	m.-1. Pleist.			
33X-CC, 11-20	304.50	304.59	B	B	B	B	B	B	B	B	B	B	B	B	B	B	B	B	B	B	B	B	B	B	B	B	B	A	B	—	B	B	?	?			
34X-CC, 13-22	311.33	311.42	R	A	F	B	C	B	B	B	C	F	B	R	B	F	B	B	B	B	B	B	B	B	B	B	B	A	F	M	B	B	?	(RW) m.-1. Pleist.			
35X-CC, 71-80	322.89	322.98	B	C	B	B	F	B	R	C	C	B	B	F	B	F	B	B	B	B	B	B	B	B	B	B	B	A	F	M	B	B	?	m.-1. Pleist.			
36X-CC, 25-34	333.04	333.13	B	A	R	B	F	B	B	C	C	B	B	B	B	B	B	B	B	B	B	B	B	B	B	B	B	C	R	M	B	B	?	m.-1. Pleist.			
37X-CC, 11-20	340.81	340.90	B	B	B	B	B	B	B	B	B	B	B	B	B	B	B	B	B	B	B	B	B	B	B	B	B	B	—	B	B	B	?	?			
38X-CC, 17-26	349.39	349.48	B	C	R	B	F	R	B	C	C	B	F	B	F	B	B	B	B	B	B	B	B	B	B	B	B	C	C	M	B	B	?	(RW) m.-1. Pleist.			
40X-CC, 67-76	368.93	369.02	B	B	B	B	B	B	B	B	B	B	B	B	B	B	B	B	B	B	B	B	B	B	B	B	B	B	—	B	B	B	?	?			

Table 5. Spores and pollen data for Hole 935A.

Core, section, interval (cm)	Top interval (mbsf)	Bottom interval (mbsf)	Pollen and spores			Dinocysts	Wood/ carbonized particles	Ericson Zone (inferred from forams.)	Age (inferred from forams.)
			Abundance	Preservation	Major types recorded				
155-935A-									
1H-1, 32-34	0.32	0.34	b			b	f	Z	Holocene
1H-2, 58-60	2.08	2.10	r	p	Monolete (psilate) spore	b	f	Z	Holocene
4H-CC, 60-61	32.91	32.92	r	m	<i>Alnus</i>	b	c	Y	late Pleist.
9H-6, 98-100	78.48	78.50	r	m	Monosulcus	b	f	Y	late Pleist.
14X-CC, 23-24	117.37	117.38	f	m	Cyatheaceae, monolete (psilate) spore	b	f	Y	late Pleist.
22X-CC, 38-39	190.73	190.74	b			b	f	X (RW)	late Pleist.
25X-5, 1-3	218.61	218.63	a	g	Gramineae, Compositae, Cyatheaceae, TCP, monolete (psilate) spore, <i>Alnus</i>	b	c	?	?
25X-5, 44-46									
25X-5, 67-69	219.04	219.06	f	m	Gramineae, Cyatheaceae, monolete (psilate) spore	b	c	X	late Pleist.
25X-CC, 28-29	219.27	219.29	r	m	Cyatheaceae	b	f	X	late Pleist.
27X-2, 76-78	225.74	225.75	b			b	r	X	late Pleist.
31X-3, 74-76	240.06	240.08	r	g	Cyatheaceae	b	f	?	Pleist.
31X-4, 38-40	280.04	280.06	b			b	f	?	m.-l. Pleist.
31X-5, 104-106	281.18	281.20	b			b	f	?	m.-l. Pleist.
33X-3, 80-85	282.71	282.73	f	m	SP, monolete (psilate) spore	b	c	?	m.-l. Pleist.
40X-3, 13-15	299.50	299.55	b			b	r	?	?
	366.13	366.15	b			b	f	?	?

Notes: TCP = tricolporate; SP = stephanoporate.

abyssal and bathyal benthics are found sporadically in lithologic Unit IV, suggesting that there was significant reworking into this unit. Unit V has high abundances of well-preserved abyssal benthic foraminifers similar to those in Unit I, indicating that this unit is in-place and not reworked. Benthic foraminifers are not found below 284 mbsf (Sample 935A-31X-CC, 41-50 cm; Fig. 17).

Siliceous Microfossils

Site 935 is barren of diatoms, except for the mud-line sample where a few solution-resistant species of marine pelagic diatoms are present. Neither marine nor freshwater diatoms were observed in the pre-Holocene section at Site 935. Siliceous sponge spicules are present in low abundances in the pre-Holocene sections (Table 3), and radiolarians are present only as fragments in the mud-line samples of Hole 935A.

Palynology

Sixteen samples were examined from Hole 935A (Table 5). In general, low abundance, moderate preservation, and low diversity are characteristic of most of these samples. The Holocene (Z Zone) pollen and spore assemblage has very low abundance and poor preservation, with only monolete spores present. The late Pleistocene (Y Zone) pollen and spore assemblage has low abundance with *Alnus*, monosulcus type (probably *Palmae*), Cyatheaceae, and monolete spores present. *Alnus* and *Palmae* tend to be representative of wetland environments and riverbank vegetation.

Three samples at 190.73 mbsf, 219.27 mbsf, and 225.74 mbsf (Samples 935A-22X-CC, 38-39 cm, -25X-5, 67-69 cm, -25X-CC, 28-29 cm) were examined from sediment assigned to Ericson Zone X (identified by planktonic foraminifers). In general, the pollen and spore assemblage has low abundance and diversity, which is similar to the Holocene assemblage. Two samples from the debris-flow deposit (lithologic Unit IV), at 218.61 and 219.84 mbsf (Samples 935A-25X-5, 1-3 cm, and -5, 44-46 cm), have high abundances and diversities of pollen and spores. The assemblage includes Gramineae, Compositae, *Alnus*, Cyatheaceae, and tricolporate (TCP) and monolete spores. This assemblage contains elements from both dryland and wetland vegetation communities and is similar to the late Pleistocene assemblages obtained at previous sites (e.g., Holes 932A and 931B). Wood particles have been observed in all sample slides in low abundance. Dinoflagellates are not present in the samples examined.

Stratigraphic Summary

There are high abundances of calcareous and siliceous microfossils (nannofossils, foraminifers, and diatoms) down to 0.65 mbsf in

the nannofossil- and foraminifer-bearing clay recovered at the top of Hole 935A. This section is defined as Z Zone or Holocene. Palynomorphs are present in low abundance in this zone. The disappearance of *G. menardii* and *G. tumida* in Hole 935A indicates the Ericson Z/Y boundary is between 0.8 and 3.5 mbsf. In the dark olive green to dark gray silty clay below the Holocene section, there are low abundances of siliceous and calcareous microfossils. Based on the planktonic foraminifer assemblage, this section is classified as Y Zone. Palynomorphs show variable abundance in this zone. The $Y_{P.obliq.}$ datum is located at 178.8 mbsf in lithologic Subunit IIIB, suggesting the sediment below this level is older than 40 ka. In these units, the abundances of nannofossils and planktonic foraminifers vary greatly. In Subunit IIIB and Unit IV the planktonic foraminifer assemblages contain sporadic occurrences of *G. tumida*, *P. obliquiloculata*, *G. menardii*, and *G. tumida flexuosa*; both abyssal and bathyal benthic foraminifers are found, suggesting that the sediment is of late Pleistocene age but is reworked to some degree.

Unit V has high abundances of planktonic and abyssal benthic foraminifers and nannofossils. The nannofossil assemblage is of Zone CN14b, suggesting an age between 0.26 and 0.46 Ma. Unit V contains *G. tumida flexuosa* and *G. calida calida*, which constrains the age from middle to late Pleistocene. The relatively high abundance of *G. tumida flexuosa* and the occurrence of *G. hexagonus* suggests that Unit V is from a full interglacial period, but an assignment of oxygen isotopic Stage 5e (120-130 ka), based on the work of Pflaumann (1986), is not consistent with the nannofossil stratigraphy. Shore-based oxygen isotope analyses of the abundant abyssal benthic foraminifers may help to constrain the age of Unit V. Palynomorphs in Unit V have a low abundance, similar to the assemblage found in the Holocene.

Unit VI has low abundances of planktonic foraminifers and is barren of nannofossils. This prevents any precise age dating of this unit. The sporadic occurrence of iron-stained *G. tumida flexuosa* suggests that this unit is heavily reworked.

PALEOMAGNETISM

Remanence Studies

Eleven archive-half APC cores and selected sections from 23 archive-half XCB cores from Hole 935A were measured on the pass-through cryogenic magnetometer. The Tensor tool provided azimuthal orientations for seven of the APC cores.

Figure 18 shows uncorrected declination and remanence intensity, after AF demagnetization to 20 mT, for all measured cores from Hole 935A. The azimuthally uncorrected declinations for the APC cores (above 100 mbsf) appear randomly distributed from core to core. However, the downcore declination data progressively swings

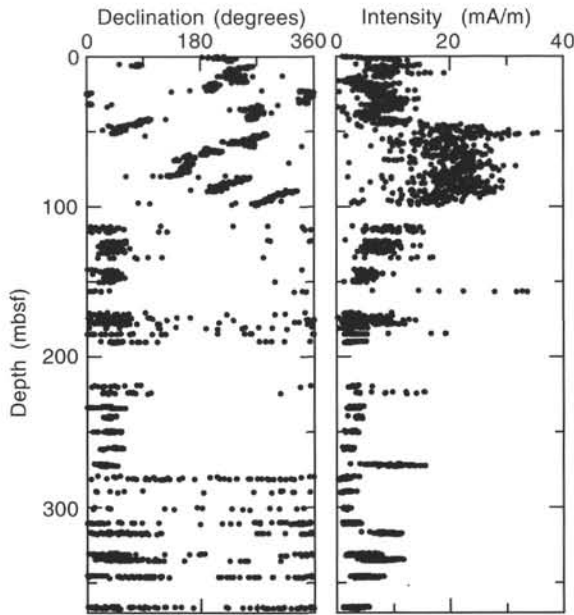


Figure 18. Uncorrected declinations and intensities for all measured archive-half core sections from Hole 935A. All sections were AF demagnetized to 20 mT.

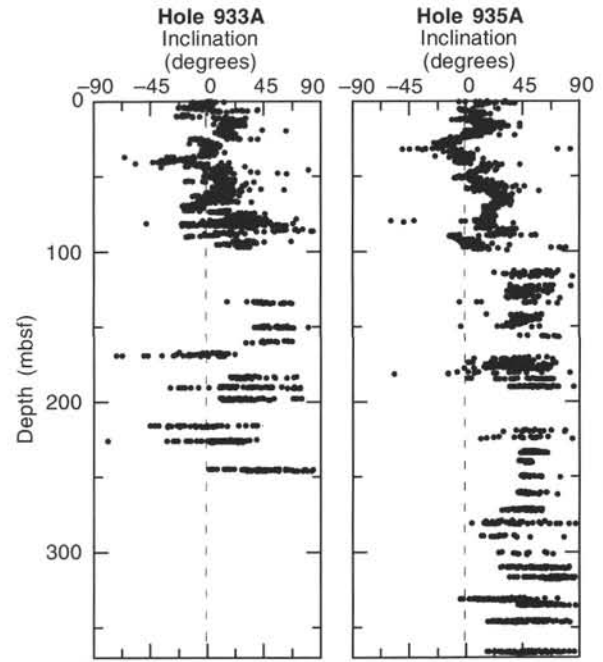


Figure 19. A comparison of inclinations for archive-half core sections from Holes 933A and 935A. All sections were AF demagnetized to 20 mT. Note contrast in the distribution of inclination values below 100 mbsf.

to the west within many cores, indicating a counter-clockwise twisting of those cores from top to bottom during recovery.

Declinations for the XCB cores are clearly biased toward 0°, again reflecting the acquisition of drill stem remanence with a unidirectional horizontal (radial?) component (see “Paleomagnetism” section, “Site 932” chapter, this volume). Mean remanence intensities for the interval between 47.5 and 100 mbsf are more than double those of the underlying and overlying sediment. This interval corresponds to a zone of silty clay characterized by closely spaced sandy-silt laminae and beds (lithostratigraphic Subunit IID).

Intra-core declinations become more variable, beginning with Core 935A-31X at the top of lithostratigraphic Unit V (calcareous clay) at a depth of 276.3 mbsf.

The inclinations for the XCB cores from Hole 935A remain high and positive after AF demagnetization to 20 mT (Fig. 19). This contrasts with the more evenly distributed inclination values for the XCB cores in Hole 933A, particularly in those cores from below the debris flow (depth > 167 mbsf). The high positive inclinations in Hole 935A indicate the persistence of a strong drill stem remanence overprint after AF demagnetization in this hole. The persistence of a drill stem remanence in the silt and sand beds of Subunit IID (43.4–98.5 mbsf) may also explain their higher remanence intensities, as their inclination values generally remain positive (Fig. 19).

Figure 20 shows oscillations in both declination (A–E) and inclination (1–5) over an ~7-m interval within Core 935A-5H. As was the case for another apparent record of secular variation in Hole 932A (see “Paleomagnetism” section, “Site 932” chapter, this volume), this interval consists of undisturbed, homogeneous clay nearly devoid of silt laminae (Fig. 5). The displacements in depth between declination and inclination peaks indicate complexities (e.g., clockwise and counter-clockwise looping) in the apparent pole path corresponding to these data.

No large, anomalous relative changes in remanence direction and intensity, which could be interpreted as a geomagnetic excursion, were observed in the APC cores from Hole 935A.

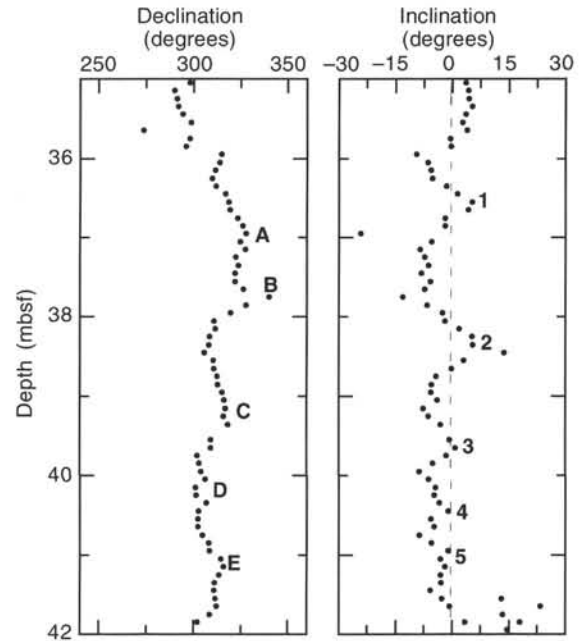


Figure 20. Declinations and inclinations for a clay interval in Hole 935A characterized by sparse silt laminae. Discernible cycles are designated A–E (declination) and 1–5 (inclination). Measurements were made on the archive-half core section after AF demagnetization to 20 mT. Declinations have been azimuthally corrected using the Tensor tool orientations.

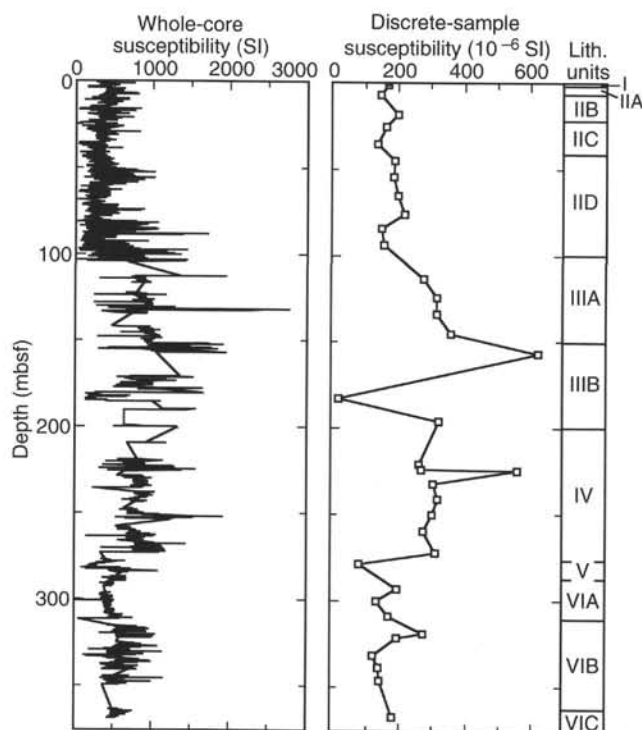


Figure 21. The magnetic susceptibility records for Site 935.

Magnetic Susceptibility

Whole-core and discrete-sample magnetic susceptibilities data show similar downhole trends for Hole 935A (Fig. 21). The highest discrete-sample susceptibilities are within Units III and IV, with the lowest mean values associated with Units I, II, V, and VI. Low values for both a discrete sample and the whole core within Subunit IIIB (about 183 mbsf) are associated with coarse to medium sand beds. In Unit V, the very low values from about 275 to 285 mbsf are associated with the nanofossil-foraminifer-rich clay.

There is no corresponding increase in magnetic susceptibility through the interval of enhanced remanence intensity (47.5–100 mbsf). This suggests that the increase in remanence is not related to increased magnetic mineral concentration. Instead, the higher intensity signal may reflect the presence of finer grained magnetic particles.

ORGANIC GEOCHEMISTRY

Volatile Hydrocarbons

Headspace methane concentrations increase rapidly below the sediment surface to a maximum value of 25,150 ppm at 11.00 mbsf (Table 6; Fig. 22). Methane concentrations remain fairly constant below this depth, ranging from 7,000 ppm to 11,000 ppm, with low values at 133.50 mbsf (590 ppm) and 223.10 mbsf (6,700 ppm). Vacutainer methane values are up to two orders of magnitude higher than headspace concentrations (Fig. 22), ranging from 149,000 ppm to 944,000 ppm in Hole 935A. Variable amounts of carbon dioxide (3,000 to 6,000 ppm) were also measured in vacutainer samples. Higher molecular weight hydrocarbons were not detected, indicating a predominantly biogenic methane source at Site 935.

Carbon, Nitrogen, and Sulfur Concentrations

Carbonate, calculated as CaCO_3 , content is 38% at 0.10 mbsf and ranges from 0.7% to 3.4% between 2.30 and 219.91 mbsf (Table 7; Fig. 23). Higher carbonate values were measured in several mud clast

Table 6. Gas concentrations in sediment from Site 935.

Core, section, interval (cm)	Depth (mbsf)	Sed. temp.* (°C)	Methane	
			HS (ppm)	VAC (ppm)
155-935A-				
1H-2, 0-5	1.50	2	4	
2H-6, 0-5	11.00	2	25,150	
3H-6, 0-5	20.50	3	9,170	203,546
4H-6, 0-5	30.00	3	7,928	438,570
5H-6, 0-5	39.50	3	6,820	922,541
6H-4, 0-5	46.00	3	8,440	
7H-6, 0-5	58.08	4	8,845	149,398
8H-7, 0-5	68.52	4	9,300	720,480
9H-7, 0-5	79.00	5	7,234	944,071
10H-7, 0-5	87.71	5	8,900	681,629
11H-5, 0-5	95.00	5	9,560	931,373
12H-4, 0-5	103.00	5	9,026	
14X-3, 0-5	115.70	6	11,388	
15X-4, 0-5	126.80	6	9,828	
16X-2, 0-5	133.50	6	590	
17X-5, 0-5	147.70	7	7,945	
18X-4, 0-5	155.90	7	9,189	
20X-5, 0-5	176.40	8	7,812	
23X-1, 0-5	199.30	8	8,851	
24X-1, 0-5	209.00	9	3,386	
25X-4, 0-5	223.10	9	6,710	
26X-3, 0-5	231.20	9	8,070	
27X-4, 0-5	242.30	10	9,387	
28X-3, 0-5	250.40	10	9,890	
29X-4, 0-5	261.60	10	8,756	
30X-4, 0-5	271.20	11	6,514	
31X-4, 0-5	280.80	11	11,843	
32X-4, 0-5	290.50	11	5,487	
33X-5, 0-5	301.70	12	16,293	
34X-5, 0-5	311.35	12	9,440	
35X-5, 0-5	321.00	12	12,182	
36X-5, 0-5	330.70	13	9,443	
37X-4, 0-5	338.80	13	9,787	
38X-2, 0-5	345.40	13	12,629	

Notes: HS = headspace; VAC = vacutainer. Geothermal gradient = 32°C/km. Bottom-water temperature = 2°C. *See "In-situ Temperature Measurements" section, this chapter.

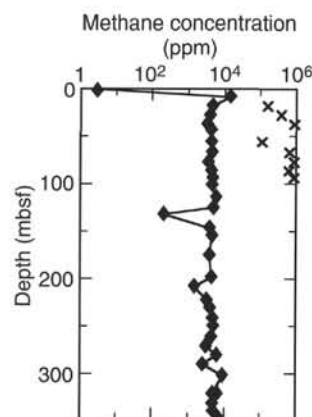


Figure 22. Methane concentrations at Site 935. Headspace (diamond) and vacutainer (x) samples are plotted.

samples below 219.91 mbsf, including 33% at 223.70 mbsf and 26.8% at 281.65 mbsf. Below 281.65 mbsf, carbonate ranges from 0.6% to 4.2%. TOC is low (0.35%) at 0.10 mbsf, then increases to 1.0% at 5.44 mbsf. Most TOC values in the rest of Hole 935A range from 0.8% to 1%. Exceptions are low concentrations, ranging from 0.7% to 0.1%, measured in silt and sand layers and in carbonate-rich zones between 219 and 283 mbsf. In addition, three elevated TOC concentrations were measured at 152.60 mbsf (3.1%), 155.58 mbsf (3.6%), and 171.12 mbsf (5.0%), corresponding to silt and sand beds rich in organic detritus.

In general, TN concentrations in Hole 935A range from 0.07% to 0.14% and display a similar downhole pattern to TOC values. Lower concentrations are observed in silt and sand beds and in carbonate-

Table 7. Elemental and organic carbon compositions of sediments from Site 935.

Core, section, interval (cm)	Depth (mbsf)	IC (%)	CaCO ₃ * (%)	TC (%)	TOC (%)	TN (%)	TS (%)	[C/N]a
155-935A-								
1H-1, 10-11	0.10	4.59	38.2	4.94	0.35	0.06	0.53	6
1H-2, 80-81	2.30	0.09	0.7	0.83	0.74	0.08	0.71	10
2H-2, 44-45	5.44	0.37	3.1	1.41	1.04	0.10	0.39	12
2H-6, 10-11	11.10	0.23	1.9	1.30	1.07	0.11	0.30	11
3H-1, 25-26	13.25	0.23	1.9	1.22	0.99	0.11	0.20	11
3H-4, 98-99	18.48	0.24	2.0	1.14	0.90	0.08	0.19	12
4H-2, 69-70	24.69	0.21	1.7	1.05	0.84	0.11	0.24	9
4H-5, 59-60	29.09	0.15	1.2	1.20	1.05	0.12	0.17	10
4H-5, 69-70	29.19	0.36	3.0	1.33	0.97	0.12	0.41	10
5H-2, 80-81	34.30	0.29	2.4	1.39	1.10	0.11	0.22	11
5H-3, 49-50	35.49	0.25	2.1	1.30	1.05	0.12	0.22	11
5H-6, 50-51	40.00	0.20	1.7	1.25	1.05	0.12	0.15	10
6H-3, 108-109	45.58	0.18	1.5	1.12	0.94	0.11	0.14	10
7H-4, 64-65	55.72	0.14	1.2	0.44	0.30	0.04	0.08	8
7H-4, 70-71	55.78	0.27	2.2	1.16	0.89	0.10	0.19	10
8H-1, 11-12	60.61	0.39	3.2	1.35	0.96	0.12	0.16	10
8H-3, 99-100	63.51	0.19	1.6	0.85	0.66	0.08	0.23	10
8H-4, 60-61	64.62	0.35	2.9	1.28	0.93	0.14	0.45	8
9H-1, 131-132	71.31	0.30	2.5	1.22	0.92	0.12	0.23	9
9H-5, 76-77	76.76	0.25	2.1	1.21	0.96	0.13	0.19	9
9H-7, 26-27	79.26	0.30	2.5	1.20	0.90	0.12	0.17	9
10H-1, 7-28	79.77	0.21	1.7	1.10	0.89	0.13	0.00	8
10H-6, 35-36	86.56	0.24	2.0	1.11	0.87	0.12	0.12	9
11H-3, 68-69	92.68	0.38	3.2	1.04	0.66	0.12	0.15	6
11H-6, 14-15	96.64	0.25	2.1	1.18	0.93	0.13	0.14	8
11H-6, 78-79	97.28	0.21	1.7	1.19	0.98	0.12	0.14	10
12H-4, 101-102	104.01	0.34	2.8	1.11	0.77	0.11	0.37	8
14X-1, 98-99	113.68	0.19	1.6	0.90	0.71	0.11	0.17	8
15X-5, 60-61	128.90	0.32	2.7	1.11	0.79	0.13	0.12	7
17X-1, 80-81	142.50	0.34	2.8	1.19	0.85	0.12	0.15	8
17X-5, 80-81	148.50	0.34	2.8	1.00	0.66	0.08	0.11	10
18X-1, 120-121	152.60	0.23	1.9	3.37	3.14	0.09	0.32	40
18X-3, 118-119	155.58	0.29	2.4	3.86	3.57	0.07	0.45	62
20X-1, 72-73	171.12	0.18	1.5	5.14	4.96	0.14	0.16	41
20X-2, 38-39	172.28	0.23	1.9	1.21	0.98	0.11	0.00	11
20X-3, 117-118	174.57	0.27	2.2	1.06	0.79	0.11	0.00	8
20X-5, 22-23	176.62	0.18	1.5	0.75	0.57	0.09	0.07	7
21X-2, 103-104	182.53	0.09	0.7	0.12	0.03	0.00	0.00	9
21X-CC, 18-19	185.28	0.24	2.0	1.00	0.76	0.07	0.10	12
22X-CC, 9-10	190.44	0.29	2.4	0.98	0.69	0.08	0.17	10
23X-CC, 1-2	200.28	0.15	1.2	0.24	0.09	0.01	0.00	8
25X-1, 131-132	219.91	0.41	3.4	1.06	0.65	0.09	0.13	8
25X-4, 60-61	223.70	3.93	32.7	4.48	0.55	0.08	0.25	8
26X-2, 50-51	230.20	0.29	2.4	1.21	0.92	0.10	0.17	11
26X-4, 50-51	233.20	0.32	2.7	1.20	0.88	0.10	0.07	10
27X-1, 49-50	238.29	0.29	2.4	1.17	0.88	0.11	0.00	10
27X-3, 49-50	241.29	0.30	2.5	1.25	0.95	0.10	0.08	11
28X-4, 39-40	252.29	1.12	9.3	1.75	0.63	0.12	0.06	6
28X-4, 55-56	252.45	0.23	1.9	0.93	0.70	0.09	0.06	9
29X-5, 12-13	263.22	0.33	2.7	1.23	0.90	0.10	0.05	11
30X-1, 103-104	267.73	0.46	3.8	0.84	0.38	0.06	0.00	8
30X-3, 97-98	270.67	0.15	1.2	0.84	0.69	0.08	0.00	10
31X-3, 12-14	279.42	0.94	7.8	1.45	0.51	0.09	1.82	7
31X-4, 85-86	281.65	3.22	26.8	3.90	0.68	0.08	0.32	10
31X-6, 9-10	283.26	0.07	0.6	0.73	0.66	0.10	0.92	8
32X-2, 29-30	287.79	0.37	3.1	1.42	1.05	0.11	0.18	12
32X-4, 50-51	291.00	0.44	3.7	1.50	1.06	0.11	0.10	11
33X-4, 25-26	300.45	0.51	4.2	1.52	1.01	0.11	0.00	10
34X-3, 93-94	309.23	0.51	4.2	1.40	0.89	0.11	0.06	9
35X-5, 20-21	321.20	0.16	1.3	0.51	0.35	0.05	0.06	8
35X-5, 22-23	321.22	0.43	3.6	1.45	1.02	0.11	0.17	11
36X-5, 105-106	331.75	0.22	1.8	0.70	0.48	0.06	0.10	10
36X-5, 109-110	331.79	0.46	3.8	1.49	1.03	0.11	0.08	11
37X-4, 99-100	339.79	0.17	1.4	0.89	0.72	0.06	0.09	14
37X-4, 105-106	339.85	0.49	4.1	1.36	0.87	0.10	0.07	10
38X-2, 2-3	345.42	0.13	1.1	0.55	0.42	0.05	0.00	10
38X-2, 29-30	345.69	0.44	3.7	1.39	0.95	0.11	0.06	10
38X-3, 41-42	347.31	0.32	2.7	1.25	0.93	0.10	0.00	11
40X-4, 39-40	367.89	0.34	2.8	1.35	1.01	0.11	0.00	10

*Calculated assuming all IC is calcite.

rich layers. Elevated TN values were not found in the three organic-rich samples at 152.60, 155.58, and 171.12 mbsf (Fig. 23). Total sulfur concentrations are slightly elevated at 0.10 mbsf (0.5%) and 2.30 mbsf (0.7%) and then decrease to values ranging from 0% to 0.4% in the rest of Hole 935A. Two major exceptions are the high TS values measured at 279.42 mbsf (1.8%) and 283.26 mbsf (0.92%). In spite of the large variations in TOC and TN concentrations associated with sediment grain size, nearly all sediment samples in Hole 935A have similar [C/N]a ratios of 8 to 12 (Table 7).

Bitumen Characterization

Four samples (29.09, 97.28, 152.60, and 171.12 mbsf) were extracted with *n*-hexane for preliminary bitumen characterization by gas chromatography (see "Explanatory Notes" chapter, this volume). A representative gas chromatogram (Sample 935A-11H-6, 78-79 cm) is shown in Figure 24. All samples contain *n*-alkanes of 25 to 33 carbon atoms as the predominant extracted compounds. The highest concentrations found were for C₂₉ and C₃₁ *n*-alkanes. The predomi-

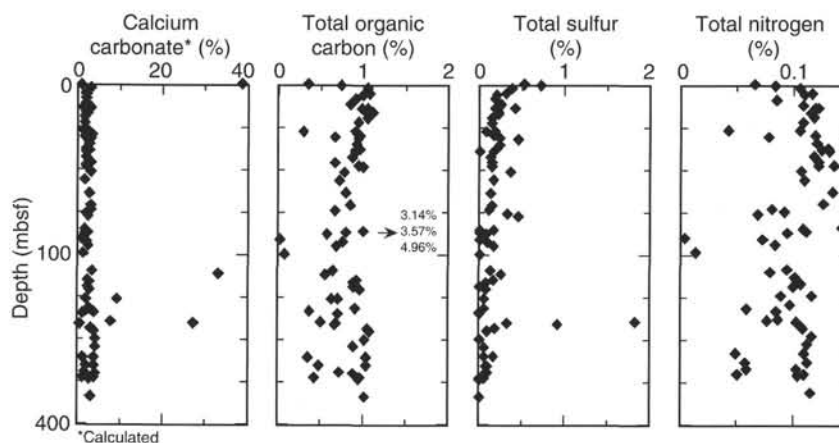


Figure 23. Concentration profiles of calcium carbonate, total organic carbon, total sulfur, and total nitrogen in Hole 935A.

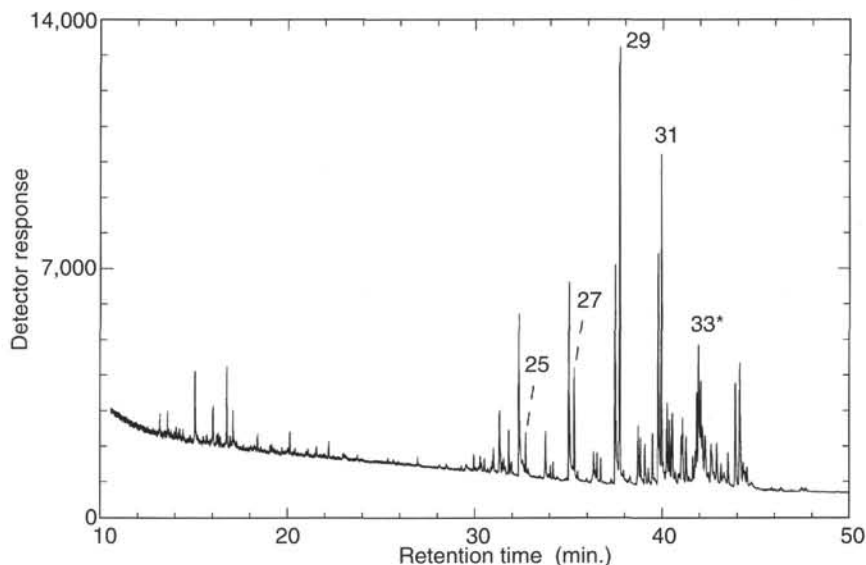


Figure 24. Gas chromatogram of *n*-hexane extract from Sample 155-935A-11H-6, 78–79 cm. The chromatographic peaks corresponding to the major hydrocarbons are identified by their carbon number. All identities are assigned based on co-injection with authentic standards. The preliminary identification of C₃₃ hydrocarbon, 33*, is based on retention time alone.

nance of odd-numbered *n*-alkanes is characteristic of cuticular waxes derived from higher plants of terrigenous origin. Though several other biomarker compounds are present in all chromatograms, it is not possible to elucidate their identities based on retention time alone. Additional analyses, such as gas chromatography/mass spectrometry, will be necessary to fully evaluate the bitumen sources.

INORGANIC GEOCHEMISTRY

Interstitial Water Analysis

Interstitial water samples were collected from 16 sediment samples at Hole 935A. Samples were taken approximately every 10 m for the upper 40 mbsf and approximately every 30 m thereafter to a depth of 365.85 mbsf (Table 8; Fig. 25).

Salinities of the water samples range from 32.0 to 34.0 (Fig. 25A). In the upper 68.42 m of the hole, salinity is rather variable, ranging from 34.0 to 32.5, with a trend of decreasing values downhole. Below 68.42 mbsf, salinity is more constant, varying between 32.0 and 33.0, with the exception of the sample from 176.30 mbsf, which has a salinity of 34.0.

Chloride concentrations increase from 558 at 2.95 mbsf to 563 mM at 94.90 mbsf (Fig. 25B). A single low chloride concentration of 555 mM was found at 149.10 mbsf. Below this depth, the values range from 560 to 564 mM.

Pore-water pH decreases from 8.02 at 2.95 mbsf to 7.25 at 20.45 mbsf (Fig. 25C). The values then increase slightly downhole to 7.71 at 223.00 mbsf. The pH decreases again to 7.39 at 250.30 mbsf, rises

to 8.11 at 309.65 mbsf, and decreases to around 7.6 for the remainder of the hole.

Pore-water alkalinity varies from 6.76 to 15.93 mM (Fig. 25D), with no overall trend downhole. In contrast to all previous sites, no shallow maximum in alkalinity was observed.

As at previous sites, dissolved magnesium and calcium concentrations decrease quickly over the first few meters of the hole. Values decrease from seawater concentrations to around 40 and 5 mM, respectively, by 10.95 mbsf (Fig. 25E and F). Below 10.95 mbsf, the values are relatively constant. Magnesium concentrations show a slight decrease downhole to values of around 35 mM in the lower 100 m of the hole.

Pore-water sulfate concentrations decrease from seawater values to 45.3 mM at 2.95 mbsf and to zero by 10.95 mbsf (Fig. 25G). The values remain zero downhole, except for values of 3.3 mM at 223.00 mbsf and 1.0 mM at 250.30 mbsf, which are likely sampling artifacts.

Ammonium concentrations increase with depth from 0.8 mM at 1.45 mbsf to 6.3 mM at 20.45 mbsf (Fig. 25H). From 29.95 to 223.00 mbsf, the ammonium concentration varies between 4.7 and 6.9 mM. Below 223.00 mbsf, the concentration increases again, to 11.7 mM in the lowermost two samples.

Pore-water phosphate concentrations show a peak of 61.3 μ M at 2.95 mbsf (Fig. 25I). From 10.95 to 250.30 mbsf, concentrations are below 10 μ M. Phosphate concentrations then increase slightly to between 11.6 and 21.8 μ M from 281.52 to 365.85 mbsf.

Dissolved silica concentrations increase quickly in the upper 10.95 mbsf, to 446 μ M (Fig. 25J). Thereafter, the values increase more slowly downhole to 713 μ M at 365.85 mbsf.

Table 8. Interstitial water chemistry, Site 935.

Core, section, interval (cm)	Depth (mbsf)	Salinity	pH	Alkalinity (mM)	Cl ⁻ (mM)	Mg ²⁺ (mM)	Ca ²⁺ (mM)	K ⁺ (mM)	HPO ₄ ²⁻ (μM)	SO ₄ ²⁻ (mM)	NH ₄ ⁺ (mM)	H ₄ SiO ₄ (μM)	Na ⁺ (μM)	Fe ²⁺ (μM)	Mn ²⁺ (μM)
155-935A-															
1H-2, 145-150	2.95	34.0	8.02	11.07	558	45.3	9.9	12.1	61.3	17.2	0.8	287	481	26.0	22.1
2H-5, 145-150	10.95	33.0	7.31	10.97	559	39.6	4.7	8.1	3.5	0.0	5.1	446	468	97.2	4.1
3H-5, 145-150	20.45	34.0	7.25	10.97	559	41.4	5.0	7.7	0.5	0.0	6.3	450	464	81.7	5.1
4H-5, 145-150	29.95	32.5	7.38	8.00	557	41.3	4.9	7.4	2.1	0.0	6.7	450	458	156.0	5.9
5H-5, 140-150	39.40	33.0	7.51	7.66	560	41.3	4.7	7.4	4.0	0.3	6.6	435	462	107.0	6.0
8H-6, 140-150	68.42	32.5	7.50	9.78	559	41.1	5.0	7.1	2.8	0.1	6.9	472	463	36.1	3.1
11H-4, 140-150	94.90	32.5	7.61	11.60	563	41.0	5.3	7.8	6.0	0.0	6.1	439	468	28.1	3.5
14X, 2, 140-150	115.60	32.0	7.58	6.76	562	39.3	5.4	8.2	1.0	0.4	4.7	487	467	54.7	6.5
17X, 5, 140-150	149.10	32.5	7.55	10.87	555	39.8	4.7	6.5	1.1	0.0	5.9	539	465	25.5	3.6
20X, 4, 140-150	176.30	34.0	7.68	15.93	562	37.7	5.3	8.9	6.1	0.4	5.6	443	478	16.8	3.4
25X, 3, 140-150	223.00	33.0	7.71	11.25	564	37.7	5.8	8.2	8.4	3.3	6.5	572	480	20.4	8.4
28X, 2, 140-150	250.30	32.5	7.39	7.91	563	36.0	5.7	7.6	3.1	1.0	6.9	628	475	11.6	3.7
31X, 4, 135-150	281.52	33.5	7.89	15.50	564	36.5	4.1	8.2	19.3	0.0	8.1	487	482	11.8	9.8
34X, 3, 135-150	309.65	33.0	8.11	12.00	562	35.0	4.6	6.7	11.6	0.0	10.0	602	478	20.3	2.2
37X, 3, 135-150	338.65	33.0	7.61	13.63	560	35.7	5.0	6.3	21.8	0.3	11.7	635	475	41.6	2.6
40X, 2, 135-150	365.85	33.5	7.55	11.75	560	36.3	5.3	6.4	12.5	1.6	11.7	713	474	34.4	2.2

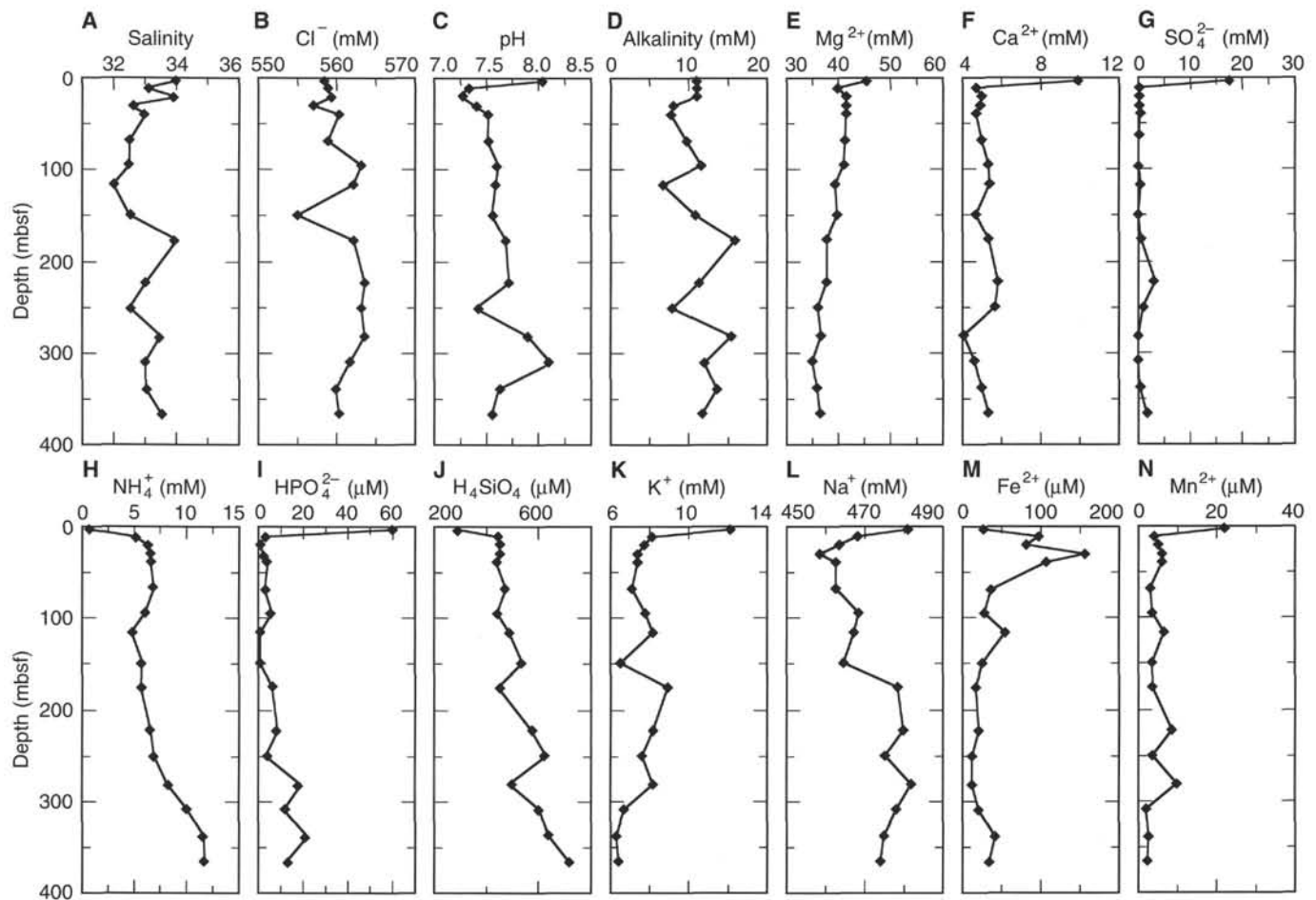


Figure 25. Downcore variation in pore-water chemistry: A. Salinity. B. Chloride. C. pH. D. Alkalinity. E. Magnesium. F. Calcium. G. Sulfate. H. Ammonium. I. Phosphate. J. Silica. K. Potassium. L. Sodium. M. Iron. N. Manganese.

Dissolved potassium and sodium concentrations exhibit similar depth profiles (Fig. 25K and -L). Concentrations of both elements decrease in the upper 29.95 mbsf, from 12.1 to around 7 mM for potassium, and from 481 to 458 mM for sodium. Potassium concentrations are then fairly constant downcore, varying from 6.5 to 8.9 mM. Sodium shows an overall downhole increase, to about 480 mM near 300 mbsf. Several small concentration changes occur concurrently in both profiles. Iron concentrations increase quickly in the upper 29.95 mbsf, to 156.0 μM (Fig. 25M), then decrease to 36.1 μM at 68.42 mbsf and remain between 11.4 and 54 μM downhole.

Manganese concentrations are a maximum of 22.1 μM at 2.95 mbsf (Fig. 25N). Thereafter, the concentration varies between 2.2 and 9.8 μM through the remainder of the hole.

Sediment Geochemistry

Five mud samples and one sand sample were analyzed for major- and trace-element geochemistry (Tables 9 and 10). These samples are from the Aqua levee through the Green levee of the Lower Levee Complex. The sand was sampled from the top of the HARP unit as-

Table 9. Major element composition (wt%) of sediment samples, Site 935.

Core, section, interval (cm)	Depth (mbsf)	Lithology	SiO ₂	TiO ₂	Al ₂ O ₃	Fe ₂ O ₃	MnO	MgO	CaO	Na ₂ O	K ₂ O	P ₂ O ₅	Total	LOI
155-935A-														
3H-5, 94-99	19.94	Mud	60.53	1.05	22.90	7.89	0.09	2.15	0.61	1.37	3.08	0.17	99.84	8.97
9H-5, 70-74	76.70	Mud	63.35	1.05	20.23	7.16	0.11	2.02	0.84	1.63	2.98	0.21	99.58	7.30
12H-1, 40-45	98.90	Sand	87.11	0.37	6.20	1.97	0.03	0.55	0.73	0.97	1.39	0.05	99.36	1.40
32X-2, 30-34	287.80	Mud	61.01	1.07	22.00	7.96	0.11	2.05	0.77	1.37	3.01	0.21	99.56	8.49
34X-3, 95-100	309.25	Mud	61.06	1.02	22.41	7.91	0.09	2.07	0.74	1.37	3.05	0.19	99.90	8.26
38X-3, 43-48	347.33	Mud	61.75	1.05	21.25	8.11	0.12	2.08	0.86	1.50	2.97	0.22	99.91	8.02

Notes: Total iron is reported as Fe₂O₃. LOI = loss on ignition.

Table 10. Trace element composition (ppm) of sediment samples, Site 935.

Core, section, interval (cm)	Depth (mbsf)	Lithology	Ba	Ce	Cr	Cu	Nb	Ni	Rb	Sr	V	Y	Zn	Zr
155-935A-														
3H-5, 94-99	19.94	Mud	455	110	65	34	22	35	135	137	78	36	126	206
9H-5, 70-74	76.70	Mud	484	103	59	29	22	31	129	155	79	38	119	251
12H-1, 40-45	98.90	Sand	319	41	13	2	10	8	49	111	0	19	26	175
32X-2, 30-34	287.80	Mud	469	115	67	31	22	33	128	145	82	40	124	231
34X-3, 95-100	309.25	Mud	495	106	67	31	22	32	131	144	76	36	125	215
38X-3, 43-48	347.33	Mud	487	107	65	30	22	34	126	153	82	39	123	237

sociated with the Aqua Channel. Mud compositions are similar to those of previous sites, with SiO₂ from 61 to 63 wt%, and Al₂O₃ between 20 and 23 wt%. CaO abundances are relatively constant between 0.6 and 0.9 wt%, indicating a dominantly silicate mineralogy.

The composition of the sand is 87% SiO₂, and has correspondingly low abundances of Al₂O₃ (6.2 wt%) and most other elements. K₂O/Al₂O₃ and Na₂O/Al₂O₃ (0.22 and 0.17, respectively) are much higher than for the muds (0.14-0.15 and 0.06-0.8), a consequence of sorting of feldspar into sand fractions at the expense of more aluminous clays. This is also reflected in comparatively elevated K₂O, Na₂O, and CaO abundances in the sand units, which are nearly as high as for the muds.

PHYSICAL PROPERTIES

Index Properties

Index properties were determined for all lithologic units in Hole 935A (Table 11). Water content displays an overall decrease with depth from 60% near the top of Unit II to 24% at the base of Hole 935A (Fig. 26). Porosity variation parallels that of water content, decreasing from 79% near the seafloor to 47% at the base of the hole. Only one sample was taken from the foraminifer-nannofossil clay of Unit I (0-0.65 mbsf), and its water content, 48%, is lower than that of the underlying silty clay. Sediment of Unit II displays the uniform, exponential decrease in water content with depth that is present in the uppermost laminated and thin-bedded silty clay units at the previous Amazon Fan sites. Within Unit II, water content decreases downhole from 60% to 28%. Increased variability in water content, with values ranging from 20% to 30%, characterizes Unit III. The mixture of abundant sand beds and mud clasts most likely accounts for the water content variability in this unit. Low water contents determined for sand beds in Unit III (Fig. 26) probably are not representative of in-situ conditions as a result of the gas expansion, and likely pore-water drainage, experienced by these layers during core recovery. The silty clays of Unit IV display a more restricted range in water content, 21% to 23%; however, within this unit anomalously high water content, 32%, was determined for a 0.12-m-thick carbonate-rich clast at 225.25 mbsf. The nannofossil clays of Unit V also have water con-

tents higher than those of overlying and underlying sediment, with values ranging from 28% to 32%. A restricted range in water content, 23% to 28%, characterizes the silty clay with silt laminae and thin-bedded silt and sand of Unit VI. Within Unit VI, water contents decrease from 25% to 24% downhole.

Grain density varies little in Hole 935A, with most of the values contained in the range of 2.7 to 2.8 g/cm³ (Table 11). Except for the coarse to medium sand beds of Subunit IIIB (Samples 935A-21X-1, 50-52 cm; -2, 50-52 cm; and -3, 50-52 cm), which have an average grain density of 2.64 g/cm³, there is little difference in grain density among lithologies. Silty clays compose the bulk of the samples measured and have an average grain density of 2.73 g/cm³. Grain density averages for sand beds (excluding the Subunit IIIB sand) and nannofossil clays are 2.72 g/cm³ and 2.74 g/cm³, respectively.

Because of the low variability of grain density, the downhole variation of wet-bulk density essentially matches the variation in water content (Fig. 26). From the top of Unit II to the base of the hole, wet-bulk density increases from approximately 1.4 to 2.0 g/cm³. GRAPE records reflect the general trends in wet-bulk density, but are characterized by densities 0.4 g/cm³ lower than the discrete sample values. The divergence in the GRAPE and discrete-sample data begins in Core 935A-2H, coinciding with the first occurrence of gas-induced sediment expansion.

The general pattern of variation of water content, porosity, and wet-bulk density is in many ways comparable to the variation at Sites 931 and 933. With the exception of Unit III in Hole 935A, the same general sequence of lithologic units is present at Sites 931, 933, and 935. Characteristics of these units, in terms of water content variation, include: (1) uniform decrease in water content in the upper interval of silty clay with silt laminae and thin-bedded silt and sand; (2) lower water content in sediment inferred to be mass transport deposits; and (3) higher water content in the interval of silty clay below the mass transport deposits. Site 935 differs from the previous sites in that below the mass transport deposits of Unit IV the silty clays show a smaller increase in water content and a lower water content gradient. At Sites 931 and 933, the boundary between mass transport deposits and underlying silty clays is marked by water content increases of 10% and 11%, respectively. At Site 935, water content is 23% at the base of Unit IV and 25% at the top of Unit VI. The 9.74-m-thick

Table 11. Index properties at Site 935.

Core, section, interval (cm)	Depth (mbsf)	Water content (%)	Wet-bulk density (g/cm ³)	Grain density (g/cm ³)	Dry-bulk density (g/cm ³)	Porosity (%)	Void ratio
155-935A-							
1H-1, 29-31	0.29	48.3	1.57	2.81	0.81	72.0	2.57
1H-1, 83-85	0.83	59.6	1.41	2.64	0.57	79.2	3.81
1H-2, 109-111	2.59	52.6	1.50	2.71	0.71	74.6	2.94
2H-2, 79-81	5.79	47.0	1.57	2.74	0.83	70.4	2.38
2H-3, 79-81	7.29	43.2	1.64	2.59	0.93	65.8	1.92
2H-4, 79-81	8.79	43.9	1.64	2.72	0.92	67.5	2.08
2H-5, 59-61	10.09	44.4	1.61	2.63	0.89	67.2	2.05
2H-6, 70-72	11.70	43.5	1.61	2.70	0.91	67.0	2.03
2H-7, 26-28	12.76	42.6	1.61	2.70	0.92	66.2	1.96
3H-1, 104-106	14.04	42.0	1.65	2.66	0.95	65.3	1.89
3H-2, 14-16	14.64	41.0	1.66	2.66	0.98	64.4	1.81
3H-3, 117-119	17.17	36.4	1.76	2.71	1.12	60.3	1.52
3H-4, 117-119	18.67	39.8	1.67	2.67	1.01	63.3	1.73
3H-5, 69-71	19.69	39.5	1.71	2.73	1.04	63.5	1.74
3H-6, 80-82	21.30	39.5	1.70	2.67	1.03	63.0	1.70
3H-7, 35-37	22.35	39.5	1.68	2.65	1.01	62.9	1.69
4H-1, 93-95	23.43	37.9	1.73	2.70	1.07	61.7	1.61
4H-2, 92-94	24.92	37.6	1.72	2.72	1.07	61.5	1.60
4H-3, 82-84	26.32	37.8	1.72	2.76	1.07	62.1	1.64
4H-4, 80-82	27.80	37.3	1.71	2.71	1.07	61.1	1.57
4H-5, 84-86	29.34	37.9	1.70	2.70	1.05	61.6	1.61
4H-6, 56-58	30.56	35.8	1.74	2.62	1.12	58.8	1.43
4H-7, 17-19	31.67	35.8	1.74	2.64	1.11	58.9	1.43
5H-1, 74-76	32.74	36.5	1.73	2.67	1.10	60.0	1.50
5H-2, 74-76	34.24	36.0	1.72	2.66	1.10	59.4	1.46
5H-3, 74-76	35.74	34.7	1.79	2.76	1.17	58.8	1.43
5H-4, 70-72	37.20	36.2	1.76	2.73	1.12	60.2	1.51
5H-5, 73-75	38.73	35.5	1.74	2.65	1.12	58.7	1.42
5H-6, 74-76	40.24	35.1	1.77	2.74	1.15	59.1	1.45
5H-7, 36-38	41.36	34.8	1.79	2.70	1.17	58.5	1.41
6H-1, 42-44	41.92	34.7	1.77	2.71	1.16	58.4	1.41
6H-2, 40-42	43.40	33.8	1.77	2.70	1.17	57.4	1.35
6H-3, 49-51	44.99	33.3	1.78	2.69	1.19	56.7	1.31
6H-4, 54-56	46.54	32.5	1.81	2.65	1.22	55.5	1.25
6H-5, 49-51	47.99	32.8	1.81	2.65	1.22	55.9	1.27
6H-6, 56-58	49.56	32.1	1.82	2.74	1.24	55.8	1.26
6H-7, 52-54	51.02	32.3	1.83	2.77	1.24	56.4	1.29
7H-1, 66-68	51.66	32.6	1.84	2.76	1.24	56.6	1.30
7H-2, 25-27	52.55	31.6	1.84	2.76	1.26	55.4	1.24
7H-3, 55-57	54.13	32.8	1.81	2.72	1.22	56.5	1.30
7H-4, 100-102	56.08	31.8	1.81	2.71	1.24	55.2	1.23
7H-5, 40-42	56.98	30.3	1.85	2.75	1.29	53.8	1.17
7H-6, 28-30	58.36	31.4	1.82	2.75	1.25	55.1	1.23
7H-7, 44-46	60.02	30.5	1.85	2.73	1.29	54.0	1.17
8H-2, 69-71	61.71	31.1	1.85	2.78	1.27	55.1	1.23
8H-3, 52-54	63.04	30.8	1.85	2.73	1.28	54.2	1.19
8H-4, 32-34	64.34	30.9	1.87	2.78	1.29	54.8	1.21
8H-5, 41-43	65.93	30.2	1.86	2.72	1.30	53.4	1.15
8H-6, 46-48	67.48	30.5	1.87	2.77	1.30	54.3	1.19
8H-7, 22-24	68.74	29.6	1.89	2.74	1.33	53.0	1.13
9H-1, 54-56	70.54	30.7	1.87	2.76	1.30	54.4	1.19
9H-2, 54-56	72.04	30.8	1.86	2.76	1.29	54.5	1.20
9H-3, 59-61	73.59	27.8	1.93	2.78	1.40	51.1	1.04
9H-4, 66-68	75.16	29.3	1.92	2.79	1.35	53.1	1.13
9H-5, 56-58	76.56	29.5	1.86	2.71	1.31	52.6	1.11
9H-6, 59-61	78.09	29.0	1.88	2.66	1.34	51.5	1.06
9H-7, 56-58	79.56	29.4	1.90	2.75	1.34	52.8	1.12
10H-2, 80-82	81.01	35.2	1.80	2.74	1.16	59.2	1.45
10H-3, 81-83	82.52	32.4	1.83	2.69	1.23	55.7	1.26
10H-4, 40-42	83.61	25.9	1.94	2.70	1.44	48.0	0.92
10H-5, 74-76	85.45	28.7	1.93	2.75	1.38	51.9	1.08
10H-6, 72-74	86.93	30.0	1.90	2.73	1.33	53.3	1.14
10H-7, 63-65	88.34	28.7	1.92	2.78	1.37	52.2	1.09
11H-1, 52-54	89.52	29.9	1.87	2.76	1.31	53.5	1.15
11H-2, 66-68	91.16	27.8	1.92	2.70	1.39	50.3	1.01
11H-3, 46-48	92.46	28.6	1.91	2.75	1.37	51.8	1.07
11H-4, 56-58	94.06	28.9	1.91	2.69	1.36	51.6	1.06
11H-5, 31-33	95.31	28.0	1.90	2.72	1.37	50.8	1.03
11H-6, 54-56	97.04	29.7	1.89	2.75	1.33	53.1	1.13
11H-7, 37-39	98.37	26.1	1.93	2.72	1.43	48.3	0.93
12H-1, 99-101	99.49	18.9	2.09	2.71	1.70	38.2	0.62
12H-4, 111-113	104.11	27.9	1.93	2.78	1.39	51.2	1.05
14X-1, 84-86	113.54	30.2	1.84	2.69	1.29	53.3	1.14
14X-2, 84-86	115.04	29.8	1.90	2.76	1.33	53.3	1.14
14X-3, 83-85	116.53	28.8	1.91	2.68	1.36	51.3	1.05
15X-1, 87-89	123.17	30.0	1.89	2.70	1.32	53.0	1.13
15X-2, 108-110	124.88	27.2	1.96	2.81	1.43	50.5	1.02
15X-3, 129-131	126.59	26.5	2.01	2.72	1.48	48.9	0.96
15X-4, 120-122	128.00	27.5	1.92	2.71	1.39	50.1	1.01
15X-5, 125-127	129.55	26.6	1.95	2.75	1.43	49.4	0.98
15X-6, 70-72	130.50	25.9	1.98	2.73	1.47	48.2	0.93
16X-1, 80-82	132.80	19.2	2.11	2.67	1.70	38.2	0.62
17X-1, 92-94	142.62	26.9	1.98	2.74	1.45	49.6	0.99
17X-2, 92-94	144.12	24.8	2.00	2.74	1.51	46.9	0.88
17X-3, 92-94	145.62	25.5	1.97	2.73	1.47	47.7	0.91
17X-4, 87-89	147.07	23.9	2.02	2.72	1.54	45.5	0.83
17X-5, 48-50	148.18	24.2	2.00	2.78	1.51	46.4	0.87
17X-6, 82-84	150.02	25.0	1.99	2.73	1.50	47.0	0.89
18X-1, 47-49	151.87	26.5	1.93	2.70	1.42	48.7	0.95
18X-2, 79-81	153.69	29.9	1.92	2.76	1.34	53.5	1.15

Table 11 (continued).

Core, section, interval (cm)	Depth (mbsf)	Water content (%)	Wet-bulk density (g/cm ³)	Grain density (g/cm ³)	Dry-bulk density (g/cm ³)	Porosity (%)	Void ratio
18X-2, 89-91	153.79	30.3	1.89	2.78	1.32	54.1	1.18
18X-3, 82-84	155.22	29.3	1.92	2.74	1.36	52.6	1.11
18X-4, 90-92	156.80	25.5	1.97	2.72	1.47	47.5	0.91
20X-1, 84-86	171.24	31.4	1.84	2.68	1.26	54.5	1.20
20X-2, 50-52	172.40	29.6	1.85	2.70	1.30	52.5	1.11
20X-3, 60-62	174.00	28.3	1.89	2.73	1.36	51.2	1.05
20X-4, 50-52	175.40	30.2	1.85	2.77	1.29	54.0	1.17
20X-5, 49-51	176.89	33.6	1.80	2.73	1.20	57.4	1.35
20X-6, 51-53	178.41	24.2	2.01	2.78	1.52	46.3	0.86
21X-1, 50-52	180.50	18.5	2.08	2.66	1.70	37.1	0.59
21X-2, 50-52	182.00	16.2	2.18	2.69	1.82	33.6	0.51
21X-3, 50-52	183.50	20.1	2.10	2.58	1.68	38.8	0.63
21X-4, 51-53	185.01	21.2	2.10	2.77	1.65	42.0	0.73
22X-1, 58-60	190.18	23.2	2.05	2.77	1.58	44.9	0.82
23X-1, 44-46	199.74	27.9	1.93	2.75	1.39	51.0	1.04
24X-1, 32-34	209.32	22.0	2.06	2.78	1.60	43.4	0.77
25X-1, 49-51	219.09	19.7	2.07	2.71	1.66	39.4	0.65
25X-2, 49-51	220.59	23.9	2.00	2.76	1.52	45.8	0.84
25X-3, 49-51	222.09	24.0	2.03	2.78	1.55	46.1	0.86
25X-4, 90-92	224.00	23.2	2.03	2.74	1.56	44.7	0.81
25X-5, 61-63	225.21	32.3	1.83	2.75	1.24	56.2	1.28
26X-1, 81-83	229.01	22.5	2.02	2.71	1.56	43.5	0.77
26X-2, 79-81	230.49	22.8	2.05	2.72	1.58	44.0	0.79
26X-3, 80-82	232.00	23.2	2.03	2.74	1.56	44.6	0.81
26X-4, 74-76	233.44	22.3	2.05	2.71	1.59	43.2	0.76
26X-5, 47-49	234.67	22.5	2.01	2.75	1.56	43.8	0.78
27X-1, 74-76	238.54	21.2	2.09	2.79	1.65	42.3	0.73
27X-2, 86-88	240.16	21.5	2.03	2.75	1.59	42.4	0.73
27X-3, 75-77	241.55	22.8	2.02	2.71	1.56	43.9	0.78
27X-4, 76-78	243.06	22.4	2.05	2.78	1.59	43.9	0.78
28X-1, 80-82	248.20	23.7	2.00	2.71	1.53	45.0	0.82
28X-2, 78-80	249.68	23.0	2.04	2.72	1.57	44.2	0.79
28X-3, 84-86	251.24	20.5	2.12	2.77	1.68	41.1	0.70
28X-4, 77-79	252.67	18.4	2.13	2.71	1.73	37.4	0.60
29X-1, 108-110	258.18	22.3	2.04	2.70	1.59	43.1	0.76
29X-2, 79-81	259.39	22.7	2.08	2.76	1.61	44.2	0.79
29X-3, 79-81	260.89	22.1	2.10	2.74	1.64	43.1	0.76
29X-4, 86-88	262.46	21.4	2.07	2.68	1.63	41.6	0.71
29X-5, 71-73	263.81	21.8	2.08	2.75	1.63	42.9	0.75
29X-6, 65-67	265.25	21.6	2.07	2.70	1.62	42.1	0.73
30X-1, 100-102	267.70	16.2	2.21	2.74	1.85	34.1	0.52
30X-2, 53-55	268.73	23.2	2.02	2.70	1.55	44.3	0.79
30X-3, 77-79	270.47	22.0	2.07	2.73	1.61	43.0	0.75
30X-4, 40-42	271.60	24.2	2.05	2.73	1.55	45.9	0.85
30X-5, 25-27	272.95	23.4	2.05	2.75	1.57	45.1	0.82
31X-1, 55-57	276.85	32.1	1.83	2.73	1.25	55.7	1.26
31X-2, 30-32	278.10	27.9	1.93	2.75	1.39	51.0	1.04
31X-3, 33-35	279.63	31.1	1.87	2.76	1.29	54.9	1.22
31X-4, 34-36	281.14	32.8	1.82	2.67	1.22	56.0	1.27
31X-5, 56-58	282.23	25.1	1.98	2.74	1.48	47.3	0.90
31X-6, 29-31	283.46	26.3	1.95	2.68	1.44	48.3	0.93
32X-1, 74-76	286.74	25.1	2.02	2.74	1.51	47.3	0.90
32X-2, 75-77	288.25	25.4	1.96	2.70	1.46	47.3	0.90
32X-3, 75-77	289.75	25.4	1.98	2.70	1.48	47.3	0.90
32X-4, 75-77	291.25	24.5	2.03	2.78	1.53	46.8	0.88
33X-1, 89-91	296.59	27.1	1.96	2.77	1.43	50.1	1.00
33X-2, 88-90	298.08	27.1	1.95	2.76	1.42	50.0	1.00
33X-3, 100-102	299.70	26.9	1.94	2.83	1.41	50.4	1.02
33X-4, 98-100	301.18	26.8	1.97	2.78	1.44	49.8	0.99
33X-5, 99-101	302.69	26.3	1.99	2.80	1.47	49.3	0.97
33X-6, 100-102	304.20	26.1	1.98	2.79	1.46	49.0	0.96
34X-1, 114-116	306.44	27.3	1.94	2.74	1.41	50.1	1.00
34X-2, 111-113	307.91	27.4	1.96	2.77	1.42	50.5	1.02
34X-3, 116-118	309.46	26.3	1.96	2.73	1.44	48.7	0.95
34X-4, 112-114	310.92	25.5	1.96	2.69	1.46	47.4	0.90
35X-1, 87-89	315.87	28.2	1.91	2.72	1.37	51.0	1.04
35X-2, 41-43	316.91	27.3	1.95	2.79	1.42	50.5	1.02
35X-3, 79-81	318.79	26.7	1.96	2.74	1.43	49.4	0.98
35X-4, 142-144	320.92	26.6	1.96	2.79	1.44	49.7	0.99
35X-5, 80-82	321.80	26.7	1.95	2.72	1.43	49.2	0.97
36X-1, 126-128	325.96	26.5	1.96	2.73	1.44	49.1	0.96
36X-2, 117-119	327.37	26.8	1.96	2.78	1.44	49.9	1.00
36X-3, 77-79	328.47	26.9	1.95	2.75	1.42	49.7	0.99
36X-4, 50-52	329.70	26.2	1.98	2.80	1.46	49.2	0.97
36X-5, 27-29	330.97	25.9	1.95	2.72	1.45	48.2	0.93
36X-6, 69-71	332.89	26.0	2.00	2.81	1.48	49.0	0.96
36X-7, 48-50	333.48	25.3	1.98	2.71	1.48	47.3	0.90
37X-1, 107-109	335.37	26.6	1.97	2.80	1.45	49.8	0.99
37X-2, 113-115	336.93	25.2	1.97	2.73	1.47	47.3	0.90
37X-3, 78-80	338.08	26.3	1.97	2.76	1.45	49.1	0.96
37X-4, 84-86	339.64	25.2	2.00	2.76	1.50	47.5	0.90
37X-5, 22-24	340.52	25.2	2.00	2.79	1.50	47.8	0.91
38X-1, 100-102	344.90	23.5	2.04	2.80	1.56	45.7	0.84
38X-2, 107-109	346.47	23.3	2.05	2.78	1.57	45.1	0.82
38X-3, 104-106	347.94	24.7	1.99	2.70	1.50	46.4	0.86
38X-4, 68-70	349.08	22.8	2.04	2.78	1.58	44.5	0.80
40X-1, 42-44	363.42	26.0	1.97	2.74	1.46	48.4	0.94
40X-2, 56-58	365.06	25.7	2.00	2.78	1.48	48.3	0.94
40X-3, 43-45	366.43	24.1	2.03	2.71	1.54	45.7	0.84
40X-4, 28-30	367.78	24.4	2.02	2.80	1.53	46.9	0.88

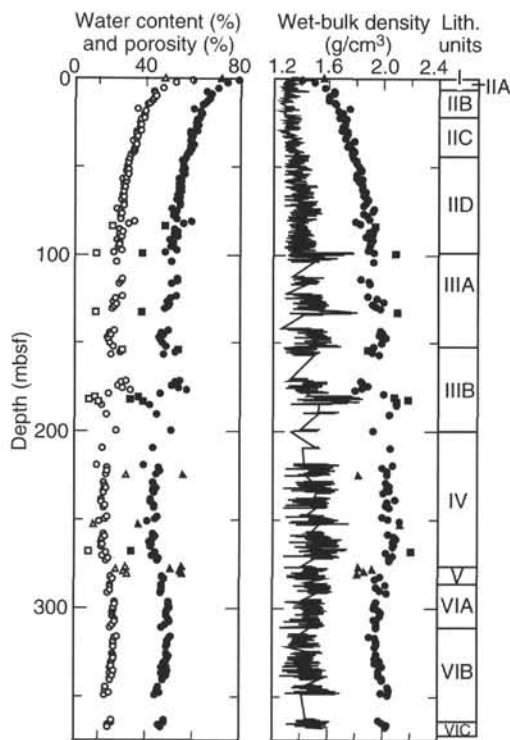


Figure 26. Water content (open symbols), porosity (solid symbols), and wet-bulk density as determined for discrete samples and by the GRAPE (line) in Hole 935A. Circles = silty clay; squares = sand and sandy silt; triangles = nanfossil clay or foraminifer-nanfossil clay.

Unit V has water contents up to 32%, but these values may be associated with the abundant biogenic constituents in this sediment. Water content decreases downhole in Unit VI from 25% to 24%. Over roughly comparable depths at Sites 931 and 933 the downhole decrease in water content is 29% to 22% and 34% to 24%, respectively.

The lowermost silty clay interval (Unit VI) in Hole 935A differs from equivalent units at Sites 931 and 933 in that it contains a higher abundance of silt laminae and thin silt and sand beds. This difference in lithology may account for differences in water content. The lower contrast between water content of the base of Unit IV and the top of Unit VI and the lower water content gradient in Unit VI may reflect the coarser grain size of this sediment or increased pore-water drainage provided by the more abundant silt and sand layers.

Compressional-wave Velocity

Compressional-wave velocity measurements were limited by pervasive microfractures in the sediment produced by gas expansion. One transverse velocity measurement of 1501 m/s was obtained with the DSV at 2.60 mbsf. Transverse velocities were obtained with the PWL for two intervals, 0 to 4 mbsf and 183 to 184 mbsf. Velocities averaged 1480 m/s in the upper 4 m. The velocities measured for a sand layer in the interval between 183 and 184 mbsf are approximately 1670 m/s.

Shear Strength

Measurements of undrained shear strength were made using the motorized shear vane on most cores from Hole 935A (Table 12). Below 65 mbsf compressive strengths were determined using a pocket penetrometer. The correlation between shear-strength values estimated from the compressive strength and those determined by the lab

vane varies among lithologic units, but it is good overall ($r = 0.88$). However, the regression equation ($S_u \text{ est} = 0.63 \cdot q_u/2 + 17.1$) indicates that the penetrometer yields measurements that overestimate the lab vane values.

Changes in the strength profile (Fig. 27) roughly correlate with the boundaries between lithologic units. Within Unit II, undrained shear strength increases from 6 to 26 kPa downhole. There is a distinct decrease in strength at 47 mbsf in Unit II and an increase in variability below this depth. Below 65 mbsf, penetrometer measurements increasingly diverge from the lab vane values. A wide scatter of shear-strength values, ranging from 29 to 107 kPa, characterizes Unit III. Shear strength decreases at the boundary between Subunits IIIA and IIIB (151 mbsf). In Subunit IIIB, the correlation between compressive strength and shear strength is better than it is in Subunit IIIA. A wide scatter in values and poor correlation between compressive and shear strength characterizes lithologic Units IV and V and the upper part of Unit VI (199 to 292 mbsf). This interval has the highest strengths measured in Hole 935A ($q_u/2 = 216$ kPa). Below 292 mbsf, the correlation between shear and compressive strengths improves. Strengths decrease to 37 kPa at 316 mbsf before increasing to about 100 kPa at the base of the hole.

The ratio of residual to peak undrained shear strength decreases with depth to about 50 mbsf and then remains constant within a general range of 0.45 to 0.65. The carbonate-rich clay clast at 225.22 mbsf has a ratio of only 0.3, which is expected for sediment with abundant biogenic constituents. The low value in these materials results from a moderately high initial strength and the lack of cohesive strength after the sediment has been disturbed.

The variation of shear strength at Site 935 is in many ways similar to its variation at the previous Amazon Fan sites. The greatest uniformity in the strength profile and best agreement between shear vane and penetrometer measurements occurs in the APC-cored section of Hole 935A. The influence of the higher abundance of sand at this site is most likely reflected in the significant divergence of shear and compressive strength in some intervals. As at the previous sites, the inferred mass transport deposits display the highest and most variable strength.

Resistivity

Longitudinal and transverse resistivity were determined for Hole 935A (Table 13). The longitudinal resistivity displays a general downhole increase that parallels the downhole decrease in porosity (Fig. 28). Unit II displays a relatively uniform increase in resistivity with depth, from 0.22 Ωm at the top of the unit to 47 Ωm at 74 mbsf. Below 74 mbsf, resistivity decreases to a minimum of 0.34 Ωm at approximately 84 mbsf before returning to a downhole increase with depth that continues through Unit III. The low resistivity in the lower part of Unit II coincides with a local decrease in porosity and increase in the sand content of the sediment. The magnitude and variability of resistivity are high in Subunit IIIB and Unit IV. Resistivity has a maximum value of 0.79 Ωm in this interval. A minimum value of 0.26 Ωm occurs in the nanfossil clay of Unit V, coinciding with anomalously high porosity. In Unit VI there is little change in resistivity, and its variability is reduced with most values clustered in the range of 0.40 to 0.50 Ωm .

Unlike at previous Amazon Fan sites, a consistent lithology-dependent variation in the resistivity anisotropy is not present in Hole 935A (Fig. 28). All units at the site are characterized by significant scatter in the anisotropy. With the exception of Unit V, all of the lithologic units have a negative mean anisotropy.

Thermal Conductivity

Thermal conductivity displays a general increase with depth in Hole 935A (Table 14), as expected for a sedimentary section with decreasing porosity with depth. Conductivity values range from 0.67 to

Table 12. Undrained shear strength at Site 935.

Core, section, interval (cm)	Depth (mbsf)	Peak undrained shear strength (kPa)	Residual undrained shear strength (kPa)	Unconfined compressive strength* (kPa)	Core, section, interval (cm)	Depth (mbsf)	Peak undrained shear strength (kPa)	Residual undrained shear strength (kPa)	Unconfined compressive strength* (kPa)
155-935A-					20X-6, 52	178.42	88.0	48.8	171.7
1H-2, 110	2.60	5.9	4.4		21X-4, 52	185.02	99.8	54.0	343.4
2H-2, 80	5.80	5.7	4.2		22X-1, 59	190.19	107.0	52.0	235.4
2H-3, 80	7.30	5.7	4.3		23X-1, 45	199.75	69.8	26.9	132.4
2H-4, 80	8.80	8.7	5.8		24X-1, 33	209.33	69.8	39.5	210.9
2H-5, 60	10.10	9.0	6.4		25X-1, 50	219.10	72.5	37.2	107.9
2H-6, 71	11.71	9.0	5.9		25X-2, 50	220.60	101.7	50.4	201.1
2H-7, 27	12.77	9.8	6.8		25X-3, 50	222.10	116.7	57.8	235.4
3H-1, 105	14.05	8.2	4.9		25X-4, 91	224.01	116.7	63.3	220.7
3H-2, 15	14.65	8.3	6.2		25X-5, 62	225.22	77.8	23.0	132.4
3H-3, 118	17.18	13.7	8.7		26X-1, 82	229.02	53.9	30.5	220.7
3H-4, 118	18.68	11.3	7.6		26X-2, 80	230.50	125.5	58.1	201.1
3H-5, 70	19.70	8.7	5.8		26X-3, 81	232.01	107.9	56.3	245.3
3H-6, 81	21.31	7.6	5.2		26X-4, 75	233.45	116.7	66.8	294.3
3H-7, 36	22.36	9.8	7.0		26X-5, 49	234.69	104.3	58.7	343.4
4H-1, 94	23.44	19.4	12.0		27X-1, 76	238.56	121.1	63.4	412.0
4H-2, 95	24.95	10.9	6.4		27X-2, 87	240.17	114.9		382.6
4H-3, 83	26.33	17.6	10.2		27X-3, 76	241.56	98.1	56.0	367.9
4H-4, 81	27.81	20.2	11.2		27X-4, 77	243.07	94.6	55.5	372.8
4H-5, 85	29.35	11.5	6.7		28X-1, 81	248.21	74.3	38.4	304.1
4H-6, 57	30.57	13.5	8.6		28X-2, 79	249.69	130.8	71.0	412.0
4H-7, 18	31.68	14.2	9.4		28X-3, 85	251.25	175.0		416.9
5H-1, 75	32.75	15.6	9.5		28X-4, 78	252.68	193.6	94.1	431.6
5H-2, 75	34.25	19.1	11.8		29X-1, 109	258.19	135.3	73.2	412.0
5H-3, 75	35.75	17.2	11.4		29X-2, 81	259.41	127.3	70.9	343.4
5H-4, 71	37.21	20.3	11.8		29X-3, 80	260.90	125.5	58.9	441.5
5H-5, 74	38.74	15.9	10.2		29X-4, 87	262.47	161.8	81.3	421.8
5H-6, 75	40.25	20.3	11.7		29X-5, 72	263.82	183.9	90.1	382.6
5H-7, 37	41.37	22.1	13.3		29X-6, 66	265.26	190.9	89.2	
6H-1, 43	41.93	22.1	11.6		30X-2, 55	268.75	106.1	63.2	284.5
6H-2, 41	43.41	23.5	12.9		30X-3, 78	270.48	116.7	62.9	358.1
6H-3, 50	45.00	24.3	13.1		30X-4, 42	271.62	138.8	76.1	382.6
6H-4, 55	46.55	30.4	16.1		30X-5, 26	272.96	148.5	75.1	343.4
6H-5, 50	48.00	21.3	11.4		31X-1, 56	276.86	90.2	47.9	230.5
6H-6, 57	49.57	21.3	10.8		31X-2, 31	278.11	107.9	58.9	284.5
6H-7, 53	51.03	19.2	8.5		31X-3, 34	279.64	96.4	50.0	294.3
7H-1, 67	51.67	15.8	10.6		31X-4, 35	281.15	128.2	60.2	269.8
7H-2, 26	52.56	21.1	11.9		31X-5, 58	282.23	115.8	61.3	372.8
7H-3, 56	54.14	17.3	10.4		31X-6, 30	283.47	138.8	60.1	318.8
7H-4, 101	56.09	20.3	12.8		32X-1, 75	286.75	137.0	84.0	323.7
7H-5, 41	56.99	22.8	11.0		32X-2, 76	288.26	110.5	59.0	323.7
7H-6, 29	58.37	21.6	13.8		32X-3, 76	289.76	137.9	73.9	363.0
8H-2, 70	61.72	34.8	16.2		32X-4, 77	291.27	136.1	73.1	358.1
8H-3, 53	63.05	28.7	17.0		33X-1, 90	296.60	88.4	40.1	171.7
8H-4, 33	64.35	36.9	19.5		33X-2, 89	298.09	80.4	41.0	157.0
8H-5, 42	65.94			88.3	33X-3, 101	299.71	75.1	42.4	137.3
8H-5, 42	65.94	35.4	21.6		33X-4, 99	301.19	84.0	46.4	186.4
8H-6, 47	67.49	36.2	19.8	78.5	33X-5, 100	302.70	103.4	47.6	201.1
8H-7, 23	68.75	25.7	13.9	68.7	33X-6, 101	304.21	115.8	53.4	215.8
9H-1, 55	70.55	35.6	21.3	73.6	34X-1, 115	306.45	61.0	38.1	161.9
9H-2, 55	72.05	27.2	13.3	73.6	34X-2, 112	307.92	57.5	31.0	117.7
9H-3, 60	73.60	37.3		98.1	34X-3, 117	309.47	69.8	39.1	142.2
9H-4, 67	75.17	41.1	20.3	107.9	34X-4, 113	310.93	99.0	55.3	215.8
9H-6, 60	78.10	41.7	25.1	107.9	35X-1, 88	315.88	37.1	24.0	68.7
9H-7, 57	79.57	35.5		98.1	35X-2, 42	316.92	39.8	25.7	78.5
10H-2, 82	81.03	21.6			35X-3, 80	318.80	49.5	23.9	112.8
10H-7, 64	88.35	25.7		78.5	35X-4, 143	320.93	87.5	44.7	137.3
11H-2, 68	91.18	37.5		103.0	35X-5, 81	321.81	53.9	28.8	98.1
11H-3, 46	92.46	38.1		98.1	36X-1, 127	325.97	66.3	33.5	161.9
11H-4, 57	94.07	26.7		117.7	36X-2, 118	327.38	56.6	32.5	112.8
11H-5, 32	95.32	25.7		142.2	36X-3, 70	328.40	43.3	16.8	93.2
14X-1, 85	113.55	29.3	18.5	103.0	36X-4, 51	329.71	47.7	27.1	137.3
14X-2, 85	115.05	47.8	27.9	161.9	36X-5, 28	330.98	76.9	38.4	161.9
14X-3, 85	116.55	50.4	29.8	29.8	36X-6, 70	332.90	83.1	41.0	196.2
15X-2, 108	124.88	71.0	39.4		36X-7, 45	333.45	58.3	20.5	122.6
15X-3, 130	126.60	81.3	44.6	210.9	37X-1, 108	335.38	54.8	35.6	117.7
15X-4, 121	128.01	68.9	36.1	196.2	37X-2, 114	336.94	72.5	41.9	171.7
15X-5, 126	129.56	73.6	38.7		37X-3, 79	338.09	47.7	29.4	147.2
15X-6, 72	130.52	98.2	50.3	260.0	37X-4, 85	339.65	62.8	37.1	186.4
17X-1, 93	142.63	45.3	29.4	171.7	37X-5, 23	340.53	79.6	44.9	171.7
17X-3, 92	145.62	81.3	44.2	255.1	38X-1, 101	344.91	61.9	37.2	122.6
17X-4, 88	147.08	92.6	49.3	240.3	38X-2, 108	346.48	85.8	50.2	166.8
17X-5, 49	148.19	88.0	46.5	299.2	38X-3, 105	347.95	143.2	76.0	318.8
17X-6, 84	150.04	97.2	48.3	289.4	38X-4, 69	349.09	175.9	92.1	363.0
18X-1, 49	151.89	36.5	21.9		40X-1, 43	363.43	69.0	42.2	176.6
18X-3, 83	155.23	23.1	14.5		40X-2, 58	365.08	95.5	50.7	196.2
18X-4, 91	156.81	50.9	24.0	117.7	40X-3, 44	366.44	90.2	50.6	220.7
20X-1, 85	171.25	31.9	21.4		40X-4, 29	367.79	76.9	47.2	186.4
20X-2, 50	172.40	47.3	27.8						
20X-3, 61	174.01	50.9	29.6						
20X-4, 51	175.41	79.2	38.5						
20X-5, 50	176.90	39.1	24.2	83.4					

Note: *Unconfined compressive strength (q_u) can be used to approximate undrained shear strength (S_u) by the relationship $q_u = 2S_u$.

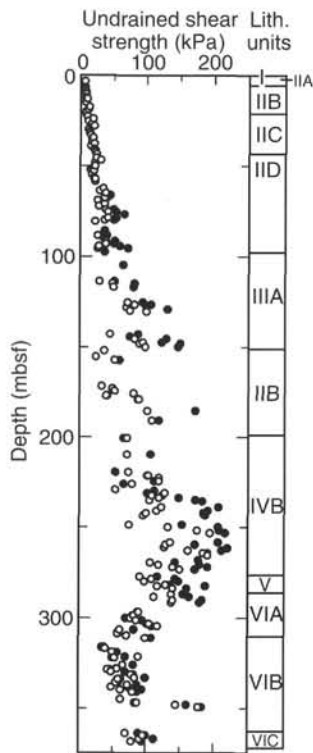


Figure 27. Undrained shear strength (open circles) and assumed undrained shear strength derived from unconfined compressive strength (closed circles) in Hole 935A.

1.94 W/(m·K). The correlation of thermal conductivity with porosity (Fig. 29) is weak, with a correlation coefficient of $r = 0.55$. As at the other Amazon Fan sites, gas expansion voids in the sediment commonly prevented full contact between the sediment and conductivity probes, resulting in questionable measurements.

DOWNHOLE LOGGING

Logging Operations and Quality of Logs

The bottom-hole assembly (BHA) was raised from a total depth (TD) of 370 mbsf to 79.5 mbsf, and the hole was reamed by lowering the BHA back to TD. The base of the BHA was set at 79.5 mbsf, and the drill string was arranged so that it could be raised to 60.5 mbsf during the upgoing logging runs. During the first logging run, a bridge was encountered at 190 mbsf. Data were obtained from the Quad-combination string (upgoing and downgoing logs) between 185 and 90 mbsf during the first run and from the Formation Micro-Scanner tool (FMS) string between 175 and 79 mbsf. We then drilled 5 m through the bridge and set the BHA at 209.5 mbsf. Another bridge was encountered at 299 mbsf. Logs were obtained from the Quad combination between 298 and 229 mbsf (upgoing logs only) and from the FMS (two passes) between 267 and 229 mbsf. In both the upper and lower logged intervals, the repeat run of the FMS tool provided additional coverage only over limited intervals. No log data were obtained from the interval between 185 and 220 mbsf (also an interval of poor core recovery.)

Despite generally poor borehole conditions overall, log quality is good and provided coverage of the interval of poor recovery between 104 and 185 mbsf. The caliper measurements indicate a markedly larger borehole for the upper logged interval from 82 to 175 mbsf (12–14 in. [30–35 cm] diameter), in comparison to the lower logged interval from 229 to 287 mbsf (10–11 in. [25–28 cm]; Fig. 30). A few

intervals (up to 2 m thick) display large (16–18 in. [40–46 cm]) borehole diameter that adversely affected all logging responses.

The velocity and density data from the upper portion of the logged interval were used to construct a synthetic seismogram to tie core observations to seismic reflection data, after removing cycle skips and noisy density data (see “Core-Seismic Integration” section, this chapter).

Offsets of up to 3 m between the depth measurements of the log and core data apparently result from errors in the assignment of core depths within intervals of incomplete core recovery. Depth offsets of up to 1 m, between the results from individual logging tools, are caused in part by incomplete heave compensation of the logging tools by the wireline heave compensator (WHC). Logging data processed on shore are shown at the end of this chapter and on the CD-ROM (back pocket).

Results

Comparison with Lithology

Logging responses show abrupt changes at 98, 118, 152, and 274 mbsf (Fig. 30) that generally correspond to lithostratigraphic unit boundaries. Lithostratigraphic Subunit IIC is characterized by a downhole increase in velocity and small-scale cyclicity in the gamma-ray logs, probably reflecting changes in the frequency of silty-sand turbidites (Fig. 31A). The boundary between Subunit IIC and Unit III at 98 mbsf is well-defined by an abrupt decrease in gamma-ray counts, as well as a sharp increase in density (Fig. 30). Velocity data are noisy at the boundary as a result of cycle skipping, but are 1.65 km/s near the base of Unit II and increase to 1.8 km/s at 110 mbsf within Unit III.

The first downhole occurrence of thick sand beds at the top of Unit III correlates with a sharp decrease in the gamma-ray and resistivity logs (Fig. 31A). The logging data suggest three main sand intervals occur between 98 and 118 mbsf. The upper sand interval was recovered in Core 935A-12H and corresponds to an upward decrease in gamma-ray counts, which is consistent with a coarsening-upward trend. The inferred two lower sand intervals occur at the depth of Core 935A-13X, which had no recovery. The gamma-ray response suggests the presence of sand at 106 to 110 mbsf, an intervening unit of thin-bedded silty sand at 110 to 113 mbsf, and an additional sand body at 113 to 118 mbsf (Fig. 31A). At 118 mbsf, a sharp increase in gamma-ray counts marks the base of this sand-rich unit. The top of Core 935A-14X probably corresponds to this boundary; however, a depth mismatch may result from incorrect assignment of core depth as a result of incomplete core recovery. At 118 mbsf, an abrupt downhole decrease in velocity and density, and a marked increase in resistivity and gamma-ray counts also are observed (Figs. 30 and 31).

Unit III below 118 mbsf is characterized by relatively high gamma-ray counts and overall higher resistivity, except for a low gamma-ray and resistivity interval that correlates to a sand bed recovered in Core 935A-16X (132–134 mbsf; Figs. 30 and 31A). The resistivity, sonic, and density measurements suggest that the material not recovered in Core 935A-16X is composed of silty sand with characteristics similar to those at the top of Subunit IIIB (Core 935A-18X). The same is true for the upper portion of Subunit IIIB (139–152 mbsf) and the lower portion of Subunit IIA (118–132 mbsf).

The boundary between lithostratigraphic Subunits IIIA and IIIB, at 152 mbsf, is well defined by an abrupt downhole decrease in gamma-ray, resistivity, sonic velocity, and density data (Figs. 30 and 31A). The interval at 158 to 170 mbsf has resistivity and density signatures that resemble the sand-rich interval observed near the top of Subunit IIIA (98–118 mbsf). Electrical resistivity increases from 170 to 180 mbsf. High resistivity at 180 mbsf correlates with the presence of clay clasts in a thick sand bed that was recovered in Core 935A-21X. A similar response was observed in the clay-clast conglomerates at Site 934. Subunit IIIB was only partially logged. Density, gamma-ray, and resistivity data suggest that the top of Subunit IIIB

Table 13. Electrical resistivity at Site 935.

Core, section, interval (cm)	Depth (mbsf)	Longitudinal resistivity (Ωm)	Transverse resistivity (Ωm)	Core, section, interval (cm)	Depth (mbsf)	Longitudinal resistivity (Ωm)	Transverse resistivity (Ωm)
155-935A-				18X-3, 83	155.2	0.488	0.455
1H-1, 30	0.3	0.261	0.246	18X-4, 91	156.8	0.589	0.503
1H-1, 85	0.85	0.217	0.209	20X-1, 85	171.3	0.554	0.546
1H-2, 110	2.6	0.212	0.210	20X-2, 50	172.4	0.487	0.485
2H-2, 80	5.8	0.283	0.264	20X-3, 61	174	0.523	0.536
2H-3, 80	7.3	0.281	0.258	20X-4, 51	175.4	0.732	0.659
2H-4, 80	8.8	0.261	0.261	20X-5, 50	176.9	0.398	0.391
2H-5, 60	10.1	0.307	0.280	20X-6, 52	178.4	0.649	0.645
2H-6, 71	11.71	0.336	0.287	21X-4, 52	185	0.775	0.732
2H-7, 27	12.77	0.341	0.296	22X-1, 59	190.2	0.644	0.563
3H-1, 105	14.05	0.361	0.322	23X-1, 45	199.8	0.505	0.464
3H-2, 15	14.65	0.315	0.278	24X-1, 33	209.3	0.675	0.592
3H-3, 118	17.18	0.317	0.388	25X-1, 50	219.1	0.794	0.583
3H-4, 118	18.68	0.314	0.309	25X-2, 50	220.6	0.614	0.507
3H-5, 70	19.7	0.304	0.280	25X-3, 50	222.1	0.704	0.521
3H-6, 81	21.31	0.302	0.362	25X-4, 91	224	0.612	0.546
3H-7, 36	22.36	0.377	0.308	25X-5, 62	225.2	0.501	0.504
4H-1, 94	23.44	0.327	0.309	26X-1, 82	229	0.708	0.827
4H-2, 93	24.93	0.340	0.295	26X-2, 80	230.5	0.661	0.565
4H-3, 83	26.33	0.338	0.340	26X-3, 81	232	0.603	0.595
4H-4, 81	27.81	0.338	0.308	26X-4, 75	233.5	0.720	0.718
4H-5, 85	29.35	0.323	0.347	26X-5, 49	234.7	0.712	0.794
4H-6, 57	30.57	0.352	0.350	27X-1, 76	238.6	0.638	0.570
4H-7, 18	31.68	0.376	0.325	27X-2, 87	240.2	0.596	0.538
5H-1, 75	32.75	0.383	0.393	27X-3, 76	241.6	0.544	0.490
5H-2, 75	34.25	0.371	0.360	27X-4, 77	243.1	0.494	0.501
5H-3, 75	35.75	0.375	0.369	28X-1, 81	248.2	0.502	0.448
5H-4, 71	37.21	0.366	0.364	28X-2, 79	249.7	0.481	0.507
5H-5, 74	38.74	0.377	0.370	28X-3, 85	251.3	0.584	0.544
5H-6, 75	40.25	0.391	0.362	28X-4, 78	252.7	0.555	0.619
5H-7, 37	41.37	0.365	0.357	29X-1, 109	258.2	0.538	0.536
6H-1, 43	41.93	0.375	0.359	29X-2, 81	259.4	0.505	0.540
6H-2, 41	43.41	0.358	0.353	29X-3, 80	260.9	0.519	0.519
6H-3, 50	45	0.392	0.345	29X-4, 87	262.5	0.537	0.554
6H-4, 55	46.55	0.417	0.367	29X-5, 72	263.8	0.541	0.587
6H-5, 50	48	0.407	0.378	29X-6, 66	265.3	0.535	0.536
6H-6, 57	49.57	0.422	0.391	30X-1, 100	267.7	0.638	0.642
6H-7, 53	51.03	0.377	0.372	30X-2, 55	268.8	0.497	0.459
7H-1, 67	51.67	0.426	0.372	30X-3, 83	270.5	0.507	0.482
7H-2, 26	52.56	0.460	0.391	30X-4, 42	271.6	0.484	0.480
7H-3, 56	54.14	0.358	0.384	30X-5, 26	273	0.467	0.469
7H-4, 101	56.09	0.455	0.407	31X-1, 53	276.8	0.384	0.365
7H-5, 41	56.99	0.419	0.435	31X-2, 31	278.1	0.386	0.411
7H-6, 29	58.37	0.432	0.516	31X-3, 34	279.6	0.401	0.385
8H-2, 70	61.72	0.445	0.379	31X-4, 35	281.2	0.248	0.259
8H-3, 53	63.05	0.406	0.410	31X-5, 58	282.3	0.345	0.348
8H-4, 33	64.35	0.415	0.398	31X-6, 30	283.5	0.352	0.370
8H-5, 42	65.94	0.441	0.400	32X-1, 75	286.8	0.411	0.394
8H-6, 47	67.49	0.444	0.417	32X-2, 76	288.3	0.422	0.392
8H-7, 23	68.75	0.465	0.414	32X-3, 76	289.8	0.410	0.409
9H-1, 55	70.55	0.412	0.390	32X-4, 77	291.3	0.434	0.422
9H-2, 55	72.05	0.455	0.418	33X-1, 90	296.6	0.429	0.391
9H-3, 60	74	0.466	0.416	33X-2, 89	298.1	0.482	0.412
9H-4, 67	75	0.436	0.392	33X-3, 101	299.7	0.419	0.411
9H-5, 59	76.59	0.407	0.384	33X-4, 99	301.2	0.433	0.414
9H-6, 60	78.1	0.411	0.418	33X-5, 100	302.7	0.446	0.438
9H-7, 57	79.57	0.425	0.414	33X-6, 101	304.2	0.426	0.407
10H-2, 82	81.03	0.384	0.386	34X-1, 115	306.5	0.411	0.393
10H-3, 79	82.5	0.376	0.372	34X-2, 112	307.9	0.468	0.409
10H-4, 41	83.62	0.336	0.314	34X-3, 117	309.5	0.402	0.394
10H-5, 75	85.46	0.371	0.365	34X-4, 113	310.9	0.570	0.422
10H-6, 73	86.94	0.371	0.366	35X-1, 88	315.9	0.451	0.395
10H-7, 64	88.35	0.385	0.383	35X-2, 42	316.9	0.470	0.449
11H-1, 54	89.54	0.398	0.374	35X-3, 80	318.8	0.474	0.442
11H-2, 68	91.18	0.423	0.406	35X-4, 143	320.9	0.462	0.431
11H-3, 46	92.46	0.392	0.392	35X-5, 81	321.8	0.428	0.411
11H-4, 57	94.07	0.419	0.446	36X-1, 127	326	0.458	0.394
11H-5, 32	95.32	0.438	0.408	36X-2, 118	327.4	0.453	0.446
11H-6, 55	97.05	0.401	0.393	36X-3, 78	328.5	0.412	0.402
12H-4, 114	104.1	0.447	0.413	36X-4, 57	329.8	0.519	0.463
14X-1, 85	113.6	0.410	0.383	36X-5, 28	331	0.480	0.403
14X-2, 85	115.1	0.432	0.384	36X-6, 70	332.9	0.440	0.425
14X-3, 85	116.6	0.424	0.424	36X-7, 49	333.5	0.443	0.465
15X-1, 90	123.2	0.398	0.426	37X-1, 108	335.4	0.423	0.417
15X-2, 108	124.9	0.446	0.428	37X-2, 114	336.9	0.452	0.401
15X-3, 130	126.6	0.475	0.479	37X-3, 79	338.1	0.419	0.422
15X-4, 121	128	0.478	0.489	37X-4, 85	339.7	0.429	0.428
15X-5, 126	129.6	0.463	0.468	37X-5, 23	340.5	0.421	0.371
15X-6, 72	130.5	0.486	0.462	38X-1, 101	344.9	0.410	0.418
17X-1, 93	142.6	0.464	0.450	38X-2, 108	346.5	0.433	0.409
17X-2, 94	144.1	0.472	0.461	38X-3, 105	348	0.445	0.416
17X-3, 92	145.6	0.500	0.492	38X-4, 69	349.1	0.434	0.404
17X-4, 88	147.1	0.512	0.489	40X-1, 43	363.4	0.464	0.414
17X-5, 49	148.2	0.498	0.490	40X-2, 57	365.1	0.394	0.385
17X-6, 84	150	0.476	0.457	40X-3, 44	366.4	0.460	0.396
18X-1, 49	151.9	0.436	0.433	40X-4, 29	367.8	0.404	0.389
18X-2, 80	153.7	0.504	0.465				

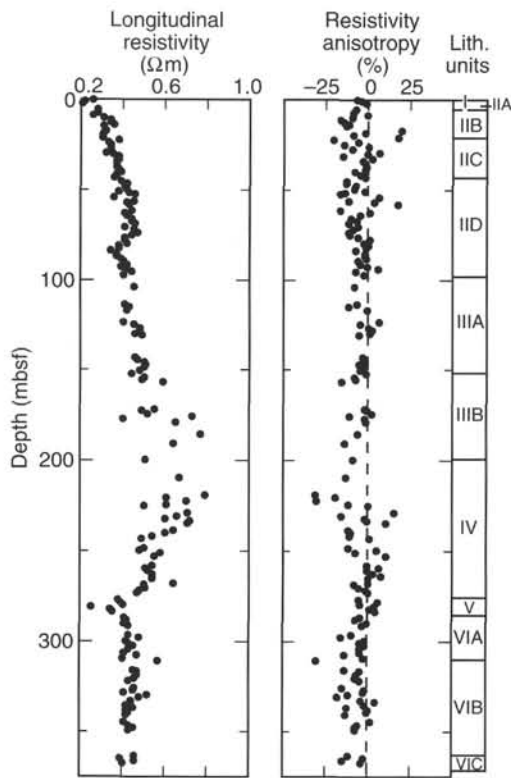


Figure 28. Longitudinal resistivity and resistivity anisotropy in Hole 935A.

is characterized by an overall upward decrease in grain size and bed thickness (Figs. 30 and 31A).

Logging data were also obtained between 229 and 290 mbsf (Figs. 30 and 31B). Except for two short intervals where large borehole diameters degraded the logging response, lithostratigraphic Unit IV is fairly homogeneous in all the logs and displays relatively high values of resistivity (~2 Ωm), density (~2.1 g/cm³), and velocity (~1.8 km/s). Near the base of Unit IV, a zone of decreased resistivity and slightly reduced density and velocity is observed that corresponds to a silty sand interval at 266 to 274 mbsf (Fig. 31B). These changes in physical properties suggest an undercompacted interval having similar characteristics as those observed beneath the mass-flow deposits logged at Sites 931, 933, and 936.

Unit V is defined by a distinct interval (274–284 mbsf) of low resistivity and density that correlates with the carbonate-rich interval recovered in Core 935A-31X (Figs. 30 and 31B). Given the thickness of the low resistivity interval (11.5 m) and the length of the carbonate-rich sediment recovered (~8 m), we infer that an additional 2 to 3 m of Unit V sediment was not recovered in the cores.

FMS Logs

We conducted two passes of the FMS tool string in each of the logged intervals. Shore-based processing of the resistivity images is expected to provide useful information regarding sedimentary structures within the channel-levee and mass-flow deposits of Subunit IID and Units III and IV.

Inclinometer measurements (from the GPIT) indicate that the borehole deviated 3.2° to 3.8° from the vertical, with an azimuth of 0° to 40° for the upper logged interval and 160° to 200° for the lower logged interval. Orthogonal two-arm caliper measurements of borehole diameter show that the upper logged interval displayed a markedly elliptical borehole, with one of the calipers measuring a diameter equal to bit size (9.875 in. [25 cm]), and the other a diameter up to 15 in. (38 cm, the maximum extension of the caliper; Fig. 32). In con-

Table 14. Thermal conductivity at Site 935.

Core, section, interval (cm)	Depth (mbsf)	Thermal conductivity (W/[m·K])
155-935A-		
1H-1, 40	0.40	1.09
1H-2, 110	2.60	0.98
2H-1, 80	4.30	0.96
2H-2, 80	5.80	0.78
2H-4, 80	8.80	0.93
2H-6, 80	11.80	0.84
5H-6, 75	40.25	0.87
5H-5, 75	38.75	0.80
5H-3, 75	35.75	0.79
5H-1, 75	32.75	0.82
6H-3, 50	45.00	1.06
6H-5, 50	48.00	1.00
7H-1, 60	51.60	0.92
7H-3, 60	54.18	0.99
7H-5, 50	57.08	1.12
8H-2, 75	61.77	0.95
8H-3, 75	63.27	0.88
8H-4, 75	64.77	0.93
8H-5, 75	66.27	1.32
9H-1, 55	70.55	0.98
9H-3, 55	73.55	0.89
9H-5, 55	76.55	1.03
9H-6, 55	78.05	0.90
10H-2, 80	81.01	0.77
10H-3, 80	82.51	0.85
10H-5, 75	85.46	0.95
10H-6, 75	86.96	1.32
11H-1, 50	89.50	1.21
11H-2, 50	91.00	1.03
11H-3, 50	92.50	0.95
11H-4, 50	94.00	0.98
12H-2, 50	100.50	1.81
15X-1, 75	123.05	1.11
15X-3, 75	126.05	1.28
15X-5, 75	129.05	1.44
17X-1, 75	142.45	1.15
17X-2, 75	143.95	1.02
17X-4, 75	146.95	1.26
17X-6, 75	149.95	1.30
18X-1, 75	152.15	1.94
18X-2, 75	153.65	1.03
18X-3, 75	155.15	0.98
18X-4, 75	156.65	1.05
20X-1, 50	170.90	0.91
20X-2, 50	172.40	1.10
20X-5, 50	176.90	1.17
20X-6, 50	178.40	0.67
21X-1, 50	180.50	1.83
21X-2, 50	182.00	1.36
21X-4, 50	185.00	1.26
22X-1, 25	189.85	1.73
23X-1, 25	199.55	1.04
24X-1, 25	209.25	1.42
25X-1, 50	219.10	1.66
25X-2, 50	220.60	1.09
25X-3, 50	222.10	0.90
25X-4, 50	223.60	1.18
26X-1, 75	228.95	0.84
26X-2, 75	230.45	1.08
26X-4, 75	233.45	1.27
26X-5, 50	234.70	1.01
27X-1, 75	238.55	1.33
27X-2, 75	240.05	1.02
27X-3, 75	241.55	1.10
27X-4, 75	243.05	1.16
28X-1, 75	248.15	1.20
28X-2, 75	249.65	0.99
28X-3, 75	251.15	1.39
28X-4, 75	252.65	1.27

trast, the lower section was nearly circular had a diameter of approximately the same as the bit size, except for a partial bridge (5 in. [13 cm] diameter) near 265 mbsf.

The long axis of the ellipse is oriented approximately parallel to the bathymetric contours on the channel-levee flank. The borehole shape may result from either drilling artifacts or from horizontal stress. In the latter case, the borehole shape indicates that the minimum horizontal stress would be oriented parallel to the topographic contours. A similar orientation of stress directions with respect to the local fan topography was inferred from borehole shape at Sites 931 and 933.

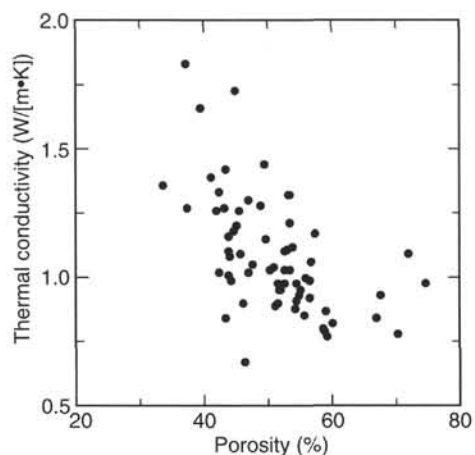


Figure 29. Thermal conductivity vs. porosity in Hole 935A.

hr after water and mud circulation had stopped. Borehole temperature in the upper portion of the hole increased from about 3.6°C at 100 mbsf to 3.9°C at 180 mbsf. About 6 hr later higher temperatures during the second run indicated borehole-temperature rebound. An additional perturbation may have resulted because a bridge at about 190 mbsf was drilled through between the first and second runs. Borehole temperatures during the second logging run (220–290 mbsf) were much warmer, between 7° and 8°C, but still about 2° to 3°C colder than that predicted by a simple extrapolation of the in-situ gradient. At about 260 mbsf, near the base of Unit IV, we observed an abrupt increase in temperature of about 0.5°C, suggesting fluid advection from the formation. A similar temperature increase was observed at the base of a mass-flow unit drilled at Site 933.

Borehole Temperature

The TLT was run with the Quad-combination tool; the TLT temperature measurements are plotted with the ADARA and WSTP in-situ measurements in Fig. 33. The first logging run occurred about 3

CORE-SEISMIC INTEGRATION

Hole 935A penetrated through the Aqua Channel-levee System, Unit R, and into the older Green Channel-levee System of the Lower Levee Complex (Manley and Flood, 1988). Seven seismic-facies units were identified on 3.5-kHz (Fig. 4) and water-gun seismic profiles (2245 UTC on 15 April 1994 during Leg 155; Fig. 34). Units 1 and 2 were classified using 3.5-kHz profiles, whereas Units 4–8 were classified from the water-gun profiles (Fig. 35). Six prominent moderate-amplitude reflections are observed at the boundaries between

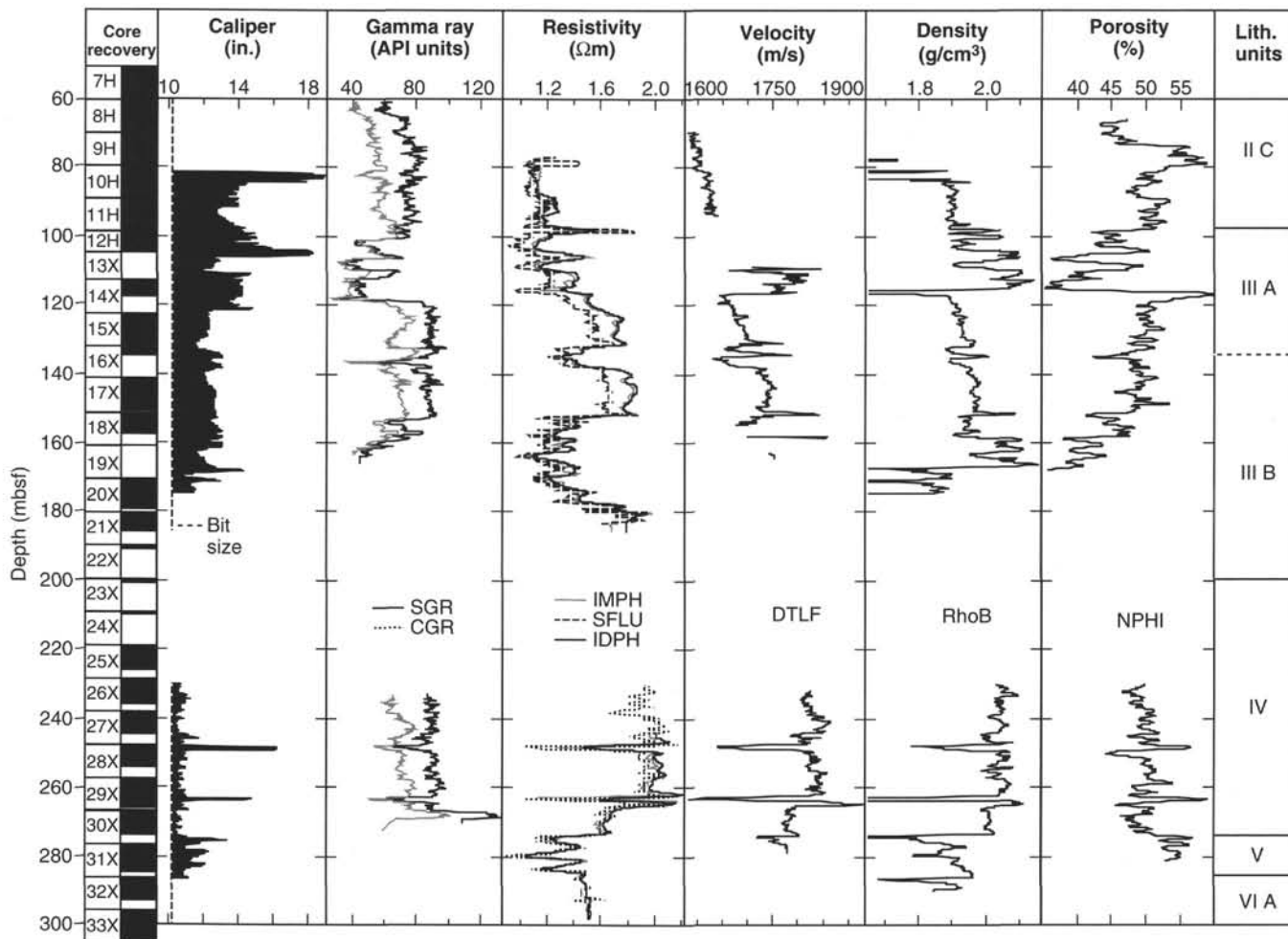


Figure 30. Partial summary of results from the Quad-combination tool string in Hole 935A. From left to right: core recovery column with core numbers; caliper measurements from the one-arm caliper on the HLDT; CGR (Th + K) = computed gamma ray SGR = spectroscopy gamma ray; SFLU = shallow, spherically focused resistivity, IMPH and IDPH = medium- and deep-induction phasor resistivity; DTLF = long-spacing (10–12 ft) interval transit time converted to velocity; RhoB = bulk density; and NPHI = neutron porosity.

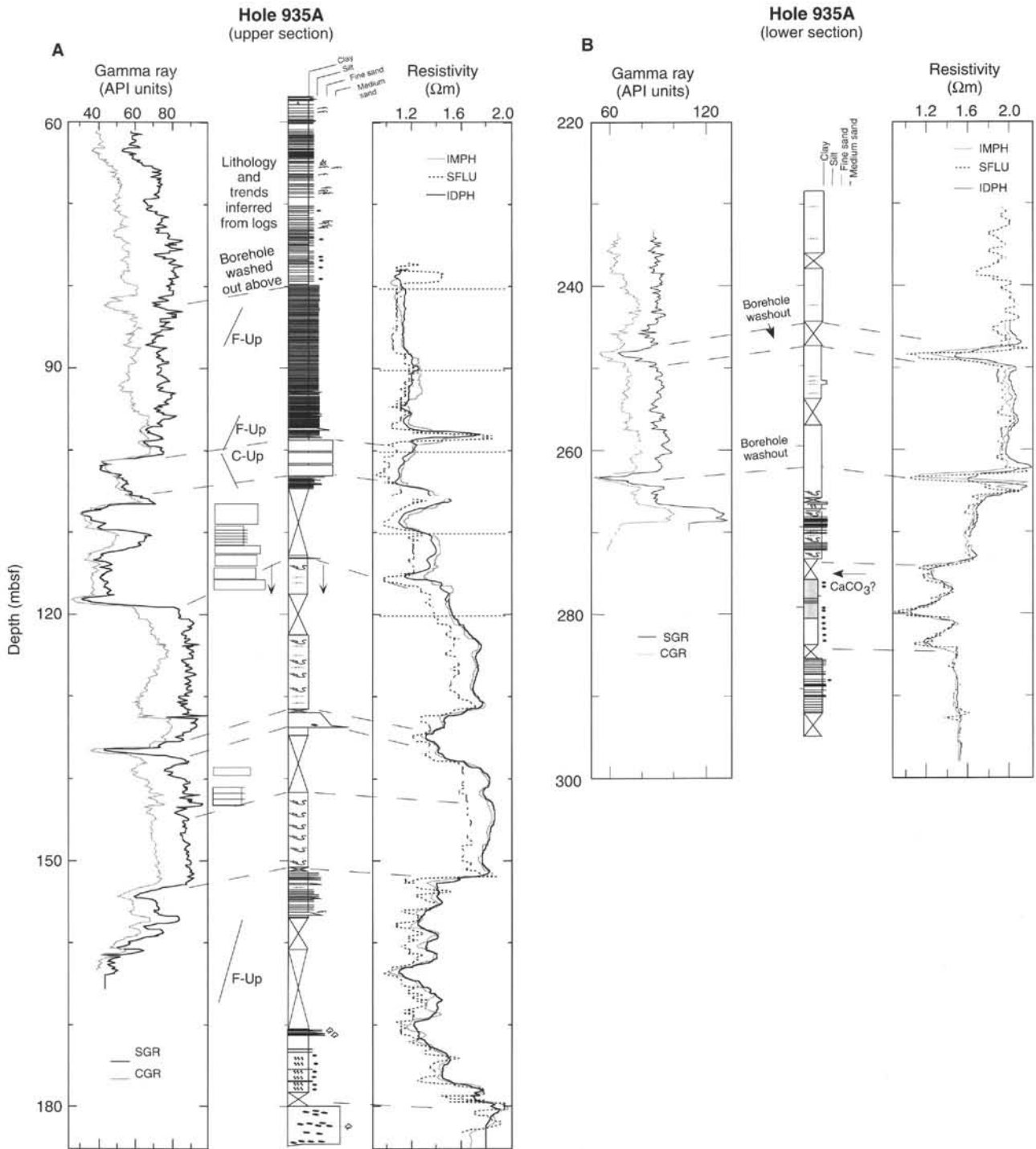


Figure 31. Comparison of gamma-ray and resistivity logs to core observations. Depth offsets between core and logs result from incomplete compensation of heave motion in the log measurements and from errors of depth assignment of incompletely recovered core sections. Gamma-ray measurements are derived from the NGT tool in the FMS string; note a small offset of about 1 m with respect to the resistivity measurements between the individual log runs. NGT data from each run will be used post-cruise to correct for depth offsets. **A.** Upper logged section (60–180 mbsf). **B.** Lower logged section (230–290 mbsf). A preliminary interpretation of the lithology from the logging data in unrecovered intervals is indicated. F-Up and C-Up refer to fining- and coarsening-upward trends, respectively, based on the logging data and inferred lithology. Core observations indicate mostly changes in the frequency of silt-sand beds and laminae, where we observed gamma-ray asymmetric trends, but subtle changes in bed thickness occur that cannot be displayed at this scale (see “Lithostratigraphy” section, this chapter). Arrows indicate possible incorrect assignment of core depths.

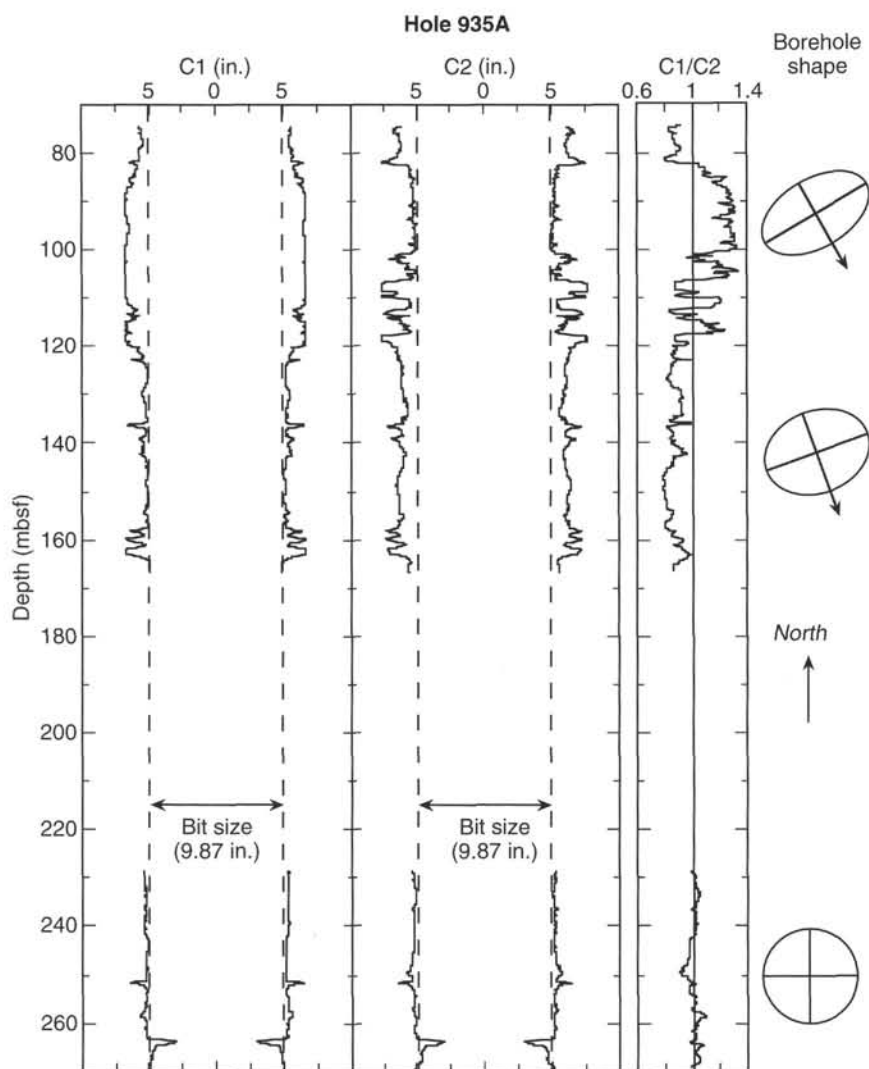


Figure 32. Borehole diameter measured by the FMS tool string. C1 and C2 are the two caliper measurements; their ratio is a measure of borehole ellipticity. The azimuth of C1 is used to determine the orientation of the ellipse with respect to north. (Arrow on borehole shape shows location of Pad 1.)

seismic-facies units (13, 20, 40, 140, 250, and 340 ms; Fig. 35). Preliminary correlation was achieved between the seismic-facies units and the lithologic units by using the time vs. depth relationship determined at Site 931 (Fig. 36).

Seismic-facies Unit 1 (0–13 ms) is characterized by high-amplitude, continuous, slightly divergent reflections returned from sediment of the Amazon and Brown Channel-levee systems and correlates with all of lithologic Unit I, Subunit IIA, and the upper 2 m of Subunit IIB (Fig. 35). Seismic-facies Unit 2 exhibits low-amplitude, discontinuous, regular migrating reflections between 13 and 20 ms. This seismic-facies unit correlates to lithologic Subunit IIB, which contains silt laminae. Seismic-facies Unit 3 is transparent and occurs from 20 to 40 ms; this unit correlates with the lower 7 m of lithologic Subunit IIB and the upper 8 m of lithologic Subunit IIC.

Low-amplitude, continuous divergent reflections from 40 to 140 ms characterize seismic-facies Unit 4, which correlates with the lower 14 m of Subunit IIC and all of Subunit IID (Fig. 35). Both lithologic Subunits IIC and IID are within the flank of the Aqua Channel-levee System and are composed of turbidites.

Seismic-facies Units 5 and 6 can be correlated with lithologic Units III and IV, respectively. Seismic-facies Unit 5 is characterized by very high-amplitude angular reflections from 140 to 250 ms, which are returned from the HARP unit(s) at the base of the Amazon and Aqua Channel-levee systems (Figs. 34 and 35). A good correlation exists between the chaotic to hummocky reflections of seismic-

facies Unit 6 (Unit R) and the mass-transport deposits of lithologic Unit IV. The low-amplitude, continuous, divergent reflections characteristic of seismic-facies Unit 7 appear to originate from the turbidite deposits of lithologic Unit V and Subunits VIA and VIB within the Green Channel-levee System (Fig. 35).

Synthetic Seismogram

Velocity and density profiles were determined between 70 and 158 mbsf from logging data. A synthetic seismogram (Fig. 36) was produced using a two-way traveltime from the seafloor to the first log data (70 mbsf; average constant velocity of 1550 m/s). The synthetic seismogram shows the correct number and locations of prominent reflections at the base of seismic-facies Unit 4 (the Aqua System) and at the top of seismic-facies Unit 5 (HARPs). The major reflectors occur about 5 ms deeper in the synthetic seismogram than in the actual record, which suggests that a faster velocity occurs in the upper 70 m. In addition, the source signature used in the convolution does not have the high-frequency component of the source at this site.

IN-SITU TEMPERATURE MEASUREMENTS

Temperature gradients and heat flow were determined using three downhole measurements and the bottom-water (mud-line) tempera-

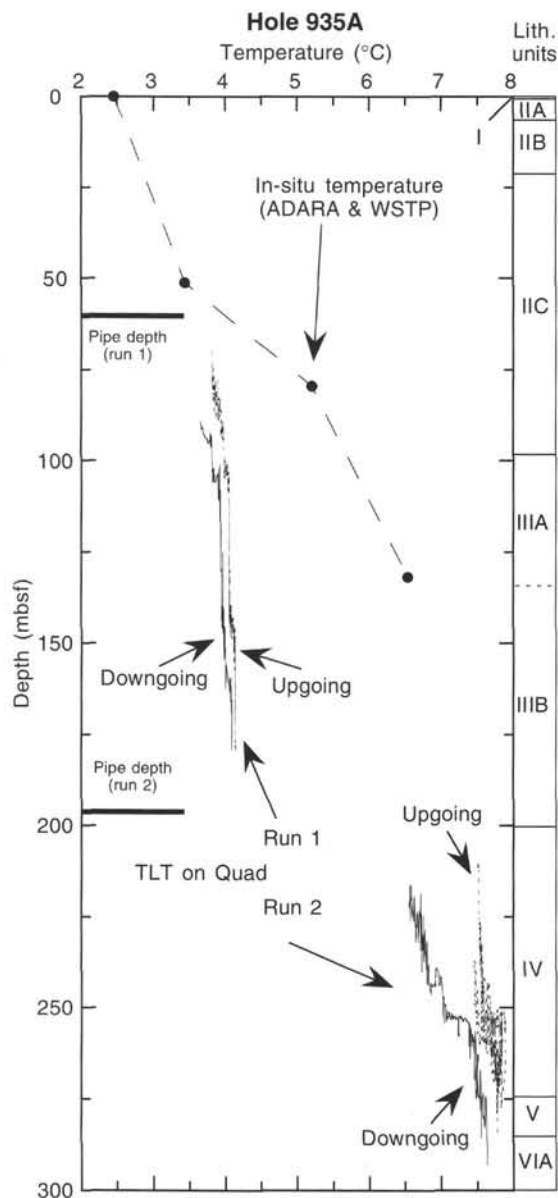


Figure 33. Borehole TLT temperature and point measurements of formation temperature using the ADARA and WSTP tools. Run 2 of the TLT occurred about 6 hr after Run 1. Note rapid increase in borehole temperature at 260 mbsf in the downgoing logging run.

ture. An ADARA measurement attempted during Core 935A-4H (32.0 mbsf) was unsuccessful, possibly as a result of movement of the coring shoe while it was in the sediment, creating friction-induced temperature increases. Two more ADARA measurements were made during Cores 935A-6H (51 mbsf) and -9H (79.5 mbsf) using instrument number 12. The mud-line temperature of 2.46°C measured from this instrument was used as the reference bottom-seawater temperature at this site. During the latter half of the Core 935A-6H measurement at 51 mbsf, there was some tool-induced frictional heating that shortened the interval suitable for reliable curve fitting. A questionable extrapolated equilibrium temperature of 3.44°C was determined. A successful measurement resulted in an extrapolated equilibrium temperature of 5.2°C at 79.5 mbsf. One WSTP measurement was made before Core 935A-16X (132 mbsf) using probe thermistor number 202. This measurement provided high-quality data yielding an extrapolated equilibrium temperature of 6.5°C at 103.5 mbsf. We

applied a correction of +177 ohms to the raw resistance values recorded by the WSTP data logger to correct for the difference in mud-line temperature recorded by the WSTP tool to that of the ADARA tool.

Equilibrium temperatures, extrapolated from synthetic curves constructed to fit transient temperature data, are plotted as a function of depth (mbsf) in Figure 37. Using the ADARA mud-line temperature, and the sub-bottom temperature from the WSTP measurement, the geothermal temperature gradient can be approximated by a linear mean of 32.28°C/km. We calculated heat flow by adopting the constant geothermal temperature gradient of 32.28°C/km and a thermal conductivity, K (as determined by the physical properties analyses), of 1.2 ± 0.15 W/(m-K), which corresponds to the average depth of 100 mbsf. This results in a calculated heat flow of 38.74 mW/m².

Depending on which data points are used, different estimates can be made of the geothermal gradient. Using the ADARA mud-line temperature and the one ADARA measurement at 79.5 mbsf, the geothermal gradient is 34.63°C/km (Fig. 37). If we use the ADARA temperature at 79.5 mbsf and the lower temperature from the WSTP measurement (Fig. 37), the geothermal gradient is 25.2°C/km.

SYNTHESIS AND SIGNIFICANCE

Stratigraphic Synthesis

Surficial Calcareous Clay (Unit I)

A 0.65-m-thick brown calcareous clay containing foraminifers and nannofossils is found at the top of the hole (Fig. 38). Five brown diagenetic color bands and crusts are present between 0.36 and 0.65 mbsf.

Mud Above the Levee of the Aqua Channel-levee System (Subunits IIA and IIB)

Subunit IIA (0.65–5.94 mbsf) is a slightly to moderately bioturbated clay, and Subunit IIB (5.94–21.20 mbsf) consists of silty clay with silt laminae. The 3.5-kHz data show that Subunit IIA corresponds to slightly divergent reflections and Subunit IIB to an interval of low-amplitude sediment waves.

Levee of the Aqua Channel-levee System (Subunits IIC and IID)

Subunit IIC (to 43.40 mbsf) consists of silty clay with infrequent laminae and thin beds of silt and fine sand. Subunit IID (to 98.50 mbsf) is similar to Subunit IIC, but has more frequent and thicker laminae and beds (1–3 cm) of silt and fine sand, with cross-lamination in about 5% of the sand beds. Overall, this interval forms a thinning- and fining-upward sequence. The extreme top of Subunit IIC probably forms the base of the Brown Channel-levee System.

HARPs (Unit III)

Unit III (98.50–199.30 mbsf) consists of fine to coarse sand beds, commonly with mud clasts, alternating with silty clay with laminae and thin beds of silt and fine sand. Recovery was only 52.3% in this unit, but the upper two-thirds of the interval was logged. Although the seismic image of this interval is dominated by high-amplitude reflections, the recovered sediment indicates a complex and varied stratigraphic section.

Subunit IIIA (to 151.67 mbsf) consists of thick beds of medium sand intercalated with thick silty clay intervals. On the basis of lithology and logs, four distinct intervals are distinguished.

- (a) From 98 to 117 mbsf, cores recovered mud interbedded with thick beds of medium sand and thin beds of fine sand and silt. Three prominent thick sand sequences are identifiable from log data. This interval corresponds to the HARP associated with the Aqua avulsion.

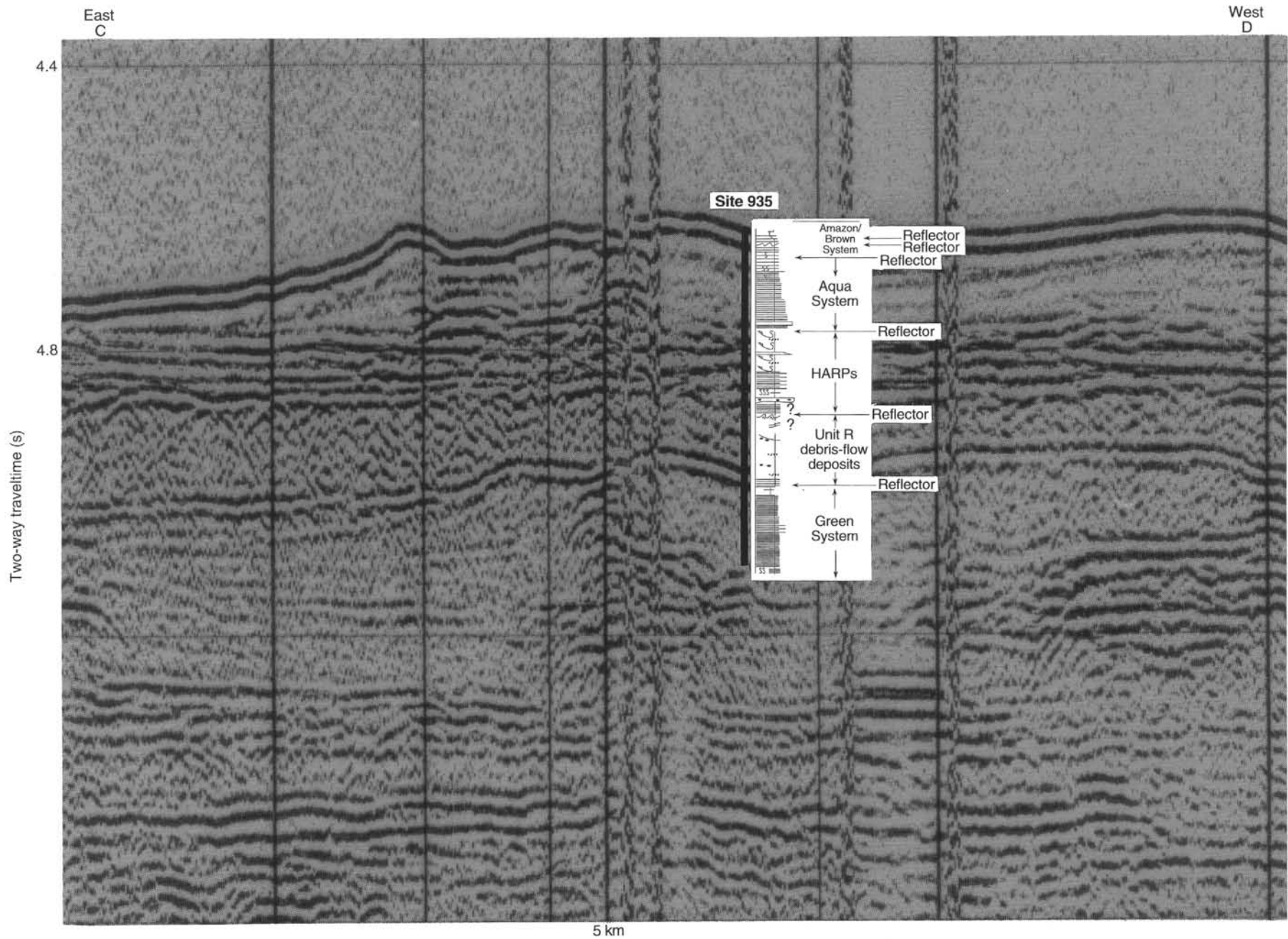


Figure 34. Seismic-reflection profile showing Site 935 with the corresponding lithostratigraphic section. Location in Figure 1.

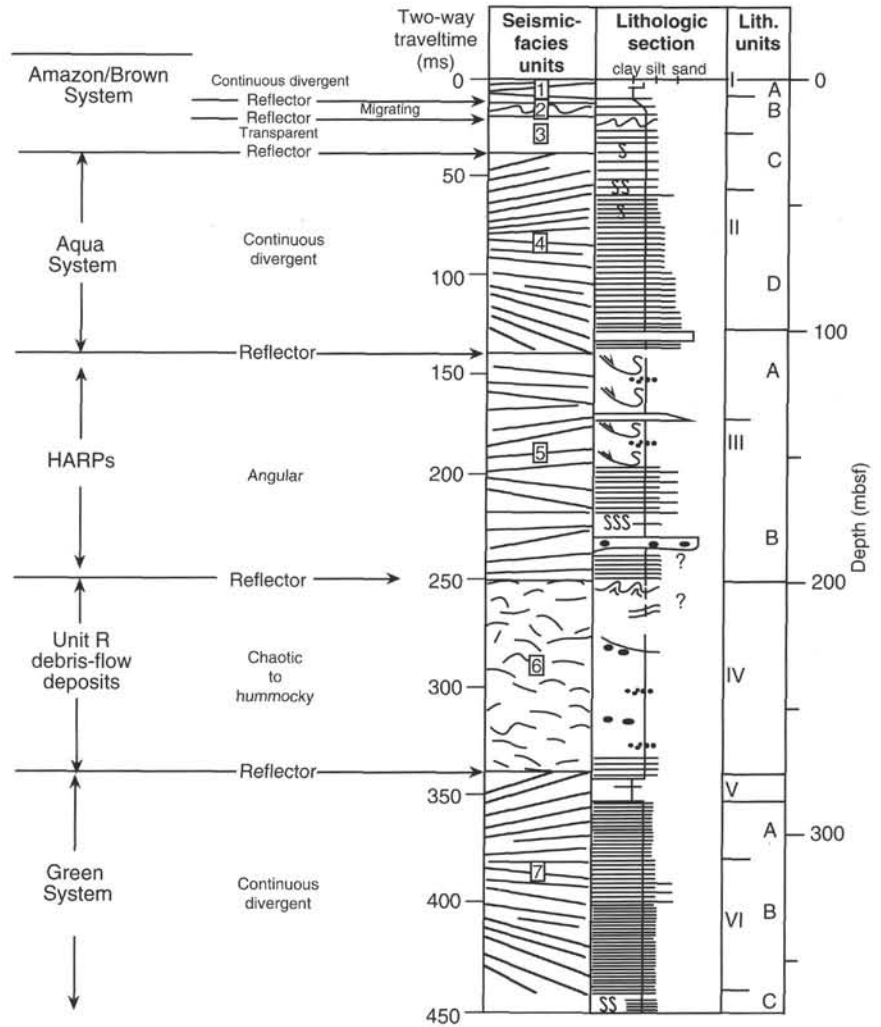


Figure 35. Correlation of lithostratigraphic observations with seismic-facies units and prominent reflections (arrows) at Site 935.

- (b) Sediment from 117 to 131 mbsf consists of mottled mud with sandy blebs. It is uncertain whether the mottling is entirely a consequence of bioturbation and drilling deformation, or whether there has also been mass transport of this interval. Shear strength in this interval is a little higher than the trend defined by sediment in Subunits IID and IIIB. Two samples contains a few cooler-water foraminifers.
- (c) Log data suggest a thick sand unit from 131 to 138 mbsf, where cores recovered medium sand with common clasts of mud and calcareous mud. The sand contains common *G. menardii* and *G. tumida* foraminifers in the size range 350 to 500 μm . The foraminifers were apparently sorted during transport. One calcareous mud clast had abundant nannofossils including abundant *E. huxleyi*, indicating an age <85 ka.
- (d) The interval 138–152 mbsf consists of well-consolidated mud with deformed bedding. The one paleontology sample contains a few cooler-water foraminifers.

Subunit IIIB (151.67–199.30 mbsf) can be divided into four intervals on the basis of lithology.

- (a) Mud with laminae and beds of sand and silt occur from 152 to 171.5 mbsf. Both core and log data show that this interval is a thinning- and fining-upward sequence of turbidites.
- (b) An intensely bioturbated mud from 173 to 179 mbsf passes up into mud with rare bioturbated silt laminae and lighter-colored

bands that contain rare nannofossils (171.5–173 mbsf). The nannofossils are poorly preserved but indicate Zone CN15 and include the cold-water species *Coccolithus pelagicus*. The one paleontology sample examined in this interval contains rare foraminifers, including common *P. obliquiloculata*, but lacks *G. menardii* and *G. tumida*, suggesting that this interval is the *Y. p. obliq.* datum at 40 ka. This interval is interpreted as a hemipelagic sediment.

- (c) One or more thick beds of coarse to medium sand containing common centimeter-sized mud clasts occur at the base of the subunit in the interval 179–190 mbsf. One calcareous mud clast has common *G. tumida* and *P. obliquiloculata* and rare *G. tumida flexuosa* and *G. menardii*, suggesting derivation from interglacial sediment. Mud with silt laminae interbedded with the sand may be in place, but some appears to occur as mud clasts. A coarse pebble of fine sandstone is present in a 30-cm-thick, graded, fine sand bed. This interval may correlate with the Orange System HARP.
- (d) The underlying mud with silt laminae, recovered at 190–191 mbsf, contains rare foraminifers, only *P. obliquiloculata* and *G. truncatulinoides*.

Mass-transport Deposit (Unit IV)

Unit IV (199.30–276.30 mbsf) consists predominantly of very dark gray silty clay. Parts of the unit include laminae and thin beds of

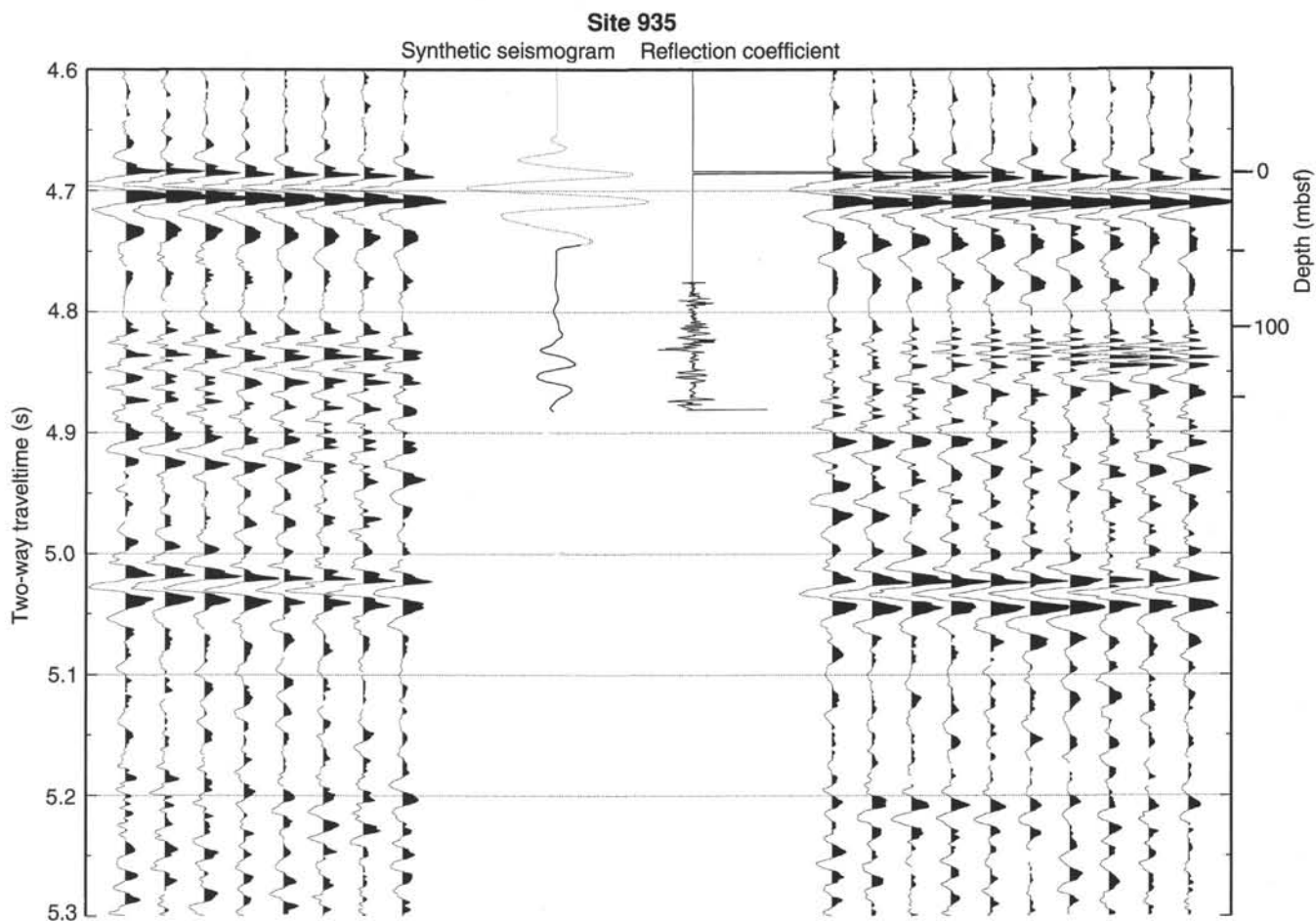


Figure 36. Synthetic seismogram for Site 935. Solid portion of synthetic seismogram was determined from log data.

silt. Some beds are contorted. At some levels, centimeter-sized mud clasts of various colors are observed. Clasts of carbonate-rich clay occur at 219–226 mbsf and 253 mbsf. Only the lower half of this unit has been logged. Index properties and shear strength determinations indicate that samples between 236 and 266 mbsf are well consolidated, whereas those higher in the unit are not. The log data show lower resistivity above 239 mbsf. The unit is divided into four intervals on the basis of recovered sediment and logs.

- (a) The upper part of Unit IV (199–218 mbsf) had only 9% recovery and no logs were obtained. Recovered sediment consists of contorted mud with silt laminae. The low recovery may indicate interbedded sand. Core-catcher samples contain rare to abundant nannofossils of Zone CN15a and common foraminifers, including common *P. obliquiloculata*. Many planktonic foraminifers appear fresh, whereas most of the benthic foraminifers (including shallow-water *Quinqueloculina*) appear iron-stained and abraded. On the basis of lithology and microfossils, this interval may be the same geologic unit as the interval IIIB(d) described above. Alternatively, the contorted bedding may indicate that the entire interval is allochthonous.
- (b) In the interval 218–237 mbsf, recovery was good. Cores contain mottled silty clay with blebs of silt and clasts of lighter-colored mud and calcareous mud. This interval has a low abundance of nannofossils from Zone CN15a, but contains common to abundant foraminifers, some of which are heavily

calcified and iron-stained. Well-preserved foraminifers include abundant *G. tumida* and *P. obliquiloculata*, sporadic occurrence of *G. menardii*, and rare *G. tumida flexuosa* (found in only one sample). One carbonate-rich clast that was examined from 225 mbsf contains a rich nannofossil assemblage similar to that in Unit V and foraminifers including common *G. menardii* and rare *G. tumida flexuosa*. The microfossil assemblage in this interval appears to result from reworking of older sediment including some interglacial calcareous mud. On the basis of the abundant mud clasts and variable sediment strength, this interval is interpreted as a muddy debris-flow deposit. Pore water at 223 mbsf contains dissolved sulfate (1.0 mM), which is characteristic of mass-transport deposits at other sites, and presumably results from re-oxidation of iron sulfides.

- (c) The interval 237–266 mbsf has a distinctive log response, with uniformly high resistivity. Two narrow zones (at 248 and 263 mbsf) are >38 cm on the caliper log and might be sand beds. The recovered core consists of well-consolidated dark mud. This is locally intercalated (at about 253 mbsf) with blocks of bioturbated sand/mud couplets and of nannofossil clay, which may suggest that this interval was emplaced by the same mass-transport event as Unit IVB(b). The well-consolidated mud is barren of nannofossils and has rare foraminifers, including a high proportion of *G. tumida* and few *P. obliquiloculata*. Pore-water sulfate concentration of 3.3 mM is found at 250 mbsf.

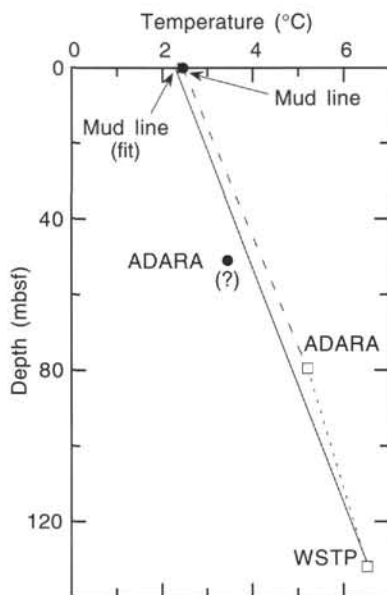


Figure 37. Estimated equilibrium temperatures in Hole 935A. A fit (solid line) through the data suggests a geothermal gradient of 32.28°C/km. A geothermal temperature gradient of 34.63°C/km is calculated (dashed line) by using the ADARA mud-line temperature and the ADARA measurement at 79.5 mbsf. A geothermal temperature gradient of 25.2°C/km is calculated (dotted line) by using the ADARA measurement at 79.5 mbsf and the lower WSTP measurement. (?) = questionable reliability of the extrapolated equilibrium temperature for the ADARA measurement at 51 mbsf.

(d) The base of Unit IV (266–276 mbsf) consists of finely color-banded mud with few silt laminae. Other than the presence of “wood-grain texture,” there is no evidence that this interval is allochthonous. Logging data is markedly different than in the rest of Unit IV and suggests that this interval is overpressured. Shear strength is similar to that in the lithologically similar Subunit VIA. There are few planktonic foraminifers, principally *G. tumida* and *G. ruber*, but no age determinant taxa. No benthic foraminifers were found. Therefore, this interval may be in its original stratigraphic position, rather than part of the mass-transport sequence as interpreted in the “Lithostratigraphy” section, this chapter.

Interglacial Hemipelagic Interval (Unit V and Top of Subunit VIA)

Unit V (276.30–286.04 mbsf) is a foraminifer-nannofossil-rich and -bearing clay, with ephemeral black color mottling and banding. This unit has higher water contents than overlying and underlying units. Lithologically, it resembles the Holocene Unit I. Its color is different, because iron is in its reduced ferrous form in Unit V. The foraminifers are an interglacial assemblage including common *G. tumida flexuosa* and the nannofossils are Zone CN14b (0.26–0.46 Ma).

Levee of the Green Channel-levee System

Unit VI (286.04–372.06 mbsf) consists of silty clay with laminae and thin beds of silt and fine sand. Subunit VIA (to 310.32 mbsf) is silty clay with rare silt laminae. Subunit VIB (to 363.00 mbsf) is silty clay with silt laminae and thin beds of silt and fine sand, some of which are cross laminated. The distribution of sand is quite variable. Subunit VIC (to 372.06 mbsf) consists of silty clay with discontinuous laminae and thin beds of silt. The presence of heavily iron-stained

foraminiferal assemblages, especially *G. tumida flexuosa* specimens, suggests that the foraminifers are reworked from older ?interglacial sediment.

Implications

Site 935 is an important chronologic reference for the Middle and Lower Levee complexes. A key stratigraphic question at this site is how much of Units III and IV are stratigraphically in place and contain microfossil assemblages that are not reworked. This issue will be addressed by further micropaleontological work and by shore-based examination of reprocessed FMS logs. In this discussion, intervals IIIA(d) (138–152 mbsf), IIIB(d) to IVA(a) (190–218 mbsf), and IV(b) and (c) (218–266 mbsf) are interpreted as mass-transport units.

The Holocene–late Pleistocene transition is similar to that at other sites from Leg 155. No geomagnetic excursion (Lake Mungo Excursion) was detected at this site. Five oscillations in magnetic declination and inclination from 36 to 42 mbsf are interpreted as secular variation cycles.

The *Y_{p.obliq.}* marker (40 ka) occurs at 179 mbsf. The absence of *G. menardii* and *G. tumida* at this level is consistent with an age of <85 ka derived from the nannofossils. *P. obliquiloculata* is absent at 117–131 mbsf, where there is a cold-water planktonic foraminiferal assemblage. The nannofossil assemblage at 174 mbsf also suggests cold water.

Unit IV(d) (266–276 mbsf) has a warm-water planktonic foraminiferal assemblage. The underlying Unit V provides a pelagic record deposited during a sea-level highstand with nannofossil assemblages dominated by 4- to 5.5- μ m-sized *Gephyrocapsa*. *P. lacunosa* and *E. huxleyi* are absent, which constrains the age to 0.26–0.46 Ma. The foraminifer assemblage is a warm (interglacial) assemblage including *Globorotalia tumida flexuosa* and *G. hexagonus*. The presence of *G. tumida flexuosa* and *G. calida calida* confirms the middle to late Pleistocene age. The abundance of *G. tumida flexuosa* might suggest that this interval is Stage 5e rather than Stage 7, 9, or 11, where this species occurs in reduced numbers in the eastern equatorial Atlantic except that this interpretation is inconsistent with the nannofossil zonation. Unit VI has common *G. tumida*, but *G. menardii* is absent except for a rare occurrence at the base of Subunit VIA, and rare *G. tumida flexuosa* is iron stained, appearing reworked. The significance of this assemblage is uncertain. The lithology is similar to that in the latest Pleistocene at the top of the hole (Subunits IIA, IIB).

Clasts of nannofossil- and foraminifer-bearing clay are found in sand beds in Unit III and as blocks in Unit IV. They potentially provide information on stratigraphic intervals that have not otherwise been sampled by coring. Most clasts in Unit III are of Zone CN15b and thus indicate the presence of a calcareous mud interval younger than 85 ka (but older than 40 ka). Calcareous mud clasts in Unit IV resemble the underlying sediment of Unit V. Most well-consolidated blocks in Unit IV(c) have low abundance of nannofossils and foraminifers, but contain a warm-water foraminiferal assemblage. The presence of *G. tumida* and lack of *G. menardii* may prove to be of some age-diagnostic value in shore-based study, because generally these two species occur together.

In summary, Hole 935A provides a stratigraphic section from the present seafloor to isotopic Stage 10 or 12. The *Y_{p.obliq.}* datum (40 ka) occurs in the middle of a composite HARP interval that includes several intervals of hemipelagic bioturbated mud with foraminiferal assemblages. The HARP interval overlies the thick mass-transport unit (Unit IV) that is correlated seismically with the Unit R Debris Flow of Manley and Flood (1988). Underlying overpressured turbidite mud with rare silt rests on calcareous clay: this sequence probably dates from isotopic Stages 9 or 11.

The clay mineral fraction of mud was systematically examined by XRD at this site. The data show that the illite/kaolinite and smectite/kaolinite ratios are particularly low in the Amazon–Aqua interval, the well-consolidated resedimented mud of Unit IV, and in the lower part

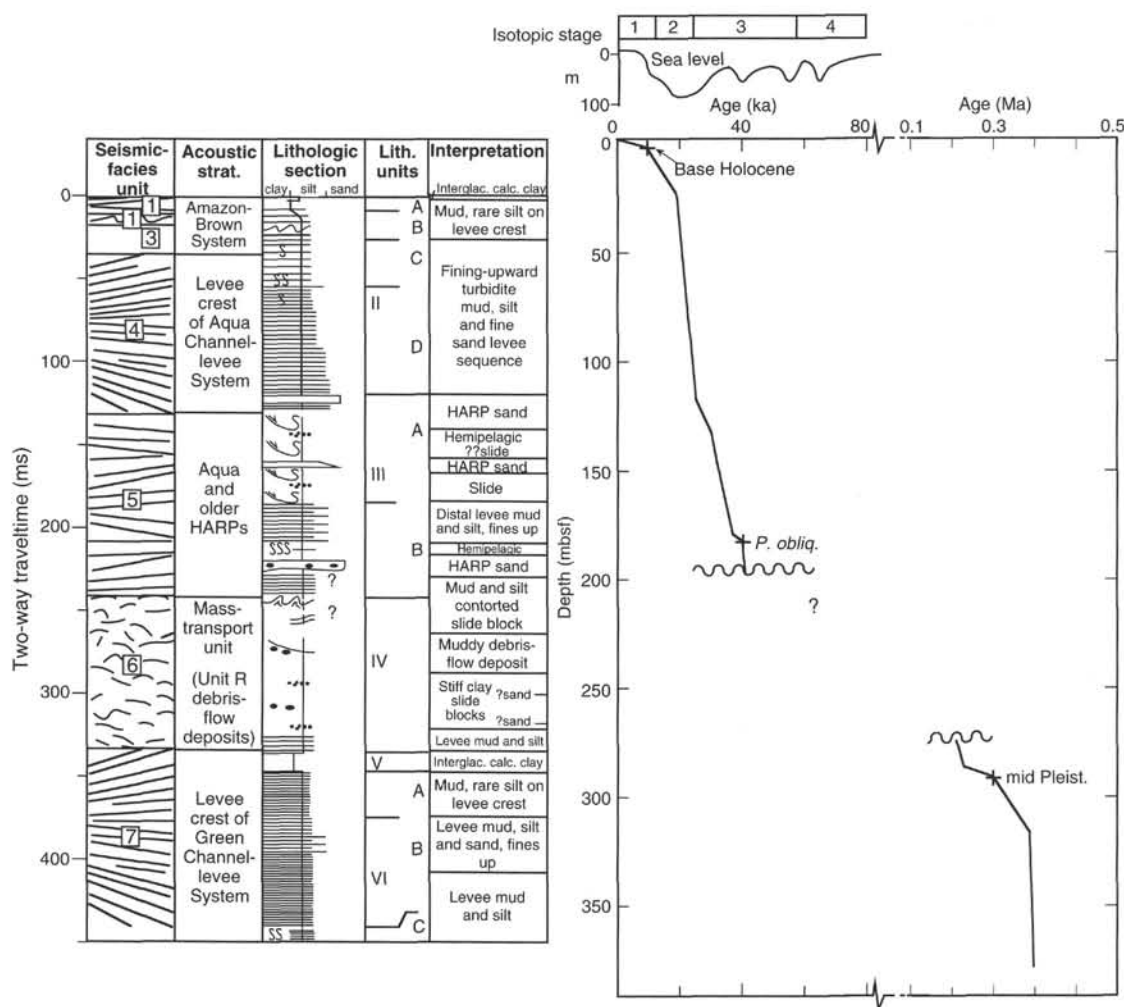


Figure 38. Summary of Site 935 showing (left to right) seismic-facies units, acoustic stratigraphy, schematic lithologic column, lithologic units, log stratigraphic units, interpreted sediment facies, chronological picks, and interpreted age-depth curve (+ = datums; variations in slope between these points are interpreted, based on dated intervals of similar facies at other sites).

of the Green levee (Subunit VIC). The early Amazon through Aqua interval may correspond to the last glacial maximum (isotopic Stage 2); the other two intervals may correspond to isotopic Stage 6. These data may indicate greater supply of kaolinite during glacial maxima, as a result of climatic changes in the Amazon Basin, but more shore-based study is needed to evaluate inter-sample variability.

Many of the sedimentological features of the levee sequences at this site confirm observations made at earlier sites. This site provides important new insights into HARPs, mass-transport units, and deeply buried calcareous clays. The core data show a more complex stratigraphy for the intervals of high-amplitude seismic reflections than was evident from the seismic-reflection profiles. The HARP immediately below the Aqua levee is a 20-m-thick sequence of three sand intervals and interbedded mud. The uppermost sand interval is a thickening- and coarsening-upward sequence of medium sand; the two lower sand intervals have no discernible trends from log data. Two deeper intervals of medium sand were cored; one 7-m-thick unit appears "blocky" on gamma and resistivity logs, showing no clear grain size trend. The lower medium sand unit, which was <11 m thick, was not logged. These sandy intervals make up less than 40% of the seismically identified HARP unit. The medium sand units are interbedded with hemipelagic and distal levee muds and with thin muddy mass-transport deposits.

The principal interval of mass-transport deposits, in Unit IV, includes muddy debris flows with polymictic mud clasts, intercalated thick sequences of well-consolidated clay in two or more blocks, and a cap of contorted mud with silt laminae that may be a large block rafted by the debris flow. At least the upper parts of the mass-transport deposit have a deep water origin, based on sedimentological character and abyssal benthic foraminiferal assemblages.

The calcareous clay of Unit V overlies a turbidite mud-silt sequence in the same manner as the Holocene Unit I overlies Unit II levee deposits and is interpreted to result from a similar major marine transgression that cut off Amazon River sediment supply to the shelf edge and thus to the fan.

Near-surface sediment has elevated total sulfur contents (0.5%–0.7% in the top 3 m). Possibly analogous high sulfur occurs in Unit V (0.3%–1.8%) and in carbonate-rich clasts in Unit IV (0.25%). Two organic-rich sand units have atomic carbon/nitrogen ratios of 20 and 34, characteristic of vascular plant debris. Four bitumen analyses show predominance of odd-carbon-numbered *n*-alkanes with maximum concentrations of *n*-C₂₉H₆₀ and *n*-C₃₁H₆₄, suggesting derivation from higher terrestrial plants.

Solid phase geochemical samples from mass-transported sediment at 176–225 mbsf have rather low nitrogen content (<0.12%). Comparably low values occur in Holocene and latest Pleistocene sed-

iment and in Unit IV(d). These low values may be characteristic of slow sedimentation rates during interglacial conditions. They are consistent with the abundance of clasts of interglacial sediment in the mass-transport sediment.

REFERENCES*

- Curry, W.B., Shackleton, N.J., Richter, C., et al., in press. *Proc. ODP, Init. Repts.*, 154: College Station, TX (Ocean Drilling Program).
- Damuth, J.E., 1977. Late Quaternary sedimentation in the western equatorial Atlantic. *Geol. Soc. Am. Bull.*, 88:695-710.
- Flood, R.D., Manley, P.L., Kowsmann, R.O., Appi, C.J., and Pirmez, C., 1991. Seismic facies and late Quaternary growth of Amazon submarine fan. In Weimer, P., and Link, M.H. (Eds.), *Seismic Facies and Sedimentary Processes of Submarine Fans and Turbidite Systems*: New York (Springer-Verlag), 415-433.
- Manley, P.L., and Flood, R.D., 1988. Cyclic sediment deposition within Amazon deep-sea fan. *AAPG Bull.*, 72:912-925.
- Masson, D.G., Huggett, Q.J., and Brunsden, D., 1993. The surface texture of the Saharan debris-flow deposit: some speculations on submarine debris-flow processes. *Sedimentology*, 40:583-598.
- Pflaumann, U., 1986. Sea-surface temperatures during the last 750,000 years in the eastern equatorial Atlantic: planktonic foraminiferal record of Meteor cores 13519, 13521, and 16415. "Meteor" *Forschungsergeb. Reihe C.*, 40:137-161.
- Westbrook, G.K., Carson, B., Musgrave, R.J., et al., 1994. *Proc. ODP, Init. Repts.*, 146 (Pt. 1): College Station, TX (Ocean Drilling Program).

*Abbreviations for names of organizations and publications in ODP reference lists follow the style given in *Chemical Abstracts Service Source Index* (published by American Chemical Society).

Ms 155IR-111

NOTE: For all sites drilled, core-description forms ("barrel sheets") and core photographs can be found in Section 4, beginning on page 703. Forms containing smear-slide data can be found in Section 5, beginning on page 1199. GRAPE, index property, magnetic susceptibility, and natural gamma data are presented on CD-ROM (back pocket).

SHORE-BASED LOG PROCESSING

HOLE 935A

Bottom felt: 3496.5 mbrf
 Total penetration: 372.6 mbsf
 Total core recovered: 268.6 m (72%)

Logging Runs

Logging string 1: DIT/LSS/HLDT/CNTG/NGT (upper part)

Logging string 2: FMS/GPIT/NGT (upper part)

Logging string 3: DIT/LSS/HLDT/CNTG/NGT (lower part)

Logging string 4: FMS/GPIT/NGT (lower part)

No open-hole logging data were acquired in the 177–216 mbsf interval.

Wireline heave compensator was used to counter ship heave.

Bottom-hole Assembly/Drill Pipe

The following bottom-hole assembly and drill pipe depths are as they appear on the logs after differential depth shift (see **Depth shift** section below) and depth shift to the seafloor. As such, there might be a discrepancy with the original depths given by the drillers on board. Possible reasons for depth discrepancies are ship heave, use of wireline heave compensator, and drill-string and/or wireline stretch.

DIT/HLDT/CNTG/LSS/NGT (upper part): Bottom-hole assembly at ~62.5 mbsf.

DIT/HLDT/CNTG/LSS/NGT (lower part): Recorded open hole.

FMS/GPIT/NGT (upper part): Recorded open hole.

FMS/GPIT/NGT (lower part): Recorded open hole.

DIT/HLDT/CNTG/LSS/NGT (upper part): Drill pipe at 20 mbsf.

Processing

Depth shift: All original logs have been interactively depth shifted with reference to NGT from FMS/GPIT/NGT main pass, and to the seafloor (–3497 m). The amount used to depth shift the data to the seafloor corresponds to the seafloor depth observed on the logs, which differs 0.5 m from the “bottom felt” depth given by the drillers. A list of the amount of differential depth shifts applied at this hole is available upon request.

Gamma-ray processing: NGT data have been processed to correct for borehole size and type of drilling fluid.

Acoustic data processing: No processing necessary because of the good quality of the data.

Quality Control

During the processing, quality control of the data is mainly performed by cross-correlation of all logging data. Large (>12 in.) and/or irregular borehole adversely affects most recordings, particularly those that require eccentricity and a good contact with the borehole wall (CNTG, HLDT).

Hole diameter was recorded by the hydraulic caliper on the HLDT tool (CALI), and the caliper on the FMS string (C1 and C2).

Data recorded through the bottom-hole assembly and drill pipe, such as the CNT and NGT data recorded above 62.5 mbsf, should be used only qualitatively because of the attenuation on the incoming signal. An invalid gamma-ray spike was detected at 54–56 mbsf.

Data from different runs were merged as follows:

Upper part:

NGT from DIT/LSS/HLDT/CNTG/NGT (repeat) from 0 to 93 mbsf

NGT from FMS/GPIT/NGT (main) from 93 to 164 mbsf

DIT/SFLU from DIT/LSS/HLDT/CNTG/NGT (repeat) from 82.5 to 120 mbsf

DIT/SFLU from DIT/LSS/HLDT/CNTG/NGT (main) from 120 to 184 mbsf

HLDT/CALI from DIT/LSS/HLDT/CNTG/NGT (repeat) from 86 to 105 mbsf

HLDT/CALI from DIT/LSS/HLDT/CNTG/NGT (main) from 105 to 176 mbsf

CNTG from DIT/LSS/HLDT/CNTG/NGT (repeat) from 86 to 105 mbsf

CNTG from DIT/LSS/HLDT/CNTG/NGT (main) from 105 to 169 mbsf

Lower part:

NGT from FMS/GPIT/NGT (main) from 216 to 238 mbsf

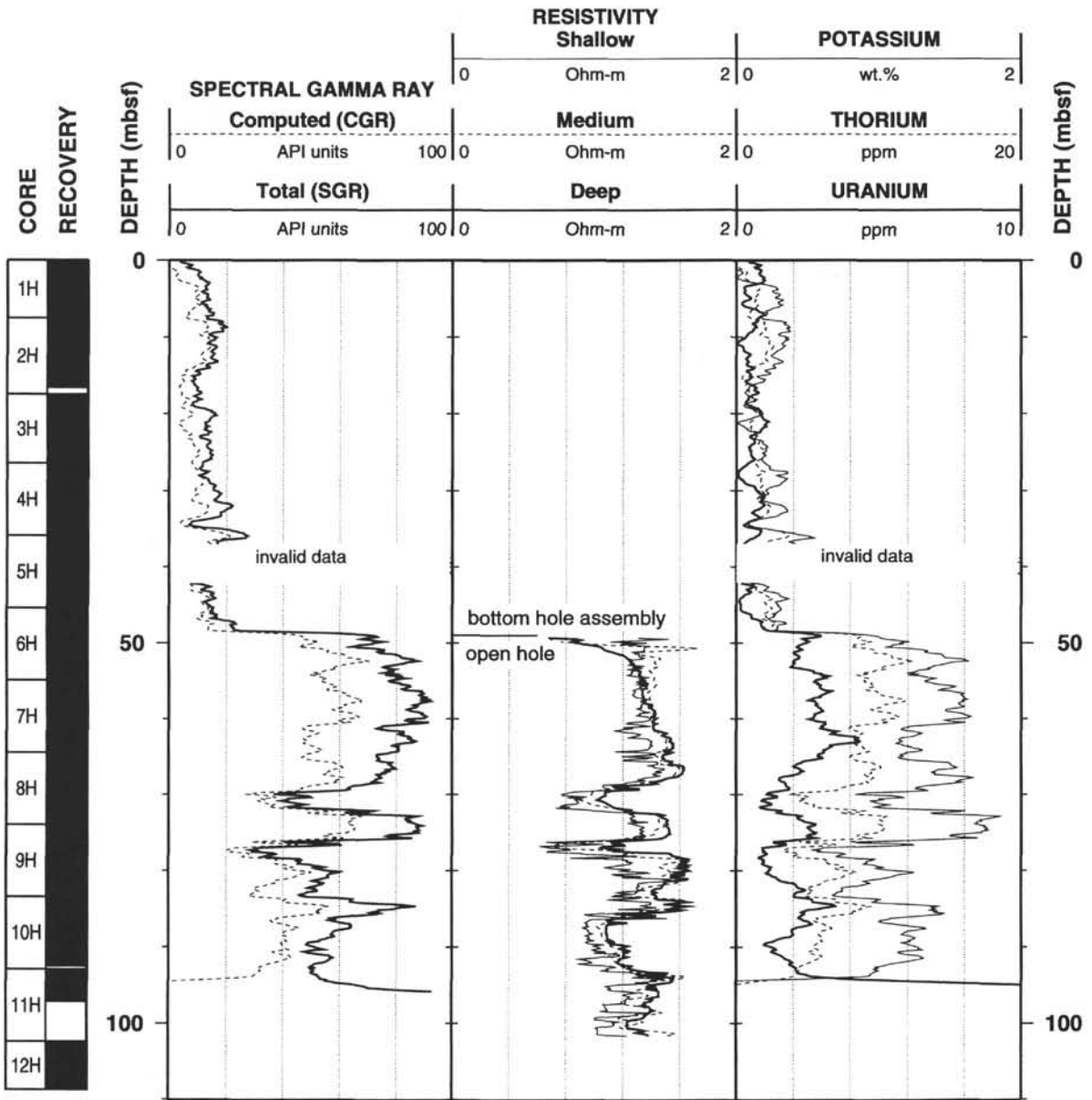
NGT from DIT/LSS/HLDT/CNTG/NGT (main) from 238 to 271 mbsf

Note: Details of standard shore-based processing procedures are found in the “Explanatory Notes” chapter, this volume. For further information about the logs, please contact:

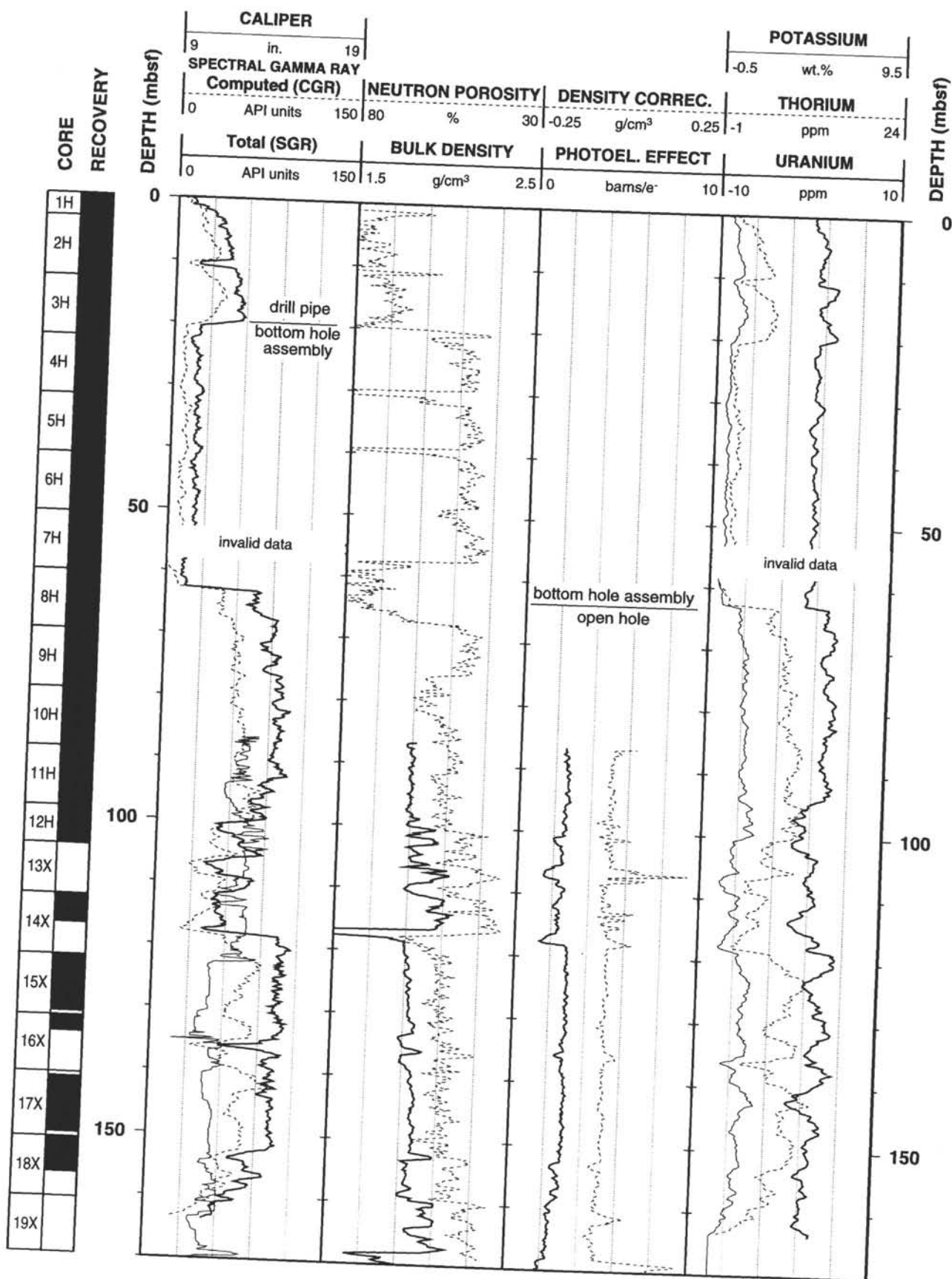
Cristina Broglia
 Phone: 914-365-8343
 Fax: 914-365-3182
 Email: chris@ldeo.columbia.edu

Elizabeth Pratson
 Phone: 914-365-8313
 Fax: 914-365-3182
 Email: beth@ldeo.columbia.edu

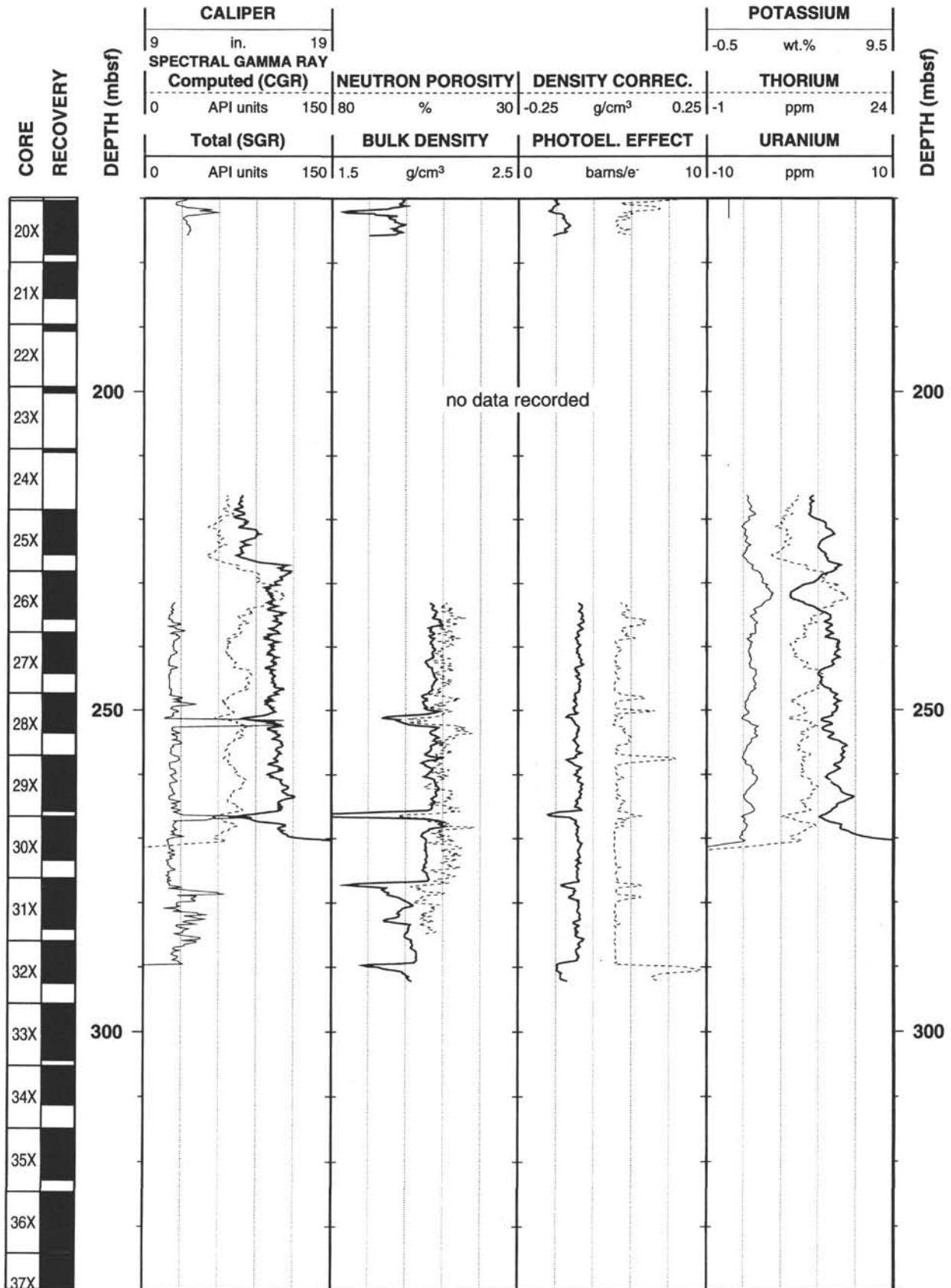
934B Natural Gamma Ray-Resistivity Logging Data



935A Natural Gamma Ray-Density-Porosity Logging Data



935A Natural Gamma Ray-Density-Porosity Logging Data (cont.)



935A Natural Gamma Ray-Resistivity-Velocity Logging Data

